AD-A095 151 NORTHEASTERN UNIV BOSTON MASS F/G 20/12
PHONON SELF-ENERGIES IN WEAKLY AND STRONGLY ANHARMONIC SYSTEMS.(U)
DEC 80 R P LOWNDES DA-ARO-D-31-124-72-G125
UNCLASSIFIED ARO-10392.14-P NL

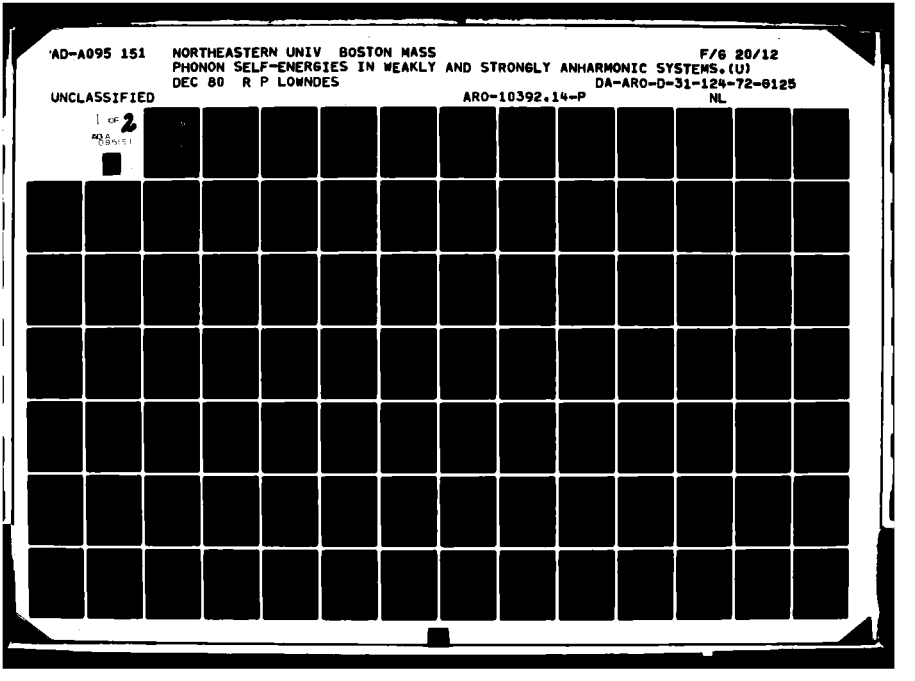

ARO 10392.14-P and 12918.10-P

(4)

AD A095151

PHONON SELF-ENERGIES IN WEAKLY AND STRONGLY ANHARMONIC SYSTEMS

LEVEL II

FINAL REPORT.

Jun 75-Dec 80

Robert P. Lowndes

December 11, 1980

U. S. ARMY RESEARCH OFFICE

DTIC ELECTE FEB 18 1981 S D E

DA-ARO-D-31-124-72-G125

DAHC04-75-G-0166

NORTHEASTERN UNIVERSITY

APPROVED FOR PUBLIC RELEASE;

DISTRIBUTION UNLIMITED.

DDC FILE COPY

81 2 17 197

THE FINDINGS IN THIS REPORT ARE NOT TO BE CONSTRUED AS AN OFFICIAL DEPARTMENT OF THE ARMY POSITION, UNLESS SO DESIGNATED BY OTHER AUTHORIZED DOCUMENTS.

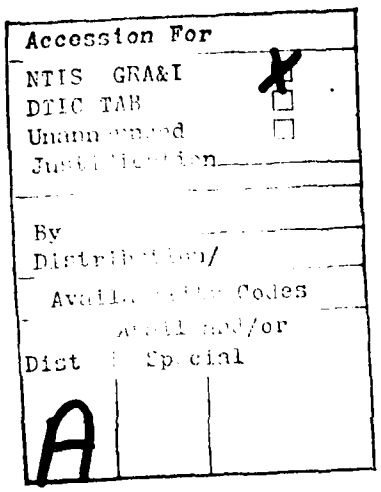

TABLE OF CONTENTS

LIST OF ILLUSTRATIONS

LIST OF TABLES

I. GENERAL INTRODUCTION

The interatomic forces in a crystal are usually strongly dependent on the interatomic spacing and consequently the lattice potential energy for a crystal can generally be written as a power series in the displacements of the atoms from their equilibrium positions. If such an expansion is terminated at the quadratic terms, then this constitutes the so-called harmonic approximation. In the harmonic approximation the lattice vibrations are true normal modes such that if energy is channeled uniquely into any one lattice mode, then it will remain undissipated in that mode. The harmonic approximation would therefore predict, for instance, that the scattering cross section for neutrons by a Bravais lattice would consist of a set of δ function peaks or, analogously, that the spectral profiles of lattice vibrations would be a set of undamped temperature independent resonances. These and other such predictions are, of course, in marked discord with experimental results. It is therefore clear that the anharmonic terms in a lattice potential must be considered if a full understanding of many of the physical properties of solids is to be achieved.

The inclusion of the anharmonic terms in a lattice potential has several consequences as far as phonons are concerned. Firstly, the phenomenon of thermal expansion is now allowed and this leads to so-called thermal strain shifts of the phonon energies away from their harmonic values. Secondly, interactions between the normal modes can now occur and this opens up channels for the decay of phonons which, in turn, causes additional so-called anharmonic self-energy shifts of phonon energies away from their harmonic values and the appearance of finite lifetimes for the phonons.[1,2] Thirdly, it opens up the possibility of interactions between certain phonons

and fluctuations in the phonon density distribution,[3,4] one of the ramifications of which (under favorable conditions) can be the appearance of a relaxing self-energy component for a mode, and it is this latter which is predicted to lead to low-frequency structure in the response function for the mode, which is now generally referred to as a central component.

Before proceeding further, it is useful to stress certain distinguishing features and certain common characteristics of these components. The thermal strain component for a mode is a frequency independent quantity, whereas the anharmonic self-energy and relaxing self-energy components are frequency dependent. The two latter, however, are differentiated in their frequency dependence because the main structure in the anharmonic self-energy occurs around 10^{12} Hz whereas the central component arising from the relaxing self-energy occurs at much lower frequencies, probably in the 10^{6}-10^{9} Hz range. The central feature which is common to all these components is that they each can contribute to the temperature dependence of a mode, sometimes in a dominant and important way. In weakly anharmonic systems, like the alkali halides for instance, the temperature dependence of all modes is generally determined by the competition or enhancement between the thermal strain and the anharmonic self-energies; for such materials the magnitude of both components for a mode is generally small compared to the harmonic energy of the mode, so that the resulting temperature dependence is also small. The effect of these two contributions, however, can be separated because the probability for phonon interaction is determined by the thermal population factors with the result that a phonon anharmonic self-energy will contribute a temperature dependence even under isochoric conditions, which is in contrast to that arising from the thermal strain component. For

certain modes in more strongly anharmonic systems, such as the soft mode in displacive ferroelectrics, this marginal imbalance between the magnitude of the thermal strain and anharmonic self-energy is broken, with the latter becoming so large as to strongly dominate both the thermal strain and the mode harmonic energy, which is imaginary, so that such systems are stabilized in their paraelectric phase by these huge anharmonic self-energy contributions to the soft mode. In certain other strongly anharmonic systems, like piezoelectric hydrogen-bonded ferroelectrics, the relaxing self-energy can also contribute importantly to the temperature dependence of the soft-mode in that it can cause the mode to condense out below the characteristic clamped-Curie temperature. In addition, the relaxing self-energy gives rise to a temperature dependence of the central component which is most pronounced as the clamped-Curie temperature is approached.

These three components, the thermal strain, the complex anharmonic self-energy and the relaxing self-energy provide the general focus of the scope of this final report. This focus is inexorably linked with the ultimate goal of achieving a satisfactory understanding and characterization, via theoretical descriptions, of anharmonic interactions, both weak and strong, and the role that these play in systems like ferroelectric materials. Ferroelectric materials are of great interest, of course, because of the enormous diversity and inter-relation of their physical properties which may be harnessed to provide solutions to technological problems such as memory function devices and the like.

Section II of this report is concerned with the determination of the thermal strain component and, more importantly, of the frequency dependence of the anharmonic self-energy and damping function of the $\underline{q} \approx 0$ transverse

optic mode in simple ionic systems. Section III deals with an experimental determination of the self-energy contributions associated with the soft mode in displacive ferroelectric materials. Section IV describes optical and dielectric investigations of the relaxing self-energy associated with the soft mode in piezoelectric hydrogen-bonded ferroelectrics.

II. WEAKLY ANHARMONIC SYSTEMS

A. Introduction

In describing the physical properties of a real anharmonic crystal it is usual to resort to the use of perturbation theory. While ordinary perturbation theory has been used to describe anharmonic interactions,[5-7] more recent discussions have appealed to the techniques of quantum field theory in which the system is described in terms of the Green's functions or propagators for the system. The use of temperature-dependent time-ordered Green's functions to describe anharmonic interactions between normal modes of vibration has been described by Maradudin and Fein[1] and Cowley.[2] These authors have shown that the dielectric and scattering properties (which are of interest here) of an anharmonic crystal are dependent on the Fourier transforms of certain time correlation functions, the simplest of which is the one-phonon Green's function defined by

$$G(\underset{\sim}{q},jj',t) = \langle TA(\underset{\sim}{q},j,t)A^{*}(\underset{\sim}{q},j',0)\rangle \qquad (1)$$

where the phonon operator $A(\underset{\sim}{q},j)$ is defined in terms of the sum of a creation and destruction operator, T is the Dyson time-ordering parameter, and the triangular parentheses represent thermal averaging. These Green's functions are periodic in the complex time direction and can be expanded in a Fourier series in that direction. The coefficients of this series are

$$G(\underset{\sim}{q},jj',\Omega) = \frac{i}{\beta\hbar}\int_{0}^{-i\beta\hbar} G(\underset{\sim}{q},jj',t)\, e^{i\Omega t}\, dt \quad , \qquad (2)$$

where $\beta = 1/kT$, k being Boltzmann's constant, and $\Omega = 2\pi xi/\beta\hbar$, x being an integer. The physical properties of the crystal can be obtained from these coefficients, analytically continued over the whole of the complex Ω plane.

The coefficients are obtained from the use of diagrammatic perturbation theory and the Dyson equation for the Green's functions obtained from these diagrams is the matrix equation

$$\sum_{j'} \left(\left[[\omega^h(\underset{\sim}{q},j)]^2 - \Omega^2 \right] \delta_{jj'} + 2\omega^h(\underset{\sim}{q},j) D(\underset{\sim}{q},jj',\Omega) \right)$$

$$\times G(\underset{\sim}{q},j'j'',\Omega) = \frac{\delta_{jj''} 2\omega^h(\underset{\sim}{q},j)}{\beta\hbar} \quad , \tag{3}$$

where $D(\underset{\sim}{q},jj',\Omega)$ is the anharmonic self-energy of the phonons. In the harmonic approximation the self-energy $D(\underset{\sim}{q},jj',\Omega)$ is zero and the left-hand side of equation (3) then plays the role of the dynamical matrix within the harmonic approximation. In the anharmonic crystal the self-energy is not zero and the matrix on the left-hand side of equation (3) couples phonons from the dispersion branches j, j', and j'' with the same wave vector. This coupling will occur whenever the modes transform according to the same irreducible representation of the space group of the crystals. The matrix $D(\underset{\sim}{q},jj',\Omega)$ has Hermitian and anti-Hermitian parts, the Hermitian parts giving rise to a shift in the normal mode frequencies, and the anti-Hermitian parts giving rise to a now finite lifetime for the phonon state. Formally the anharmonic contribution to the Hermitian part of the self-energies of the normal modes can be included by renormalizing the frequencies and eigenvectors of the normal modes. If the off-diagonal Hermitian terms in the matrix equation are neglected, then the Green's function for the anharmonic crystal becomes similar to that of the harmonic crystal if $[\omega^h(\underset{\sim}{q},j)]^2$ is replaced by $[\omega(\underset{\sim}{q},j)]^2$ such that

$$[\omega(\underset{\sim}{q},j)]^2 = [\omega^h(\underset{\sim}{q},j)]^2 + 2\omega^h(\underset{\sim}{q},j) D(\underset{\sim}{q},jj,\Omega) \quad , \tag{4}$$

where

$$D(\underline{q},jj,\Omega) = \Delta(\underline{q},jj,\Omega) - i\Gamma(\underline{q},jj,\Omega) \quad . \tag{5}$$

Detailed expressions for the self-energy $D(\underline{q},jj',\Omega)$ have been evaluated by a number of authors.[1,2,8,9] To second order in both cubic and quartic anharmonicity, the real part of the total anharmonic self-energy may be written

$$\Delta(\underline{q},jj',\Omega) = \Delta^{E}(\underline{q},jj') + \Delta^{A}(\underline{q},jj',\Omega) \quad , \tag{6}$$

where $\Delta^{E}(\underline{q},jj')$ is the thermal-strain contribution given by

$$\Delta^{E}(\underline{q},jj') = \frac{2}{\hbar} \Sigma V_{\alpha\beta}(\underline{q}j;\ -\underline{q}j')\ u^{T}_{\alpha\beta} \quad , \tag{7}$$

and $\Delta^{T}(\underline{q},jj',\Omega)$ is the anharmonic self-energy contribution given by

$$\Delta^{A}(\underline{q},jj',\Omega) = \Delta^{A}(\underline{q},jj') + \tilde{\Delta}^{A}(\underline{q},jj',\Omega) \quad , \tag{8}$$

where $\Delta^{A}(\underline{q},jj')$ is a frequency-independent contribution and $\tilde{\Delta}^{A}(\underline{q},jj',\Omega)$ is a frequency-dependent contribution to $\Delta^{A}(\underline{q},jj',\Omega)$ given by

$$\Delta^{A}(\underline{q},jj') = \Delta^{(4)}(\underline{q},jj') + \Delta^{(8)}(\underline{q},jj') \quad , \tag{9}$$

with

$$\Delta^{(4)}(\underline{q},jj') = \frac{12}{\hbar} \sum_{\underline{q}_1 j_1} V(\underline{q}j;\ \underline{q}j';\ \underline{q}_1 j_1;\ -\underline{q}_1 j_1)(2n_1 + 1) \quad , \tag{10}$$

$$\Delta^{(8)}(\underline{q},jj') = \frac{144}{\hbar^2} \sum_{\underline{q}_1 j_1} \sum_{j_2} \sum_{\underline{q}_3 j_3} V(\underline{q}j;\ \underline{q}j';\ -\underline{q}_1 j_1;\ -\underline{q}_1 j_2)$$

$$\times V(\underline{q}_1 j_1;\ -\underline{q}_1 j_2;\ \underline{q}_3 j_3;\ -\underline{q}_3 j_3)\left(\frac{n_1 + n_2 + 1}{\omega_1^{\ h} + \omega_2^{\ h}} - \frac{n_1 - n_2}{\omega_1^{\ h} - \omega_2^{\ h}}\right)$$

$$\times (2n_3 + 1) \quad , \tag{11}$$

and

$$\bar{\Delta}^{A}(\underline{q},jj',\Omega) = \Delta^{(6)}(\underline{q},jj',\Omega) + \Delta^{(8)}(\underline{q},jj',\Omega) \quad , \tag{12}$$

with

$$\Delta^{(6)}(\underline{q},jj',\Omega) = -\frac{18}{\hbar^2} \sum_{\underline{q}_1 j_1} \sum_{j_2} |V(\underline{q}j;\ \underline{q}_1 j_1;\ -\underline{q}_1 j_2)|^2\, R(\Omega) \quad , \tag{13}$$

$$\Delta^{(8)}(\underline{q},jj',\Omega) = -\frac{96}{\hbar^2} \sum_{\underline{q}_1 j_1} \sum_{\underline{q}_2 j_2} \sum_{\underline{q}_3 j_3} |V(\underline{q}j;\ \underline{q}_1 j_1;\ \underline{q}_2 j_2;\ \underline{q}_3 j_3)|^2 S(\Omega) \, , \tag{14}$$

where

$$R(\Omega) = \left(\frac{n_1 + n_2 + 1}{\Omega + \omega_1{}^h + \omega_2{}^h} - \frac{n_1 + n_2 + 1}{\Omega - \omega_1{}^h - \omega_2{}^h} + \frac{2(n_1 - n_2)}{\Omega - \omega_1{}^h + \omega_2{}^h} \right) \quad , \tag{15}$$

$$\begin{aligned} S(\Omega) = \Big[& [(n_1 + 1)(n_2 + 1)(n_3 + 1) - n_1 n_2 n_3] \left(\frac{1}{\Omega + \omega_1{}^h + \omega_2{}^h + \omega_3{}^h} \right. \\ & \left. - \frac{1}{\Omega - \omega_1{}^h - \omega_2{}^h - \omega_3{}^h} \right) + 3 \Big[n_1 (n_2 + 1)(n_3 + 1) \\ & - (n_1 + 1) n_2 n_3 \left(\frac{1}{\Omega - \omega_1{}^h + \omega_2{}^h + \omega_3{}^h} - \frac{1}{\Omega + \omega_1{}^h - \omega_2{}^h - \omega_3{}^h} \right) \Big] \Big] \, . \end{aligned} \tag{16}$$

The imaginary part of the self-energy is given by

$$\Gamma(\underline{q},jj',\Omega) = \Gamma^{(6)}(\underline{q},jj',\Omega) + \Gamma^{(8)}(\underline{q},jj',\Omega) \quad , \tag{17}$$

where

$$\bar{\Delta}^{A}(\underline{q},jj',\Omega) = \frac{1}{\pi} \int_{-\infty}^{\infty} \frac{\Gamma(\underline{q},jj',\Omega)}{(\Omega - \Omega')_P} \, d\Omega' \quad . \tag{18}$$

In these equations the n's are phonon population numbers, the V coefficients are the Fourier-transformed anharmonic force constants, and the superscripts

on the Δ and Γ label that part of the quantity coming from the contributions to that order in parameter μ when the Hamiltonian is of the form

$$H = H_0 + \eta^3 H_3 + \eta^4 H_4 \quad . \tag{19}$$

In this section of the report, we are concerned with the theoretical and experimental determination of the quantities defined by equations (7), (8) and (17) determined at $\underset{\sim}{q} \approx 0$ and with $j = j' = t$, that is for zone-center transverse optic phonons in simple cubic ionic systems like the alkali halides.

B. Numerical Evaluations of Self-Energy Components

As can be seen from the previous section, the self-energy components of interest here involve complex lattice dynamical summations which require significant computational times even on today's high-speed computers. As a result, reports of such calculations have been somewhat limited and to date have been confined to a few simple ionic materials. [2,10-14]

Such numerical estimates of the different self-energy components can be made providing the harmonic frequencies $\omega^h(\underset{\sim}{q}, j)$ are known throughout the Brillouin zone and provided the V coefficients can be evaluated. For simple cubic materials like the alkali halides reasonable lattice-dynamical calculations of the dispersion curves throughout the Brillouin zone can be made thus generating the eigenvectors and eigenvalues necessary for the evaluation of the lattice sums contained in equations (7)-(18). Alternatively, these can be obtained by fitting measured low-temperature dispersion curves to particular lattice-dynamical models. In order to evaluate the V coefficients, certain assumptions must be made concerning the nature of the forces that interact between the ions in the lattice. The procedure gener-

ally chosen is to assume a short-range central-force repulsive potential and to ignore any anharmonicity in the Coulomb contributions to the lattice potential because of the expected dominance of the former contribution (the anharmonicity of the Coulomb interactions can be included if necessary, though).

The specifics of the various lattice dynamical calculations that are used to generate the harmonic frequencies, $\omega^h(\underline{q},j)$, and of the procedures to evaluate the V coefficients are lengthy and, since they have been discussed in the literature,[2,10-16] we will not detail them here.

This group has made numerical calculations of $\Delta^E(0,t)$, $\Delta^A(0,t,\Omega)$ and $\Gamma(0,t,\Omega)$ and their temperature dependence for all of the alkali halides. In making our calculations of the principal parts and δ functions occurring in equations (7)-(18), we used the representation method suggested by Maradudin and Fein,[1] which involves the approximation

$$[(x)_p]^{-1} - i\pi\delta(x) = (x + i\epsilon)^{-1} \quad , \tag{20}$$

where ϵ has a small but finite value. In our calculations[13,14] we used a mesh of 8000 points in the Brillouin zone for $\Gamma^{(6)}(0,t,\Omega)$ and $\Delta^{(6)}(0,t,\Omega)$, but only a mesh of 1000 points for the lengthier calculations of $\Gamma^{(8)}(0,t,\Omega)$ and $\Delta^{(8)}(0,t,\Omega)$. In general we used a value of $\epsilon = 0.01\ \omega_L$, where ω_L is the value of the highest frequency in the Brillouin zone.

C. Experimental Determinations of Self-Energy Components

(1) Introduction

Under normal conditions, experimental measurements do not lead straightforwardly to a separation of the thermal strain and anharmonic self-energy components. However, as Lowndes and Martin[17] first pointed out,

they can be separated out by a suitable combination of the constraint of high pressure and variable temperature because the anharmonic self-energy components will contribute a temperature dependence to a phonon energy that occurs even when a crystal is maintained under isochoric conditions. Lowndes and Martin[17] used this approach via high-pressure/variable temperature low-frequency ($\sim 10^3$ Hz) dielectric constant measurements to make first estimates of the thermal strain, $\Delta^E(0,t)$, and low-frequency anharmonic self-energies, $\Delta^A(0,t,0)$, of the $\underset{\sim}{q} \approx 0$ transverse optic phonons in simple ionic solids. In the course of the work covered by this final report, this group has[14,18] developed high-pressure far infrared techniques in order that a similar approach via high-pressure/variable temperature far infrared measurements could be made to make separate estimates of the thermal strain component, $\Delta^E(0,t)$, and first estimates of the far infrared ($\sim 10^{12}$ Hz) anharmonic self-energy components, $\Delta^A(0,t,\omega_t)$, of the $\underset{\sim}{q} \approx 0$ transverse optic phonons in the same simple ionic compounds.

But, as equations (8) and (17) show, the anharmonic self-energy components are frequency dependent and their full frequency dependence really needs to be determined in order to more fully test the current anharmonic theories. To achieve this, one needs in principle to be able to measure the frequency dependence of both the real and imaginary parts of the mode response function via some convenient physical property. Unfortunately, most measurements do not lead directly to the form of both the real and imaginary part of the system response (conventional power far infrared spectroscopy, for example, leads directly to only the reflection amplitude, whereas the phase angle needs also to be determined in order to evaluate the

real and imaginary parts of the dielectric response; similarly, inelastic light-scattering techniques lead directly to only the imaginary part of the susceptibility). Of course, in principle, such measurements can be used to calculate the other component via an appeal to causality, such as when the Kramers-Kronig relations are used, but such procedures have only limited accuracy. One measuring technique which overcomes these problems is the comparatively new and novel technique of dispersive Fourier transform spectroscopy[19,20] (DFTS), in which a sample is placed in one arm of a Michelson interferometer rather than outside it as in conventional spectroscopy. DFTS leads directly to a simultaneous determination of the system reflection amplitude and phase angle, and hence of the real and imaginary parts of the dielectric response. This in turn can then be used to make determinations of the frequency dependence of $\Delta^A(0,t,\Omega)$ and $\Gamma(0,t,\Omega)$. During the work covered by this final report, this research group, in collaboration with Dr. T. J. Parker of the University of London, has developed and used this technique to lead to a determination of the full frequency dependence of $\Delta^A(0,t,\Omega)$ and $\Gamma(0,t,\Omega)$ for a number of simple ionic materials.[21]

(2) Determination of $\Delta^E(0,t)$

The current theories of anharmonicity lead to the conclusion that the quasi-normal frequency of a phonon measured in any resonance experiment is given by

$$\omega_{T,0}(0,t) = \omega^h(0,t)^2 + 2\omega^h(0,t)\{\Delta^A(0,t,\omega_r) + \Delta^E(0,t)\} \equiv \omega_t \quad , \qquad (21)$$

where the subscripts T and 0 denote the operative temperature and pressure of the system, respectively. It is readily shown[14] that $\Delta^E(0,t)$ is determined by

$$\Delta^E(0,t) \approx - \frac{[\omega_{T,P}(0,t)^2 - \omega_{T,0}(0,t)^2]}{2\omega_{00}(0,t)} \quad , \qquad (22)$$

where $\omega_{0,0}(0,t)$ has been taken as a reasonable estimate of $\omega^h(0,t)$, and $\omega_{T,P}(0,t)$ is the lattice vibration frequency measured at a temperature T and at a pressure P which is such as to reduce the volume of the crystal to that which it has at 0 K and zero pressure. The right-hand side of equation (22) contains all experimentally measurable parameters thus enabling an experimental determination of $\Delta^E(0,t)$.

A separate determination of $\Delta^E(0,t)$ can be made as follows. At $\Omega = 0$, $\Gamma(0,t,0) = 0$, and the lattice contribution to the static dielectric response can be written as

$$\epsilon^L(0) = \frac{\omega^h(0,t)^2 S(0)^2}{\omega^h(0,t)^2 + 2\omega^h(0,t)[\Delta^A(0,t,0) + \Delta^E(0,t)]} \quad . \qquad (23)$$

Providing the oscillator strength $S(0)^2$ is reasonably temperature independent, it is readily shown[17] that equation (23) leads to

$$\Delta^E(0,t) \approx -\frac{\omega_{T,0}(0,t)^2}{\omega_{0,0}(0,t)} \frac{\Delta\varepsilon^L(0)]_T}{\varepsilon^L_{T,0}(0)} \quad , \tag{24}$$

where the subscripts on ω and ε^L again refer to temperature and pressure, respectively. $\Delta\varepsilon^L(0)]_T$ is a measure of the change in $\varepsilon^L(0)$ on raising the pressure isothermally at a temperature T so as to restore the volume of the crystal to that which it has at 0 K and zero pressure. The approximation sign used in this equation stems from two sources. Firstly, as discussed above we have used values of the lattice vibration frequency determined at close to T - 0 K and at zero pressure, $\omega_{00}(0,t)$, to approximate $\omega^h(0,t)$. Secondly, it is assumed that $S(0)^2$ is reasonably temperature independent; justification for this for temperatures up to 500 K has been given by Lowndes and Martin.[17] The right hand side of equation (24) contains all experimentally measurable parameters and hence can lead to a second determination of $\Delta^E(0,t)$.

In our work, we have determined $\Delta^E(0,t)$ from both equations (22) and (24) and have generally found good agreement between the two approaches.

The determination of $\Delta^E(0,t)$ by these two separate procedures therefore requires the measurement of the isobaric (at 1 bar) temperature dependence of $\omega_{T,0}(0,t)$ and the corresponding high-pressure and temperature dependence of $\omega_{T,P}(0,t)$ to determine $\Delta^E(0,t)$ from equation (22), and the additional measurement of the isobaric (1 bar) temperature dependence of the dielectric response, $\varepsilon^L_{T,0}(0)$, and the corresponding appropriate high pressure and temperature dependence of $\varepsilon^L(0)$ to determine $\Delta^E(0,t)$ from equation (24). The lattice vibration

frequency for the $\underset{\sim}{q} \approx 0$ transverse optic mode in the alkali halides is most conveniently studied via (conventional) far infrared spectroscopic transmission measurements. This laboratory has developed high-pressure far infrared techniques sufficiently so as to facilitate the necessary determinations of $\omega_{TO}(0,t)$ and $\omega_{T,P}(0,t)$.

(3) Determination of $\Delta^A(0,t,\omega_t)$ and $\Gamma(0,t,\omega_t)$

At T =0K and at zero pressure, equation 21 becomes

$$[\omega_{00}(0,t)]^2 = [\omega^h(0,t)]^2 + 2\omega^h(0,t)\Delta_0^A(0,t,\omega_t') \tag{25}$$

where $$\omega_t' = \omega_{00}(0,t) \tag{26}$$

while at a temperature T and a suitably chosen applied pressure P so as to maintain the crystal volume at that found for the crystal at 0K and zero pressure, equation 21 becomes

$$[\omega_{T,P}(0,T)]^2 = [\omega^h(0,t)]^2 + 2\omega^h(0,t)\Delta_T^A(0,t,\omega_t) \tag{27}$$

which leads to

$$\Delta_T^A(0,t,\omega_t) - \Delta_0^A(0,t,\omega_t') = \frac{[\omega_{T,P}(0,t)]^2 - [\omega_{00}(0,t)]^2}{2\omega_{00}(0,t)} \tag{28}$$

$$\approx \frac{[\omega_{T,P}(0,t)]^2 - [\omega_{00}(0,t)]^2}{2\omega_{00}(0,t)} \tag{29}$$

$$\equiv -A'(T) \tag{30}$$

Equation (30) therefore allows an experimental determination of the change in the anharmonic self-energy between a temperature T and 0K via suitable studies of the temperature and pressure dependence of $\omega(0,t)$. $\Delta_0^A(0,t,\omega_t')$ is not necessarily zero because anharmonic interactions can persist in the presence of zero point fluctuations. However, experimental estimates of $\Delta_0^A(0,t,\omega_t')$ can be made as follows. For temperatures close to the Debye

temperature and above, it can be shown that the thermal population factors vary linearly with T and also that the leading terms in both the cubic and quartic anharmonic contributions to $\Delta_T^A(0,t,\omega_t)$ are linear in T. If such a linearity is found for A'(T), therefore, extrapolations of these linear parts back to T = 0 will yield an intercept of $\Delta_0^A(0,t,\omega_t')$ and hence $\Delta_T^A(0,t,\omega_t)$ can be determined from equation (29).

(4) The Determination of $\Delta^A(0,t,\Omega)$ and $\Gamma(0,t,\Omega)$

A simple cubic material, such as an alkali halide, has a single branch of transverse optic phonons and the lattice contribution to the dielectric response at a frequency Ω, $\epsilon^L(\Omega)$, is proportional to the Fourier transform of the propagator for such phonons with the wave vector $\underset{\sim}{q} \approx 0$. The Fourier transform of the propagator leads to a complex lattice contribution to the dielectric response at a frequency Ω of the form[1,2]

$$\epsilon^L(\Omega) = \frac{\omega^h(0,t)^2\, S(\Omega)^2}{\omega^h(0,t)^2 + 2\omega^h(0,t)D(0,t,\Omega) - \Omega^2} \quad , \tag{31}$$

where $S(\Omega)^2$ is the oscillator strength associated with the $\underset{\sim}{q} \approx 0$ transverse optic mode and is related to the effective dipole moment between the ions in the crystal. The mode anharmonic self-energy and the damping can be expressed in terms of the dielectric response of the system as[21]

$$\Delta^A(0,t,\Omega) = \tfrac{1}{2}\left\{\omega^h(0,t)[S(\Omega)^2\eta'(\Omega) - 1] + \frac{\Omega^2}{\omega^h(0,t)}\right\} - \Delta^E(0,t) \quad , \tag{32}$$

and

$$\Gamma(0,t,\Omega) = -\frac{\omega^h(0,t)\eta''(\Omega)S(\Omega)^2}{2} \quad , \tag{33}$$

where

$$\eta'(\Omega) = \frac{[\epsilon'(\Omega) - \epsilon(\infty)]}{[\epsilon'(\Omega) - \epsilon(\infty)]^2 + \epsilon''(\Omega)^2} \quad , \tag{34}$$

and

$$\eta''(\Omega) = \frac{\epsilon''(\Omega)}{[\epsilon'(\Omega) - \epsilon(\infty)]^2 + \epsilon''(\Omega)^2} \quad , \tag{35}$$

where $\epsilon'(\Omega)$ and $\epsilon''(\Omega)$ are the real and imaginary part, respectively, of the (total) dielectric response of the system.

Equations 32-35 reveal that experimental determinations of the frequency dependence of $\Delta^A(0,t,\Omega)$ and $\Gamma(0,t,\Omega)$ can be made if values of $\omega^h(0,t)$, $S(\Omega)$, $\eta'(\Omega)$ and $\eta''(\Omega)$, and $\Delta^E(0,t)$ can be determined. We have discussed the determination of $\omega^h(0,t)$ and $\Delta^E(0,t)$ in section C(2) above.

Bilz et al.[22] and Cowley[2] have shown that the oscillator strength $S(\Omega)^2$ has only a very weak frequency dependence compared to that arising from $\Delta^A(0,t,\Omega)$ and $\Gamma(0,t,\Omega)$. Furthermore, Lowndes and Martin[18,23] have shown that $S(0)^2$ has only a very weak temperature dependence. At $T = 0$ and $\Omega = 0$ the dielectric response described by equation (31) reduces to a good approximation to $S(0)^2 \approx \epsilon^L(0)$ and so values of $S(\Omega)^2$ may be obtained to a good approximation from values of $\epsilon^L(0)$ which have previously been reported by this author.[18]

Equations (34) and (35) reveal that the frequency dependence of $\eta'(\Omega)$ and $\eta''(\Omega)$ are determined by a knowledge of $\epsilon'(\Omega)$ and $\epsilon''(\Omega)$ and $\epsilon(\infty)$. $\epsilon(\infty)$ has little temperature dependence.[18,23] We have used <u>dispersive</u> Fourier transform reflection spectroscopy (DFTS) to determine $\epsilon'(\Omega)$ and $\epsilon''(\Omega)$ with high accuracy. DFTS will allow measurements of $\epsilon'(\Omega)$ and $\epsilon''(\Omega)$ to be made <u>simultaneously</u> to an accuracy of $\pm$ 2% throughout the far

infrared region (5-600 cm^{-1}). It is to be noted here that the temperature measurements of $\epsilon'(\Omega)$ and $\epsilon''(\Omega)$ need to be determined only at zero pressure in order to determine $\Delta^A(0,t,\Omega)$ and $\Gamma(0,t,\Omega)$.

(5) Experimental Techniques

A variety of experimental techniques were needed to measure the various parameters required in the determination of $\Delta^A(0,t,\Omega)$, $\Gamma(0,t,\Omega)$ and $\Delta^E(0,t)$ (see equations (32)-(35), (22), (24)). $\Delta^E(0,t)$ was determined in two separate ways: through (conventional far infrared Fourier transform spectroscopic studies of the phonon frequency and through studies of the low-frequency dielectric response, both made at high pressures and variable temperatures. The determination of $\Delta^A(0,t,\Omega)$ and $\Gamma(0,t,\Omega)$ required the use of Dispersive Fourier Transform Spectroscopy to measure the frequency dependence of the complex dielectric response.

(a) (Conventional) Fourier Transform Spectroscopy

Cubic ionic solids like the alkali and thallium halides have one $\underline{q} \approx 0$ transverse optic mode which is most conveniently studied by far infrared spectroscopy. The frequencies and lifetimes of these modes are readily determined from suitable measurements of the normal incidence transmission spectra of thin films of the material under investigation. Electromagnetic analyses of thin-film behavior shows that the minimum in the spectral transmission for such a thin film occurs at $\omega(0,t) \equiv \omega_t$ providing the film is thin compared to the vacuum wavelength of the incident radiation.[24] A similar analysis reveals that $2\Gamma(0,t,\omega_t)$ is determined by the

spectral damping measured at a transmission T', where T' is given by

$$T' = \frac{2T_o}{1 + T_o} \tag{36}$$

with T_o being the transmission at $\omega(0,t)$. The use of thin film transmission studies, therefore, allows a direct determination of $\omega(0,t)$ and $2\Gamma(0,t,\omega_t)$ without lengthy analysis of the data, as would be required using reflection data from bulk samples.

Values of $\omega_{T,0}(0,t)$ and $\omega_{T,P}(0,t)$, which were required to determine $\Delta^E(0,t)$ (see equation (22)), were measured by transmission studies on thin films using conventional far infrared Fourier Transform Spectroscopy. Values of $\omega_{T,0}(0,t)$ were also obtained from the far infrared DFTS measurements (to be discussed below) made in reflection from bulk single crystals and hence these allowed a check on these measurements. It is to be noted that, because of severe technical problems, the DFTS technique cannot as yet be used with samples under pressure and hence no check values of $\omega_{TP}(0,t)$ were obtained.

The measurements of $\omega(0,t)$ were obtained by means of Fourier Transform Spectroscopy using Michelson interferometers. A germanium bolometer (Infrared Laboratories, Tucson) operating at 2 K, was used as a detector in the frequency range 3-300 cm^{-1}; a Golay cell was used at higher frequencies.

(b) High Pressure Fourier Transform Spectroscopy

The requirements of hydrostatic pressure containment and far-infrared spectroscopy are somewhat conflicting. The first requires small apertures for maximum strength while the second requires large apertures to provide maximum energy throughput from the comparatively weak far-infrared sources. These requirements are further complicated because of the scarcity of readily available window materials which satisfy the competing demands

of strength and transmissivity in the far infrared. As a result of these difficulties, much of the very limited far-infrared high-pressure research has been confined to date to work achieved with the opposed diamond anvil system.[25] When used properly this cell is a powerful tool in the very-high-pressure domain, but, in the important 0-10 Kbar range involved in the present work, reliable far-infrared measurements are difficult to perform with this cell. This is primarily because of the difficulty in accurately determining the system operating pressure but also because of the inherent difficulty of achieving true hydrostatic pressure conditions because of residual pressure gradients across the anvil faces. The consequences of these problems have been that it is difficult to precisely determine the pressure dependence of mode eigenfrequencies, especially at the low pressures necessary for the evaluation of $\omega_{T,P}(0,t)$, and it is virtually impossible to reliably measure the (small) pressure dependence of the associated linewidths using the diamond anvil system.

Accordingly, this group has developed a high-pressure far-infrared cell which goes some way to solving these problems,[26] and this is illustrated in figure 1. The cell body, window mounts, and retaining closures were machined from 4340 alloy steel and then heat treated to a hardness of RC45 giving a yield strength of 14 Kbars. The critical bores and surfaces of the cell and its components were ground and honed to size after the hardening process. The cell body measures 17 × 14 × 10 cm and fully assembled the cell has an effective speed of f2.4.

The window mounts used in the cell give a supported to unsupported area ratio of about 3 with an unsupported port diameter of 5 mm. The window high-pressure seal is achieved by lapping and polishing the mating surfaces of the window and its mount to be flat and parallel to better than 300Å.

The windows are prevented from sliding off their mounts by brass retaining rings attached to the window mounts. The window mount pressure seal is achieved using a stainless-steel, brass, and Teflon packing assembly.

In choosing both the cell windows and the pressure transmission medium, care must be used to avoid materials which have characteristic electromagnetic resonances in the spectral region under investigation. The choice of materials available for both window and pressure transmission media for far-infrared service is extremely restricted however. For windows we have used $\frac{1}{4}$-in.-thick fused quartz for the spectral range below 125 cm^{-1} and $\frac{1}{2}$-in.-thick silicon for the spectral range 125-400 cm^{-1}. For a pressure transmission medium we have used either helium or argon gas since these exhibit no characteristic far-infrared resonances as do most of the organic oils and molecular gases conventionally used in high-pressure research.

Figure 2 shows the experimental arrangement for a high-pressure far-infrared transmission experiment. The high-pressure cell is located in an isolated evacuated thick-walled module B designed to protect the interferometric and detector modules A and C, respectively. The cell window axis is deliberately chosen to be off line with both the entrance and exit ports to module B to avoid any possible damage to the interferometer or detector due to a high-pressure window failure.

The hydrostatic pressure for these experiments was generated from a two-stage gas compressor. The pressure was measured using a suitably aged and calibrated manganin cell. With this high-pressure spectroscopic arrangement we were able to make spectral studies in the far infrared under truly hydrostatic pressure conditions with a pressure accuracy of better than $\pm$ 1% whilst at the same time achieving signal-to-noise values of better than 100.

(c) Low Frequency Dielectric Constant Measurement

The low-frequency dielectric response, $\epsilon(0)$, was determined via three-terminal capacitance measurements made in the frequency range 1-100 kHz with a measuring accuracy of ±0.1%.[17,23,27] The capacitance measurements were recorded on a General Radio model 1615A transformer-ratio-arm bridge used in conjunction with a tuned amplifier and null detector. The measuring electrodes were evaporated onto the single crystal samples using gold as the electrode material.

(d) Dispersive Fourier Transform Spectroscopy

In order to determine the frequency dependence of $\Delta^A(0,t,\Omega)$ and $\Gamma(0,t,\Omega)$ from equations (32) and (33), it is necessary to precisely determine the dispersion of $\epsilon'(\Omega)$ and $\epsilon''(\Omega)$.

The conventional method for determining $\epsilon'(\Omega)$ and $\epsilon''(\Omega)$ is to measure the power reflectivity, $R(\Omega)$, at near normal incidence over as wide a spectral range as possible, and then to obtain the phase spectrum, $\varphi(\Omega)$, by calculation from the Kramers-Kronig relation[28]

$$\varphi(\Omega) = \frac{2\Omega}{\pi} \int_0^\infty \frac{\ell n\, r(\Omega')}{\Omega'^2 - \Omega^2}\, d\Omega' \quad . \tag{37}$$

In this expression $r(\Omega)\exp[i\varphi(\Omega)]$ is the complex amplitude reflection coefficient and $r(\Omega) = \sqrt{R(\Omega)}$. From this $\epsilon'(\Omega)$ and $\epsilon''(\Omega)$ can then be obtained from the Fresnel relations. The main problem with this procedure is that the complete dispersion of $R(\Omega)$ must be measured, but this is often not

possible especially if there is significant dispersion at very low-frequencies (such as for soft modes) or at high frequencies, which therefore necessitates other measuring techniques to be utilized to complete the measurement of $R(\Omega)$. A second problem is that $\varphi(\Omega)$ is not well determined in those frequency ranges where $r(\Omega) \rightarrow 0$ because of the inaccuracies in measuring the magnitude of $r(\Omega)$.

Conventional Fourier transform spectroscopy, as described in a previous section, yields the power spectrum from a sample placed externally to the interferometer. However, if the sample is inserted in one arm of the Michelson interferometer, then it is possible to perform amplitude-phase or dispersive Fourier transform spectroscopy.[19,20] The asymmetric sample-interferogram from such spectroscopy can be transformed into the spectral functions of the phase and amplitude of the reflectance, from which the real and imaginary parts of the complex dielectric response of the system can be measured directly, and without having to measure the infinite spectrum. Furthermore, since DFTS measures $r(\Omega)$, rather than $r^2(\Omega) = R(\Omega)$ as in conventional spectroscopy, it has an automatic improvement in the accuracy of $\epsilon'(\Omega)$ and $\epsilon''(\Omega)$ which is especially important as $r(\Omega) \rightarrow 0$.

The apparatus used by this group is illustrated schematically in figures 3 and 4.[29-31] The fixed mirror of the Michelson interferometer is replaced by an optically flat reflector whose surface is divided

up into an outer metallized ring C and two inner semicircular rings, one of which, B, is metallized and the other is the sample. By an arrangement of opaque screens each of these parts may in turn be used as the reflector. In practice, the outer ring is first used to align the whole reflector so that the incident beam is perpendicular to the surface. Since it has a large radius it provides a readily reproducible alignment. Then a specimen interferogram is recorded with part A exposed and a reference interferogram is recorded with part B exposed. The interferograms are Fourier transformed and the educed spectra are ratioed to give the complex reflectivity. To reduce systematic errors caused by asymmetry between the two sides of the instrument this output spectrum is re-ratioed against a ratioed calibration spectrum obtained in a separate experiment with both parts A and B metallized.

Although the specimen is on a collimated beam, the method is suitable for measurements on fairly small samples of area of 1 cm^2 or larger, which is satisfactory for all the materials studied in this research project.

The procedure of metallizing part of the sample surface for use as a phase reference surface therefore allows the sample temperature to be changed and overcomes the problems experienced by earlier workers using DFTS which confined their measurements to room temperature only.[19,20,32-34] The group at Northeastern University, in collaboration with Dr. T. J. Parker of the University of London, has used this technique to determine $\epsilon'(\Omega)$ and $\epsilon''(\Omega)$ for several alkali halides (NaF, NaCℓ, KCℓ, KBr, KI, RbCℓ, RbBr and RbI) in the range 100-300 K, and hence to determine $\Delta^A(0,t,\Omega)$ and $\Gamma(0,t,\Omega)$.[21,35,36]

D. Results and Discussion

a) Theoretical Calculations of $\Delta^{A}(0,t,\Omega)$, $\Gamma(0,t,\Omega)$ and $\Delta^{E}(0,t)$

Figure 5 shows the frequency dependence calculated for the different contributions to $\tilde{\Delta}^{A}(0,t,\Omega)$ and $\Gamma(0,t,\Omega)$ for NaBr and Figure 6 shows the calculated frequency dependence of $\Delta^{A}(0,t,\Omega)$ for NaBr at different temperatures. Such results are generally typical for all of the alkali halides crystallizing in the NaCl structure.

Tables 1-4 summarize our calculated results for $\Delta^{E}(0,t)$, $\Delta^{A}(0,t,0)$, $\Delta^{A}(0,t,\omega_t)$ and $\Gamma(0,t,\omega_t)$ and their component contributions for the lithium, sodium, potassium and rubidium halides, respectively. The data for $\Delta^{A}(0,t,\omega_t)$ and $\Gamma(0,t,\omega_t)$ and their respective components are given for the calculated value of ω_t.

An analysis of the data in Tables 1-4 reveals a number of overall qualitative features which should be commented on:

(i) The frequency-independent contribution $\Delta^{A}(0,t)$ is always dominated by the positive contributions from the first-order quartic term $\Delta^{(4)}(0,t)$; $\Delta^{(8)}(0,t)$ is always less than 10% of $\Delta^{(4)}(0,t)$ even above the characteristic Debye temperature.

(ii) $\tilde{\Delta}^{A}(0,t,0)$ is always dominated by the negative second-order cubic term $\Delta^{(6)}(0,t,0)$. Although $\Delta^{(8)}(0,t,0)$ is generally less than 10% of $\tilde{\Delta}^{A}(0,t,0)$ at low temperatures, it has a much stronger temperature dependence and can be as much as 30% of $\tilde{\Delta}^{A}(0,t,0)$ at the characteristic Debye temperature.

(iii) $\Delta^A(0,t,0)$ is always positive at low temperatures because of the dominance of the first-order quartic term $\Delta^{(4)}(0,t)$, but this usually becomes negative at higher temperatures because of the stronger temperature dependence of the negative contributions of $\Delta^{(6)}(0,t,0)$, $\Delta^{(8)}(0,t)$ and $\Delta^{(8)}(0,t,0)$.

(iv) $\tilde{\Delta}^A(0,t,\omega_t)$ is always dominated by the negative second-order cubic term $\Delta^{(6)}(0,t,\omega_t)$. At low temperatures $\Delta^{(8)}(0,t,\omega_t)$ is always less than 10% of $\tilde{\Delta}^A(0,t,\omega_t)$ but because of a strong temperature dependence it can be as much as 40% of $\tilde{\Delta}^A(0,t,\omega_t)$ at the characteristic Debye temperature.

(v) $\Delta^A(0,t,\omega_t)$ can be either positive or negative at low temperatures depending on the balance between $\Delta^{(4)}(0,t)$ and $\Delta^{(6)}(0,t,\omega_t)$. At higher temperatures $\Delta^A(0,t,\omega_t)$ is generally negative, however, because of the stronger temperature dependence of the negative contributions from $\Delta^{(6)}(0,t,\omega_t)$, $\Delta^{(8)}(0,t,\omega_t)$, and $\Delta^{(8)}(0,t)$.

(vi) $\Gamma(0,t,\omega_t)$ is totally determined at low temperatures by the second-order cubic terms, $\Gamma^{(6)}(0,t,\omega_t)$. However, $\Gamma^{(8)}(0,t,\omega_t)$ has a much stronger temperature dependence than $\Gamma^{(6)}(0,t,\omega_t)$ and both contributions to $\Gamma(0,t,\omega_t)$ are generally very close in magnitude at the characteristic Debye temperature.

b) Experimental Results for $\Delta^A(0,t,0)$, $\Delta^A(0,t,\omega_t)$, $\Gamma(0,t,\omega_t)$ and $\Delta^E(0,t)$

Using the appropriate measurements of the temperature and pressure dependence of $\omega(0,t)$ and $\varepsilon(0)$, we have determined experimental values of $\Delta^E(0,t)$, $\Delta^A(0,t,0)$ and $\Delta^A(0,t,\omega_t)$ via the procedures outlined earlier, and

these values are summarized in Tables 5-10 for the lithium, sodium, potassium, rubidium, cesium, and thallium and silver halides, respectively. Table 11 summarizes the temperature dependence of $2\Gamma(0,t,\omega_t)$ for all these materials.

A number of qualitative trends emerge from these results: (i) the $\Delta_0^A(0,t,\omega_t)$ are generally quite small and are no more than a few percent of $\omega_{00}(0,t)$. (ii) The $\Delta_T^A(0,t,\omega_t)$ for the silver and alkali halides crystallizing in the NaCl structure are generally negative in sign at all temperatures and increase in magnitude with increasing temperature. (iii) The $\Delta_T^A(0,t,\omega_t)$ for the thallium and alkali halides crystallizing in the CsCl structure may be negative or positive at lower temperatures but are always positive at higher temperatures. (iv) The $\Delta_T^A(0,t,\omega_t)$ have a smaller temperature dependence than $\Delta^E(0,t)$ for all the materials studied except the thallium halides.

Tables 5-8 also compare the theoretical calculations and experimental results for the anharmonic self-energies of the experimental lithium, sodium, potassium and rubidium halides. The results have allowed separate determinations of $\Delta^E(0,t)$ to be made at $\Omega = 0$ and $\Omega = \omega_t$. Equation (7) shows $\Delta^E(0,t)$ to be a frequency-independent quantity and the experimental results generally support this within the limits of the experimental accuracy. The exceptions to this are the results for the cesium and thallium halides at higher temperatures, but these differences may indicate the importance of the volume dependence of the dipole moments associated with the transverse-optic modes in these materials which have been neglected in the determination of $\Delta^E(0,t)$ at $\Omega = 0$. It is for this reason that the results for $\Delta^E(0,t)$ determined at $\Omega = \omega_t$ are considered more reliable, and a comparison of these with the theoretical results reveals a good agreement within the accuracy limits for all the materials.

The results for $\Delta_T^A(0,t,0)$ are qualitatively very good in that both experiment and theory show a reversal in sign as the temperature is raised,

and furthermore show this reversal to take place at about the same temperature. Quantitatively, the low-temperature results are in good agreement for all the materials and this reasonable agreement is maintained for the potassium and rubidium halides at higher temperatures. For the lithium and sodium halides, however, serious discrepancies arise between the two sets of data at higher temperatures, with the calculated results showing a much stronger temperature dependence.

The agreement between theory and experiment is less good for $\Delta_T^A(0,t,\omega_t)$. Qualitatively, the experimental results suggest that the second-order anharmonic contributions always dominate so that $\Delta_T^A(0,t,\omega_t) < 0$, whereas the calculated results reveal that this is not always so at the lower temperatures. Quantitatively, although the results for many of the compounds agree within the error limitations, the experimental results generally tend to vary somewhat faster with temperature than the calculated theoretical predictions. The preceding comments have been made for the calculated values of $\Delta_T^A(0,t,\omega_t)$ determined at the calculated value of ω_t. In order to test the sensitivity of the calculated values of $\Delta_T^A(0,t,\omega_t)$ to any frequency dispersion, we have also listed values of $\Delta_T^A(0,t,\omega_t)$ calculated at the experimentally determined values of ω_t in Tables 5-8. With the exception of the higher temperature data for LiBr and LiI (which in any case must be treated with some caution for the reasons given earlier), the two sets of calculated values for $\Delta_T^A(0,t,\omega_t)$ are quite close and generally differ at most by no more than $\pm$ 15%. However, the values of $\Delta_T^A(0,t,\omega_t)$ calculated at $(\omega_t)_{exp}$ are generally in no better agreement with the experimental values than the $\Delta_T^A(0,t,\omega_t)$ calculated at $(\omega_t)_{calc}$.

The results for $\Gamma(0,t,\omega_t)$ show the theoretical predictions at low temperatures to usually be somewhat smaller than the experimental values

and, as the temperature is increased, to generally have a somewhat faster temperature dependence than the experimental results. The calculated theoretical results at the higher temperatures are generally in reasonable agreement with the experimental results for the lithium and sodium halides but are significantly bigger than the experimental results for the potassium and rubidium halides.

The experimental studies of the pressure dependence of $\Gamma(0,t,\omega_t)$ suggest that its volume dependence is small. Equations (17) and (18) reveal that such a volume dependence can arise only from that of the anharmonic coupling coefficients or from that of the $\omega^h(\underset{\sim}{q},j)$. We have attempted to calculate approximately what Eqs. (17) and (18) would predict for the volume dependence of $\Gamma(0,t,\omega_t)$ for a number of alkali halides by allowing all the $\omega^h(\underset{\sim}{q},j)$ to have the same pressure dependence as that measured for $\omega(0,t)$ and by using values of r_o and β suitably corrected for the effects of pressure. Such assumptions lead to the conclusion that $\Gamma(0,t,\omega_t)$ will always decrease with increasing pressure by (1-2)% per kbar. Although the absolute magnitude of this calculated pressure dependence for $\Gamma(0,t,\omega_t)$ is in agreement with that found experimentally, these results do not explain the small increases with pressure found for $\Gamma(0,t,\omega_t)$ for some materials.

The reason for the less good agreement between the calculated and experimental anharmonic self-energies at $\Omega = \omega_t$ is not clear. The discrepancy between calculation and experiment for $\Gamma(0,t,\omega_t)$ at low temperatures could simply arise from an underestimate of $\Gamma^{(6)}(0,t,\omega_t)$ or $\Gamma^{(8)}(0,t,\omega_t)$ or from some sample artifact in the low-temperature experimental measurements: this latter would seem most unlikely, however, in view of the equivalent results that we obtain from single-crystal reflection measurements and thin-film transmission measurements. The generally good agreement between cal-

culation and experiment for the higher temperature $\Gamma(0,t,\omega_t)$ for the sodium, potassium, and rubidium halides suggests, but does not prove, that the calculated form of $\tilde{\Delta}^A(0,t,\omega_t)$ may be correct; if this were true then this in turn would suggest that the general disagreement between calculation and experiment for $\Delta_T^A(0,t,\omega_t)$ might arise from the calculation of $\Delta^A(0,t)$ (see Eq. (9)).

c) Experimental Results for $\Delta^A(0,t,\Omega)$ and $\Gamma(0,t,\Omega)$

Figures 7-14 show the experimental determinations of the frequency dependence of $\Delta^A(0,t,\Omega)$ and $\Gamma(0,t,\Omega)$ for NaCl and RbCl at 105K and 300K. In all we have measured the frequency dependence of the self-energies, as a function of temperature, for NaF, NaCl, KCl, KBr, KI, RbCl, RbBr and RbI.

Our results indicate that there is a reasonable qualitative agreement, within experimental error, between the experimental and theoretical values of the self-energies for all materials. Quantitatively, the results are in very good agreement for the rubidium and potassium halides, but there are marked discrepancies between the two sets of data for NaF and NaCl, as the figures show. It should be noted that these measurements are in good agreement with our earlier measurements of the self-energies at specific frequencies, i.e. $\Delta^A(0,t,0)$, $\Delta^A(0,t,\omega_t)$ and $\Gamma(0,t,\omega_t)$.

d) Conclusion

In assessing the obvious qualitative and quantitative agreement for the calculated and experimental determinations of these anharmonic self-energies, it is useful to place in perspective the errors associated with each kind of determination.

Given the approximations contained within the anharmonic theory, the

errors associated with the calculated values of the anharmonic self-energies stem primarily from those involved with the $\omega^h(\underset{\sim}{q},j)$ and the anharmonic force constants. The errors associated with the $\omega^h(\underset{\sim}{q},j)$ are difficult to assess, but it can be stated that our lattice-dynamical calculations are in close agreement with available low-temperature dispersion curves, reported from inelastic neutron scattering experiments, with the most extreme differences being less than 10% over small regions of the Brillouin zone, and that anharmonic calculations for a few compounds using $\omega^h(\underset{\sim}{q},j)$ values differing uniformly by 10% throughout the Brillouin zone lead to only 10% changes in the real and imaginary anharmonic self-energies. The anharmonic force constants are sensitive to the input values of r_o and β, and in both cases values of these at low temperatures are needed. Values of β are typically determined directly at 4 K with an error of about $\pm$ 2%. Such an error in β will lead to errors of 2% or less in the various coefficients associated with the anharmonic force constants. Although r_o is usually determined quite precisely at 290 K to better than $\pm$ 0.1% via X-ray measurements, values of r_o at lower temperatures are often not directly measured but are determined from the known 290 K value of r_o and the known thermal-expansion data. This leads to a typical error of about $\pm$ 0.2% in r_o at 4 K. Such an error will generate errors of between 6-10% for the various coefficients associated with the anharmonic force constants. The accumulated errors in these coefficients will, of course, lead to errors in the individual contributions to the different total self-energy quantities. It should be recalled that $\Delta_T^A(0,t,\Omega)$ is obtained as a sum of $\Delta^{(4)}(0,t)$, $\Delta^{(8)}(0,t)$, $\Delta^{(6)}(0,t,\Omega)$ and $\Delta^{(8)}(0,t,\Omega)$, and although the errors on the individual contributions to the self-energy stemming from errors in r_o and β are no larger than about 10%, the accumulated error on $\Delta_T^A(0,t,\Omega)$ is considerably larger

because of the opposite signs of these individual contributions and because of the often close equivalence of the two dominant, but competing, terms $\Delta^{(4)}(0,t)$ and $\Delta^{(6)}(0,t,\Omega)$. However, $\Gamma(0,t,\Omega)$ is simply the sum of two components, $\Gamma^{(6)}(0,t,\Omega)$ and $\Gamma^{(8)}(0,t,\Omega)$, both of which are accurate to about $\pm$6%, and hence the accumulated error on $\Gamma(0,t,\Omega)$ will be smaller than that for $\Delta_T^A(0,t,\Omega)$. In Tables 5-8 we have listed our estimates of the possible errors associated with the different calculated self-energy components based on the known errors on r_o and β only.

The errors on the experimental determinations of $\Delta^E(0,t)$, $\Delta_T^A(0,t,\Omega)$, and $\Gamma(0,t,\omega_t)$ can vary significantly. The errors on the measured $\omega_{T,0}(0,t)$ are generally quite small and at worst no larger than about $\pm$1%, but the errors on $\omega_{T,P}(0,t)$ will be somewhat larger than this due to the error in calculating P. The experimental and theoretical results strongly suggest that the zero-temperature anharmonic self-energies are quite small, so that the use of the approximation $\omega_{U0}(0,t) \approx \omega^h(0,t)$ should not generate errors of more than a few percent in the determinations. Consequently we believe that the determinations of $\Delta^E(0,t)$ and $A'(T)$ are generally accurate to better than $\pm 1.5\ cm^{-1}$. Of course, the determinations of $\Delta_T^A(0,t,\omega_t)$ are somewhat worse than this depending on the accuracy of the extrapolation procedure used to determine $\Delta_0^A(0,t,\omega_t')$. The errors on the measured $\Gamma(0,t,\omega_t)$ are determined to be no better than $\pm$15% for the longer phonon lifetimes and no better than $\pm$25% for the shorter phonon lifetimes.

In conclusion, therefore, we have found a good agreement between theory and experiment concerning the sign, magnitude and temperature dependence of $q \tilde{\approx} 0$ transverse optic phonon self-energies in a range of weakly anharmonic systems. Although discrepancies do exist, they are generally within the errors associated with either the calculations and/or the exper-

iments. For the range of temperatures and frequencies covered by our work, therefore, the current theories of weak anharmonicity appear to satisfactorily describe the anharmonic interactions in materials like simple cubic ionic solids.

III. STRONGLY ANHARMONIC SYSTEMS: DISPLACIVE FERROELECTRICS

A. Introduction

Over the past two decades the existence of a soft mode has been observed in many ferroelectric materials. Soft mode behavior, that is the rapid movement to lower frequencies by a lattice mode as the temperature is decreased, was first proposed by Cochran[37] and Anderson[38] to explain the anomalous temperature dependence of the dielectric response of ferroelectric materials.

As discussed in the carlier sections, the temperature dependence of any lattice mode frequency arises through the anharmonic terms in the lattice potential energy. As shown in the previous section, the hermitean self-energy contributions to the normal mode frequencies in most systems are smaller than the harmonic contributions. In displacive ferroelectrics, however, it was theorized that the anharmonic contributions to the soft mode were larger than the harmonic contributions and were thereby responsible for stabilizing the paraelectric states. In this section we describe our experimental measurements of the temperature and frequency dependence of the self-energies associated with the soft mode in displacive ferroelectrics which were the first to directly confirm these theoretical predictions.

B. Experimental Results for $\Delta^A(o,t,0)$ and $\Delta^E(o,t)$

Cowley[39] has discussed the stability of an anharmonic crystal using the techniques of quantum field theory and has analyzed the dielectric response of such an anharmonic crystal. The lattice contribution to the complex dielectric constant at a frequency Ω is of the form

$$\varepsilon^L(\Omega) = \sum_j \frac{\omega^h(o,j)^2 f_j^2}{\omega^h(o,j)^2 + 2\omega^h(o,j)D(o,j,\Omega) - \Omega^2} \qquad (38)$$

where $\omega^h(o,j)$ is the harmonic frequency of the j^{th} q = o transverse optic mode and f_j is its associated oscillator strength. In the following discussion

we shall assume that the dielectric response is determined primarily by the summation term in equation (38) associated with the soft mode and shall neglect contributions from the other q = o transverse optic phonons and any temperature dependence of the f_j. The self-energy $D(o,j,\Omega)$ is defined by equations 5-18 of the previous section.

At $\Omega = o$, the self-energy terms associated with the soft-mode can be related to experimental parameters involving the lattice contribution to the static dielectric response as follows:[40]

$$\frac{2\omega^h(o,t)\Delta^E(o,t)}{\omega^h(o,t)^2 + 2\omega^h(o,t)\Delta^A_{T_i}(o,t,o)} = \frac{\Delta\varepsilon^L(o)]_T}{\Delta\varepsilon^L(o)]_p + \varepsilon^L_{T_i}(o)} \tag{39}$$

and

$$\frac{\omega^h(o,t)^2 + 2\omega^h(o,t)\Delta^A_T(o,t,o)}{\omega^h(o,t)^2 + 2\omega^h(o,t)\Delta^A_{T_i}(o,t,o)} = \frac{\varepsilon^L_{T_i}(o)}{\varepsilon^L_{T_i}(o)+\Delta\varepsilon^L_T(o)]_V} \equiv A(T) \tag{40}$$

where (o,t) denotes the soft mode, $\Delta\varepsilon^L(o)]_p$ is the change in $\varepsilon^L(o)$ in raising the temperature from T_i to TK isobarically at 1 bar, $\Delta\varepsilon^L(o)]_T$ is the change in $\varepsilon^L(o)$ in raising the pressure isothermally at a temperature T so as to restore the volume of the crystal to that which it has at T_iK and 1 bar pressure, and $\Delta\varepsilon^L_T(o)]_V$ is the change in $\varepsilon^L(o)$ on raising the temperature T_i to TK isobarically at the crystal volume at T_iK and 1 bar pressure. The equations show that suitable measurements of the temperature and pressure dependence of $\varepsilon^L(o)$, therefore, will lead to assessments of the soft mode self-energy components.

Figures 15 and 16 show the results of such measurements for the temperature dependence of the soft mode self-energy components for $KTaO_3$ and $SrTiO_3$. An estimate of $\omega^h(o,t)^2$ can be made from this data. At sufficiently high temperatures, if the thermal population factors contained in the theoretical

expression for $\Delta^A(o,t,o)$ are expanded in terms of $\hbar\omega/kT < 1$, it is found that the leading terms in both the cubic and quartic contributions to $\Delta^A(o,t,o)$ are linear in T. The temperature dependence of the function A(T) is shown in figures 15 and 16 and does appear to be reasonably linear with temperature thereby implying a linear dependence of $\Delta^A(o,t,o)$ on T. An extrapolation of this linear part back to T = o should therefore yield an interept of approximately $\omega^h(o,t)^2/\omega_{T_i}(o,t)^2$. Using measured low-temperature values of $\omega_{T_i}(o,t)^2$ of $\omega_o(o,t)^2 = 0.35 \times 10^{24}$ H_2 for $KTaO_3$ and $\omega_{100}(o,t)^2 = 1.79 \times 10^{24}$ H_2 for $SrTiO_3$ yields values of $\omega^h(o,t)^2 = -0.004 \times 10^{24}$ H_2 for $KTaO_3$ and $\omega^h(o,t)^2 = -1.43 \times 10^{24}$ for $SrTiO_3$.

Our results imply, therefore, that the soft mode harmonic frequency in $SrTiO_3$, and probably in $KTaO_3$, is imaginary and, furthermore, is stabilized by the large anharmonic self-energy components $2\omega^h(o,t)\Delta^A(o,t,o)$ which dominate all the self-energy contributions combined.

C. Experimental Results for $\Delta^A(o,t,\Omega)$ and $\Gamma(o,t,\Omega)$

Following the theoretical and experimental analyses presented in section II, we have also determined the frequency dependence of the self-energy terms $2\omega^h(o,t)\Delta^A(o,t,\Omega)$ and $2\omega^h(o,t)\Gamma(o,t,\Omega)$ via Dispersive Fourier Transform Spectroscopy. The frequency dependence of the self-energies determined in this way are shown for $KTaO_3$ in figures 17 and 18. The results reveal again that these soft mode self-energies are extremely large compared to those found in weakly anharmonic systems. In addition, these self-energies have a strong temperature dependence throughout the frequency range covered. It is of interest also to note that the determinations of $2\omega^h(o,t)\Delta^A(o,t,\Omega)$ at Ω = o determined from the static dielectric constant measurements discussed in part B of this section are closely consistent with the values determined via the DFTS measurements.

IV. HYDROGEN BONDED FERROELECTRICS

A. Introduction

Recent discussions of the transition in hydrogen-bonded ferroelectric systems have examined the consequences of interactions between the ferroelectric mode and fluctuations in the phonon density. Coombs and Cowley[3] have used a weakly anharmonic theory, within the framework of the Landau theory of phase transitions, to consider the coupling of the ferroelectric mode to fluctuations in the acoustic phonon density, and they find a response function for the ferroelectric mode of

$$G_i(\omega) = \frac{2\omega_i}{\bar{\omega}_i^2 - i\omega\gamma_i - \omega^2 - [\Sigma\, L_i/(1 - i\omega\bar{\tau})]} \quad . \tag{41}$$

Here ω_i is the harmonic ferroelectric mode wavenumber, $\bar{\omega}_i$ the renormalized ferroelectric mode wavenumber containing conventional anharmonic self-energy contributions, γ_i the mode damping, $\bar{\tau}$ an average lifetime for the acoustic phonon density and L_i is given by

$$L_i = \frac{72\omega_i}{kT\hbar}\left|V(0,1,-1)\right|^2 n_i(n_i + 1) \tag{42}$$

where the V coefficients are second-order cubic anharmonic coupling coefficients and the n_i are thermal population factors. Young and Elliott[4] have extended the pseudospin model of Kobayashi[41] to include coupling between the soft pseudospin mode and fluctuations in the phonon density via two-phonon terms in the Hamiltonian, and they find a response function for the ferroelectric mode of

$$G_i(\omega) = \frac{4\Gamma\langle\sigma^x\rangle}{h^2(\bar{\omega}_i^2 - i\omega\gamma_i - \omega^2) - [4\Gamma\langle\sigma^x\rangle\bar{L}/(1 - i\omega\bar{\tau})]} \quad . \tag{43}$$

Here Γ is the energy of the pseudospin mode, $\langle\sigma^x\rangle$ the thermal average of the spin operator and $\bar{L}$ is given by

$$\bar{L} = \frac{1}{2N} \sum_{1,2} |V(0,1,-1)|^2 \frac{2n_i(n_i + 1)}{kT} \quad . \tag{44}$$

The responses from these two different theoretical approaches are structurally identical, but differ from the characteristic response of normal phonons by the addition of a relaxing self-energy contribution. This has two important consequences: it predicts the existence of a quasi-elastic central component and the divergence of the ferroelectric mode susceptibility at a temperature, T_A, below the characteristic clamped Curie-Weiss temperature.

Attempts to determine the magnitude of the relaxing self-energy have been made for a number of hydrogen-bonded ferroelectrics via experiments to measure T_A and via searches for the central component. The former suffer from the fact that the ferroelectric mode wavenumber is determined from extrapolations of data which are deduced from fits to a simplified, and possibly ambiguous, model involving the coupling of the ferroelectric mode to other phonons.[42-44] Such experiments generally have led to the conclusion that, if present, the relaxing self-energy is quite small, but the inaccuracy of the method often precludes a definitive statement as to whether the relaxing self-energy is finite or not. Although Lagakos and Cummins[44] have reported on a preliminary observation of a central component in KH_2PO_4 (KDP) which also suggests that the relaxing self-energy is quite small, the same authors[45] have found no evidence for a central component in CsH_2AsO_4 (CsDA).

The possibility of a separate determination of the magnitude of the relaxing self-energy has been pointed out by Young and Elliott.[4] They have commented that the inclusion of spin-two-phonon coupling in their Hamiltonian also causes a splitting of the E-modes in the ferroelectric phase where the corresponding singly degenerate modes have symmetries of B_1, B_2. This splitting will be in addition to any reststrahlen splitting, and may be distinguished from it because their combined effect is dependent on the propagation direction of the phonon. They predict the splitting to be given by

$$\omega_A^2 - \omega_B^2 = S^2 \qquad \text{for } \underset{\sim}{k} \text{ along } (0,0,1) \tag{45}$$

$$\omega_A^2 - \omega_B^2 = S^2 + R^2 \qquad \text{for } \underset{\sim}{k} \text{ along } (1,1,0) \tag{46}$$

$$\omega_A^2 - \omega_B^2 = (S^4 + R^4)^{\frac{1}{2}} \qquad \text{for } \underset{\sim}{k} \text{ along } (1,0,0) \tag{47}$$

where S^2 is the relaxing self-energy splitting,

$$S^2 = \frac{4\omega_T\langle\sigma^2\rangle V(0,1,2)}{\hbar} \quad , \tag{48}$$

and R^2 is the reststrahlen splitting,

$$R^2 = \omega_L^2 - \omega_T^2 \tag{49}$$

where ω_L and ω_T are the zone-centre longitudinal and transverse optic wavenumbers, respectively.

Suitable experimental measurements of any E-mode splitting, therefore, can lead to separate estimates of the magnitude of the relaxing self-energy. Such measurements can also lead to important information concerning the central component because the anharmonic coupling coefficients that determine the magnitude of the E-mode splitting are also related to the behavior of the amplitude and wavenumber of the central component.

The following sections describe laser-Raman investigations by this group[46] of such E-mode splitting in hydrogen-bonded ferroelectrics, the results of which suggest that the relaxational processes responsible for the central components have sufficiently long lifetimes as to make their observation feasible through electronic, rather than optical, techniques. The final sections describe such a search via radio-frequency dielectric constant measurements.

B. E-Mode Splitting Investigations

Figure 19 shows schematically the laser-Raman scattering geometries used to study the E-mode splitting.

Figure 20 shows in detail the low low-frequency B_1, B_2 spectra recorded in the ferroelectric phase of KDP, KDA and KD*A for the three scattering geometries consistent with equations (45)-(47), and figure 21 shows the full B_1, B_2 spectra for RbDA and RbD*A for two of the scattering geometries. As these figures show, many, but not all, of the E-modes do show definitive splittings arising from non-reststrahlen effects. For reasons we have described elsewhere,[46] these splittings cannot arise from either strain or birefrigence artifacts, and hence we believe the splittings to originate from the relaxing self-energy.

The response function given in equation (43) leads to the conclusion that the ferroelectric mode will condense out at a temperature T_A such that $T_A < T_c^x$, where T_c^x is the clamped Curie temperature. A measure of the relative strength of the relaxing self-energy to the mode total self-energy is given by α, where

$$\alpha = \frac{T_c^x - T_A}{T_c^x} \quad . \tag{50}$$

This response function also leads to a Debye relaxation form for the central component of

$$\frac{\text{Im } G(\omega)}{G(0)} = \frac{4\Gamma\langle\sigma^x\rangle\bar{L}}{\hbar^{2-2}\omega} \frac{\omega\tau^*}{1 + \omega^2\tau^{*2}} \tag{51}$$

where

$$\tau^* = \frac{\hbar^{2-2}\omega^{2-2}\tau}{\hbar^{2-2}\omega^{2-2} - 4\Gamma\langle\sigma^x\rangle\bar{L}} = \frac{1}{\omega_c}$$

and ω_c is the central component wavenumber. In the high-temperature limit, equation (51) leads to the conclusion that ω_c will have a temperature dependence given by

$$\omega_c = \frac{(1 - \alpha)(T - T_c^x)}{[T - T_c^x(1 - \alpha)]} \frac{1}{\tau} \tag{52}$$

whilst the amplitude of the central component will be given by

$$\text{Im } G(\omega_c) = A \frac{\alpha(1 + \epsilon)}{\epsilon(1 - \alpha)(\alpha + \epsilon)} \tag{53}$$

where $A = 1/kT_c^x$ and ϵ is given by

$$\epsilon = \frac{T - T_c^x}{T_c^x} \quad . \tag{54}$$

Analogous results to those given in equations (52) and (53) can also be obtained from the response function given by Coombs and Cowley[3] for the ferroelectric mode. However, it is to be noted that, although the two theories both require the ferroelectric mode to condense out below T_c^x, the

temperature at which this occurs is not necessarily the same because of the different temperature dependence predicted for the ferroelectric mode by the two theories.

The lack of information on $\bar{\tau}$ prevents any utilization of equation (52) to assess the specific temperature dependence of ω_c. However, estimates of the temperature dependence of the central component amplitude can be made via equation (53) providing measurements of T_c^x and α are available.

T_c^x is readily determined with good precision via suitable dielectric or elastic constant measurements. α is given by equation (50) and as[4]

$$\alpha = \sum_1 \left(\frac{V(0,1,-1)}{h\omega_1}\right)^2 \tag{55a}$$

$$\alpha = \sum_1 \left(\frac{\delta\omega_1}{2\omega_1}\right)^2 \tag{55b}$$

where $\delta\omega_1$ is a mode splitting from the spin-two-phonon interactions for k along (0,0,1) as given in equation (45). Although α can be determined via equation (50), as mentioned earlier, such calculations are not reliable because of the inaccuracies in determining T_A. The fundamental difficulty with equations (55a) and (55b) is that they cannot be applied to those modes which are not doubly degenerate in the paraelectric phase and for which splittings may thus not be observed. This requires, ultimately, that α be estimated using equations (45)-(47) and (35) and a means of attributing values to V(0,1,-1) for those modes where measurement is not possible. Table 12 lists values of α calculated in a number of different ways. α_E is determined using only the measured E-mode splittings in equation (55b). α_E^S is determined via equations (48) and (55a), by using the most consistent

values of S^2 determined from equations (46)-(47). It is to be noted that there is little difference between α_E and α_E^S, and this reflects the close fits of the experimental data to the form of equations (45)-(47). $\langle\alpha\rangle$ and $\langle\alpha\rangle_m$ are calculated on the assumption that all 48 phonon branches contribute equally to α; $\langle\alpha\rangle$ uses the observed splittings averaged over all 13 allowable E-modes, whilst $\langle\alpha\rangle_m$ uses the splittings averaged over only the observed split modes.

Table 12 also contains estimates of α determined via equation (50) using data determined from studies of the temperature dependence of the ferroelectric mode. Using measured values of T_c^x (from Brody and Cummins[47] for KDP and from Spillman and Lowndes[48] for the arsenate family), α_a and α_p were then calculated using appropriate values of T_A determined by fitting the measured temperature dependence of the ferroelectric mode of these materials (Lowndes et al.,[43] J. F. Ryan 1972 (unpublished) quoted by Lagakos and Cummins[44]) to the temperature dependence predicted by the theories of Coombs and Cowley[3] and Young and Elliott[4], respectively.

Inspection of Table 12 reveals a number of differences between the two basic approaches to determining estimates of α. Firstly, the α values determined from the E-mode splittings are consistently smaller than the values determined from studies of the temperature dependence of the ferroelectric mode. Secondly, for a given anion, the α values determined from the E-mode splittings increase with increasing mass of the cation, whereas the reverse is true for α_a and α_p. Thirdly, the α values determined from the E-mode splittings are always positive, whereas α_a and α_p are negative for the deuterated arsenates. As mentioned earlier, T_A is difficult to determine precisely, and this is especially true for the deuterated arsenates where two

or more low-frequency optical phonons are coupled to the ferroelectric mode,[43] thus casting doubt on the adequacy of the two coupled oscillator fit used to determine the ferroelectric mode spectra characteristics from the Raman spectra; we believe this is the reason for $T_A > T_c^x$ and hence for the negative values determined for α_a and α_p for the deuterated arsenates.

Because of these and other difficulties in precisely determining the temperature T_A at which the ferroelectric mode condenses out, and because T_A and T_c^x are apparently very close for the materials considered here, we believe that the α_a and α_p values provide less reliable estimates of α than those determined from the E-mode splittings. Although these latter do not lead directly to an estimate of the total contributions to α, they do provide a basis for establishing a range of possible values for α. For instance, α_E provides a reasonably precise lower bound on α since actual observed contributions are included in its calculation, whilst $\langle\alpha\rangle_m$ provides a reasonable, but less distinctive, upper limit on α.

Figure 22 shows the results of calculating the temperature dependence of the central component amplitude for the hydrogenated materials using α_E, $\langle\alpha\rangle$ and $\langle\alpha\rangle_m$ for α in equation (53). Figure 23 shows the results of similar calculations for the deuterated arsenates. Although the quantitative details vary somewhat depending on the particular value of α used, the qualitative trends are very similar irrespective of the α value used. The central feature of importance to emerge from these figures is that, although the central component amplitude grows strongly as T_c^x is approached, in all cases this growth is curtailed by the onset of the ferroelectric transition. The data indicate that, at the characteristic transition temperature, the largest growth in the central component amplitude occurs for KDP and the smallest for

CsDA. This may be an important contributing factor in explaining why Lagakos and Cummins[44,45] were able to find evidence for a central component in KDP but not in CsDA. In commencing on their failure to find a central component in CsDA, Lagakos and Cummins[45] have derived two upper limits for α: firstly, a value of 10^{-4} for an unresolvably narrow central component, and, secondly, a value of 10^{-2} for a central component linewidth exceeding the free spectral range of their Fabry-Perot interferometer. The values of α determined here from the E-mode splittings are nicely bracketed by these limits, but tend to support the larger value.

C. Radiofrequency Dielectric Constant Investigations

a) Experimental Studies

The light scattering measurements of the E-mode splittings in hydrogen-bonded ferroelectrics described in the preceding section suggest that a central component may exist in these materials but at frequencies which may be too small to be resolved by optical measurements. Recent acoustic alternation,[49] electron spin resonance[50] and electron paramagnetic resonance[51] work also suggest that such relaxational processes do occur but with lifetimes sufficiently long as to make their observation feasible through electronic, rather than optical, techniques. We have therefore searched for the existence of central components via radiofrequency dielectric constant measurements.

In the paraelectric phase of KDP, the dielectric response measured in the 5-80 MHz range exhibits no frequency dependence which would be characteristic of a relaxation process and generally displays a temperature dependence commensurate with measurements at lower frequencies. Within the

sensitivity of our experiments, therefore, no significant evidence was found for any contribution to the dielectric response in this frequency range which arises from the existence of a central component.

However, as we have reported,[52] the response for CsDA in the paraelectric phase does exhibit a marked frequency-dependent dielectric loss, especially at the higher frequencies, for temperatures just above the transition. Unfortunately, the characteristic frequency of the mechanism associated with the dielectric loss appears to be above the 80 MHz upper limit of our applied field frequency using this measuring technique. Although ϵ' shows a continuous decrease with increasing temperature from the transition at 149 X 5K, ϵ'', especially at the higher frequencies, first grows rapidly as the temperature is raised from the transition and then decreases with a further increase in temperature until it is barely measurable at about 170K.

It is difficult to comment on the origins of the mechanism causing this dielectric loss in the absence of a full scan of its frequency dependence. The results are unlikely to stem from impurities or defects in the sample which typically lead to relaxation times several orders of magnitude longer than those that could be involved here. Rather, the results are more likely to be intrinsically related to the onset of the transition, in view of the growth of this dielectric loss as the transition temperature is approached. Although the results could be interpreted as being consistent with the findings of Lagakos and Cummins (in the sense that if the central peak for KDP lies at a higher frequency than that for CsDA then the optical measurements would be more favorable for studying the central peak in KDP and the dielectric measurements for studying it in CsDA), the present data for

CsDA would not seem to be described by a simple Debye relaxation form with an amplitude growing continuously as the clamped Curie temperature at 126 K is approached, as is suggested by the current theories.

The results for the ferroelectric phase of both materials also reveal some significant dielectric behaviour which has not previously been reported. For both materials, the dielectric response exhibits a pronounced dependence on frequency which is well described by a Debye form of relaxation:

$$\varepsilon(\omega) = \varepsilon'(\omega) + i\varepsilon''(\omega) = \varepsilon(\infty) + \frac{A}{1 + i\omega\tau} \qquad (56)$$

where $\varepsilon(\omega)$ is the complex dielectric response at a frequency ω, $\varepsilon(\infty)$ is the complex dielectric response at $\omega \gg 100$ MHz, A is the amplitude and τ the characteristic relaxation time. Data at representative temperatures, together with their associated fits to the form of equation (56), are shown in figures 24 and 25. Table 13 summarizes values of the parameters characterizing the Debye relaxation process for both materials. Although the dielectric relaxation occurs at somewhat lower frequencies for KDP than for CsDA, the relaxation data for the two materials are qualitatively similar with the τ decreasing dramatically with increasing temperature in the range $T \simeq 0.8\ T_{tr}$ to $T \simeq T_{tr}$ where T_{tr} is the transition temperature. The amplitude also increases substantially over much of this same temperature range but appears to level off close to the transition temperature for KDP and to actually go through a maximum about 5 K below the transition temperature for CsDA. Two further aspects of these parameters should be noted. Firstly, $\varepsilon(\infty)$ has a real part whose temperature depencence is weakly suggestive of divergent behaviour but which is not described by a Curie-Weiss behaviour, and an imaginary part which suggests a source of high-frequency conductivity which is independent of the relaxation process. Secondly,

values of τ are well fitted by the thermal activation form

$$\tau = \tau_o \exp(E/kT)$$

with $\tau_o = 4.114 \times 10^{-10}$s and E = 0.0466 eV for KDP, and $\tau_o = 1.586 \times 10^{-10}$s and E = 0.0603 eV for CsDA.

b) Theoretical Discussion

Almost simultaneously with our observation of the central component in the power spectrum of homogeneous polarization fluctuations in the ferroelectric phase of KDP and CsDA discussed above, Memelstein and Cummins[53] reported on a central component observed in the power spectrum of polarisability fluctuations in the ferroelectric phase of KDP.

Our subsequent analysis of the results for KDP (and by implication for CsDA, etc.) suggests that both effects may be attributed to a homogeneous exponential decay of the polarization. In our dielectric experiments, the response of the polarization due to an applied electric field,

$$\chi(\omega) = (\delta P/\delta E)_{\omega + i0^+} , \tag{57}$$

was directly measured in the ordered phase of KH_2PO_4. In equation (44), δP and δE are in the direction of the spontaneous polarization. As reported, the complex dielectric constant was well fitted by the simple form

$$\chi(\omega) \simeq \left(\frac{\chi_T}{1 - i\omega\tau}\right) , \qquad (T < T_c) \tag{58a}$$

in the $(\omega) \sim 10^7$ Hz range. The fluctuation-dissipation theorem for polarization fluctuations

$$\langle|\Delta P_{Q\omega}|^2 = \frac{k_B T}{\pi} \frac{I_m \chi(Q,\omega)}{\omega} \tag{58b}$$

may therefore be rewritten as a Lorentzian central component,

$$\lim_{Q\to 0} \langle|\Delta P_{Q\omega}|^2 \simeq (k_B T \chi_T/\pi)[\tau/(1 + (\omega\tau)^2)], \quad (T < T_c). \tag{59}$$

The light-scatterin rate in the low-frequency regime, $\omega \ll (k_B T/\hbar)$, is well known to obey

$$\left(\frac{d^2 h(i \to f)}{d\Omega_f d\omega_f}\right) = \left(\frac{\omega_f^3 \omega_i}{c^4}\right) \langle |\Delta\chi_{Q\omega}^{fi}|^2 \rangle , \tag{60}$$

where $\omega_i = c|k_i|$, $\omega_f = c|k_f|$, and ε_i, ε_f represent the frequencies and polarizations, respectively, of the initial (i) and final (f) states.

$$\underset{\sim}{Q} = \underset{\sim}{k}_i - \underset{\sim}{k}_f, \quad \omega = \omega_i - \omega_f, \tag{61}$$

the polarization matrix elements of the fluctuating polarisability are

$$\Delta\chi_{\underset{\sim}{Q}\omega}^{fi} = \underset{\sim}{\varepsilon}_f^* \; X \; \Delta\underset{\sim}{\chi}_{\underset{\sim}{Q}\omega} \; X \; \underset{\sim}{\varepsilon}_i, \tag{62}$$

and c is the speed of light in the ferroelectric medium. Since we wish to establish the extent to which the experimental result in equation (59) will be observed by measuring the effect given by equation (60), we need to consider the total light scattering into a given solid angle

$$\frac{dh(i \to f)}{d_f} = \left(\frac{\omega_i}{c}\right)^4 \langle |\Delta\chi_{\underset{\sim}{Q}}^{fi}{}^2 \rangle . \tag{63}$$

With F as the free energy per unit volume we have

$$dF = -SdT + \underset{\sim}{E} \cdot d\underset{\sim}{P} + \sum_j X_j dx_j, \tag{64}$$

where X_j and x_j are the stress and strain components. A complete assessment of the conributions to light scattering arising from thermal fluctuations will require the following thermal response functions to be considered:

$$C_{\underset{\sim}{P},x} = T(\partial S/\partial T)_{\underset{\sim}{P},x} , \tag{65a}$$

$$\chi_T = (\partial \underset{\sim}{P}/\partial \underset{\sim}{E})_{T,X}, \tag{65b}$$

$$\underset{\sim}{\alpha}_j = (\partial P/\partial X_j)_{T,E,X} = (\partial x_j/\partial E)_{T,E,X}. \tag{65c}$$

and

$$\lambda_{jk} = (\partial x_j/\partial X_k)_{T,E,X} = (\partial x_k/\partial X_j)_{T,E,X}. \tag{65d}$$

The following are valid as $\underset{\sim}{Q} \to 0$:

$$\langle |\Delta T_{\underset{\sim}{Q}}|^2 \rangle = (k_B T^2 / C_{\underset{\sim}{P},x}), \tag{66a}$$

$$\langle \Delta T^*_{\underset{\sim}{Q}} \Delta P_{\underset{\sim}{Q}} \rangle = 0, \tag{66b}$$

$$\langle \Delta T^*_{\underset{\sim}{Q}} \Delta x_j \rangle = 0, \tag{66c}$$

$$\langle \Delta P^*_{\underset{\sim}{Q}} \Delta P_{\underset{\sim}{Q}} \rangle = k_B T \underset{\sim}{\chi}_T , \tag{66d}$$

$$\langle \Delta P^*_{\underset{\sim}{Q}} \Delta x_{jQ} \rangle = k_B T \underset{\sim}{\alpha}_j , \tag{66e}$$

$$\langle \Delta x^*_{jQ} \Delta x_{kQ} \rangle = k_B T \lambda_{jk} . \tag{66f}$$

Equations (66) represent a complete list of thermal fluctuations which can contribute to light scattering.

Expanding χ^{fi} in the local thermal parameters $T, \underset{\sim}{P}$ and strains $\{x_j\}$, we get

$$d\chi^{fi} = \Gamma^{fi}_T dT + \underset{\sim}{\Gamma}^{fi}_{\underset{\sim}{P}} \cdot d\underset{\sim}{P} + \sum_j \Gamma^{fi}_j dx_j \tag{67}$$

which defines the Γ coefficients. The full static form factor from equations (66) and (67) is therefore

$$\begin{aligned} \lim_{\underset{\sim}{Q} \to 0} \langle |\Delta \chi^{fi}_{\underset{\sim}{Q}}|^2 \rangle = {} & |\Gamma^{fi}_T|^2 (k_B T^2 / C_{\underset{\sim}{P},x}) + (\underset{\sim}{\Gamma}^{fi}_{\underset{\sim}{P}})^* \cdot (k_B T \underset{\sim}{\chi}_T) \cdot (\underset{\sim}{\Gamma}^{fi}_{\underset{\sim}{P}}) \\ & + \sum_{jk} (\Gamma^{fi}_j)^* (k_B T \lambda_{jk}) (\Gamma^{fi}_k) + \sum_j [(\underset{\sim}{\Gamma}^{fi}_{\underset{\sim}{P}} \Gamma^{fi}_j) \\ & + (\underset{\sim}{\Gamma}^{fi}_{\underset{\sim}{P}} \Gamma^{fi}_j)^*] \cdot k_B T \underset{\sim}{\alpha}_j \end{aligned} \tag{68}$$

which may be substituted in equation (63) to give the total light-scattering cross-section. To generalize the result to frequency power spectra via the transformation

$$\langle |\chi^{fi}_{\underset{\sim}{Q}}|^2 \rangle \to \langle |\chi^{fi}_{\underset{\sim}{Q}\omega}|^2 \rangle , \tag{69}$$

one must replace the fluctuation matrix (equations 66)

$$\lim_{\underset{\sim}{Q} \to 0} \langle \Delta Y^*_{j\underset{\sim}{Q}} \Delta Y_{k\underset{\sim}{Q}} \rangle = k_B T R^T_{jk}, \tag{70}$$

by dynamic fluctuations

$$\langle \Delta Y^{*}_{j\underset{\sim}{Q}\omega} \Delta Y_{k\underset{\sim}{Q}\omega} = \frac{k_B T}{2\pi i\omega} [R_{jk}(\underset{\sim}{Q},\omega) - R^{*}_{kj}(\underset{\sim}{Q},\omega)] \tag{71}$$

leaving the Γ coefficients in equation (68) unchanged. The dynamical equivalent of equations (65) must then be obtained:

$$C(\underset{\sim}{Q},\omega) = T(\delta S/\delta T)_{\underset{\sim}{Q},\omega + i0^{+}} , \tag{72a}$$

$$\underset{\sim}{\chi}(\underset{\sim}{Q},\omega) = (\delta \underset{\sim}{P}/\delta \underset{\sim}{E})_{\underset{\sim}{Q},\omega + i0^{+}} , \tag{72b}$$

$$\underset{\sim}{\alpha}_j(\underset{\sim}{Q},\omega) = (\delta x_j/\delta E)_{\underset{\sim}{Q},\omega + i0^{+}} , \tag{72c}$$

$$\lambda_{jk}(\underset{\sim}{Q},\omega) = (\delta x_j/\delta X_k)_{\underset{\sim}{Q},\omega + i0^{+}} , \tag{72d}$$

Since the derivation of the ten linearised equations required to evaluate equations (72) is not necessary here, we will limit our evaluation of the contributions to equation (68) to an estimation employing only thermodynamic considerations.

Mermelstein and Cummins[53] attribute the central component observed in their measurements to a thermal diffusion mode. If one takes only the first term in our equation (68), their equation (11) is the result. Hence they effectively write

$$\left(\frac{d^2 n}{d\Omega_f d\omega_f}\right) \text{(central component)} \simeq (\omega_f^3 \omega_i / c^4) |\Gamma_T^{fi}|^2 \cdot (k_B T^2/\pi\omega) \mathrm{IM}[1/C(\underset{\sim}{Q},\omega)], \tag{73}$$

with a dynamic heat capacity of the thermal diffusive form

$$[C_{Px}/C(\underset{\sim}{Q},\omega)] \simeq [iD_T \underset{\sim}{Q}^2/(\omega + iD_T \underset{\sim}{Q}^2)]. \tag{74}$$

Here, $D_T = K/C_{Px}$ is the thermal diffusivity, and K is the heat conductivity. This yields a Lorenztian central component of width

$$1/\tau_{\underset{\sim}{Q}} = D_T Q^2 . \tag{75}$$

If the central component stems from the second term of equation (68) we may write

$$\frac{d^2h}{d\Omega_f d\omega_f}(\text{central component}) = \left(\frac{\omega_f^3\omega_i}{c^4}\right)\left(\frac{k_B T}{\pi\omega}\right)\mathrm{Im}[(\underset{\sim}{\Gamma}_{\underset{\sim}{P}}^{fi})^* \cdot \underset{\sim}{\chi}(Q,\omega) \cdot (\underset{\sim}{\Gamma}_{\underset{\sim}{P}}^{fi})], \qquad (76)$$

$$= \left(\frac{\omega_f^3\omega_i}{c^4}\right)\langle|\underset{\sim}{\Gamma}^{fi} \cdot \Delta\underset{\sim}{P}_{Q\omega}|^2\rangle . \qquad (77)$$

From equations (59) and (77) one would then expect a Lorentzian central component with a Q independent width of $1/\tau$. This would allow the observations of both experiments to be described by the same microscopic physical process which, however, cannot be unambiguously identified at this time.

First let us consider the width of the central component. The light-scattering width agrees with both $D_T Q^2$ and the dielectrically-measured width (which is obviously a $Q \simeq 0$ homogeneous mode). One has two possibilities: (i) The light-scattering central component arises from a thermal diffusion mode with a width given by equation (75), while the polarisation central component arises from some other mechanism. The similarity of the two line-widths would then be purely coincidental. (ii) Both central components have the same physical source. Then the agreement with equation (75) is purely coincidental. This dichotomy could be resolved experimentally, of course, by changing Q in the light-scattering work and observing whether or not the width appreciably changes.

Secondly, let us consider the relative intensities of the scattered light given by the first and second terms in equations (77). These are

$$h(\text{thermal diffusion}) \propto \left(\frac{T}{\underset{\sim}{C}_{Px}}\right)\left|\underset{\sim}{\varepsilon}_f^* \cdot \frac{\partial \underset{\sim}{\chi}_T}{\partial T} \cdot \underset{\sim}{\varepsilon}_i\right|^2 . \qquad (78)$$

$$h(\text{polarisation}) \propto \frac{\partial}{\partial \underset{\sim}{P}}(\underset{\sim}{\varepsilon}_f^* \cdot \underset{\sim}{\chi}_T \cdot \underset{\sim}{\varepsilon}_i)^* \cdot \frac{\partial}{\partial \underset{\sim}{P}}(\underset{\sim}{\varepsilon}_f^* \cdot \underset{\sim}{\chi}_T \cdot \underset{\sim}{\varepsilon}_i). \qquad (79)$$

An analysis of equation (78) has been carried out by Mermelstein and

Cummins[53]. An equivalent analysis of equation (79) is much more difficult in that $(\partial/\partial P)\underline{\chi}_T$ is a third-order tensor which has not (to our knowledge) been directly measured. The depolarization effects will be substantial and not qualitatively different from equation (77). For an estimate of absolute size we take the Landau approach and expand the free energy in powers of P,

$$F(P,T) = \sum_{n=1}^{\infty} a_n(T)P^{2n} \tag{80}$$

stopping at n = 2 for second-order and n = 3 for first-order phase transitions. The $a_n(T)$ which change sign at $T = T_c$ are well known[54]. The coefficients are fit to E = 0 and $(\partial\underline{\chi}_T/\partial P)$ is estimated via equations (64) and (80). Although this procedure is only a rough approximation, it allows an order-of-magnitude comparison between the light-scattering intensities given by terms 1 and 2 of equation (68)

$$\frac{h(\textit{thermal diffusion})}{H(\text{polarization})} \propto \frac{\chi_T^2}{\chi_T^3} \sim 10^{-2} \text{ to } 10^{-1} . \tag{81}$$

This suggests that the homogeneous polarization effects would dominate those of a thermal diffusion mode if it were present, and hence supports our view that the central components observed by the two techniques have the same origin.

REFERENCES

1. A.A. Maradudin and A.E. Fein, Phys. Rev. 128, 2589 (1962).
2. R.A. Cowley, Adv. in Phys. 12, 421 (1963).
3. C.J. Coombs and R.A. Cowley, J. Phys. C6, 121, 143 (1973).
4. A.P. Young and R.J. Elliot, J. Phys. C7, 2721 (1974).
5. G. Leibfried and W. Ludwig, Sol. State Phys. 12 (1961).
6. B. Szigeti, Proc. Roy. Soc. Lond. A252, 217 (1959).
7. B. Szigeti, Proc. Roy. Soc. Lond. A258, 377 (1960).
8. H. Bilz, in Phonons in Perfect Lattices and in Lattices with Point Imperfections (Oliver and Boyd, Edinborough 1966), p. 208.
9. R.F. Wallis, I.P. Ipatova and A.A. Maradudin, Sov. Phys. Sol. State 8, 850 (1966).
10. I.P. Ipatova, A.A. Maradudin and R.F. Wallis, Phys. Rev. 155 882 (1967).
11. K.W. Johnson and E.E. Bell, Phys. Rev. 187, 1044 (1969).
12. E.R. Cowley, J. Phys. C5, 1345 (1972).
13. A. Rastogi, J.P. Hawranek and R.P. Lowndes, Phys. Rev. B9, 1938 (1974).
14. R.P. Lowndes and A. Rastogi, Phys. Rev. 14, 3598 (1976).
15. A.M. Karo and J.R. Hardy, Phys. Rev. 181, 1272 (1969).
16. U. Schroder, Sol. State Comm. 4, 347 (1966).
17. R.P. Lowndes and D.H. Martin, Proc. Roy. Soc. Lond. A354, 351 (1970).
18. R.P. Lowndes, Phys. Rev. B6, 1490 (1972).
19. J. Chamberlain, J.E. Gibbs and H.A. Gebbie, Nature 198, 874 (1963).
20. E.E. Bell, Infrared Physics 6, 57 (1966).
21. A. Rastogi, K.F. Pai, N.E. Tornberg, T.J. Parker and R.P. Lowndes, Phys. Lett 62A, 239 (1977).
22. H. Bilz, L. Genzel and H. Happ, Z. fur Phys. 160, 535 (1960).
23. R.P. Lowndes and D.H. Martin, Proc. Roy. Soc. Lond. A308, 473 (1969).

24. M. Born and K. Huang, in Dynamical Theory of Crystal Lattices (Oxford UP, 1954), p. 124.

25. C.E. Weir, E.R. Lippincott, A. van Valkenburg and E.N. Bunting, J. Res. Nat. Bur. Standards, A63, 55 (1959).

26. R.P. Lowndes in Proc. 4th Int. Conf. on High Pressure (Physico-Chemical Society, Kyoto, 1974), p. 805.

27. R.P. Lowndes, Phys. Rev. B6, 969 (1953).

28. T.S. Robinson and W.C. Price, Proc. Phys. Soc. B66, 969 (1953).

29. T.J. Parker, W.G. Chambers and J.F. Angiers, Infrared Phys. 14, 207, (1974).

30. T.J. Parker and W.G. Chambers, IEEE Trans. MTT-22, 1032 (1974).

31. T.J. Parker and W.G. Chambers, Infrared Phys. 16, 349 (1976).

32. J. Chamberlain, J.E. Gibbs, and H.A. Gebbie, Infrared Phys. 9 185 (1969).

33. E.E. Russell and E.E. Bell, Infrared Phys. 6, 75 (1966).

34. J.I. Berg and E.E. Bell, Phys. Rev. B4, 3572 (1971).

35. K.F. Pai, A. Rastogi, N.E. Tornberg, T.J. Parker and R.P. Lowndes, Proc. 2nd Int. Conf. on Submillimeter Waves in J.O.S.A. 67, 914 (1977).

36. A. Rastogi, K.F. Pai, T.J. Parker and R.P. Lowndes Proc. Int. Conf. on Lattice Dynamics (Flammarion: Paris, 1978), p. 142.

37. W. Cochran, Adv. in Phys. 9, 387 (1960).

38. P.W. Anderson, Fiz. Dielectrik (Akad. Nauk. SSR) (1970).

39. R.A. Cowley, Phil. Mag. 11, 673 (1965).

40. R.P. Lowndes and A. Rastogi, J. Phys. C6, 932 (1973).

41. K. Kobayashi, J. Phys. Soc. Japan 24, 497 (1968).

42. R.S. katiyar, J.F. Ryan and J.F. Scott, in Proc. Int. Conf. on Light Scattering in Solids (Flammarion, Paris 1971) p436.

43. R.P. Lowndes, N.E. Tornberg and R.C. Leung, Phys. Rev. B10, 911 (1974).

44. N. Lagakos and H.Z. Cummins, Phys. Rev. B10 1063 (1974).

45. N. Lagakos and H.Z. Cummins, Phys. Rev. Lett. 34, 883 (1975).

46. R.C. Leung, N.E. Tornberg and R.P. Lowndes, J. Phys. C9, 4477 (1976).

47. E.M. Brody and H.Z. Cummins, Phys. Rev. Lett. 21, 1263 (1968).

48. W.B. Spillman and R.P. Lowndes (to be published)

49. E.M. Alexander and R.W. Gammon, Feroelectrics.

50. K. Hukuda J. Phys. Soc. Japan 38 150 (1975).

51. K.A. Muller, N.S. Dalal and W. Berlinger, Phys. Rev. Lett. 36, 1504 (1976).

52. N.E. Tornberg and R.P. Lowndes, J. Phys. C10, L549 (1977).

53. M.D. Mermelstein and H.Z. Cummins, Phys. Rev. B16, 2177 (1977).

54. A. Widom, N. E. Tornberg and R. P. Lowndes, J. Phys. C11, L433 (1978).

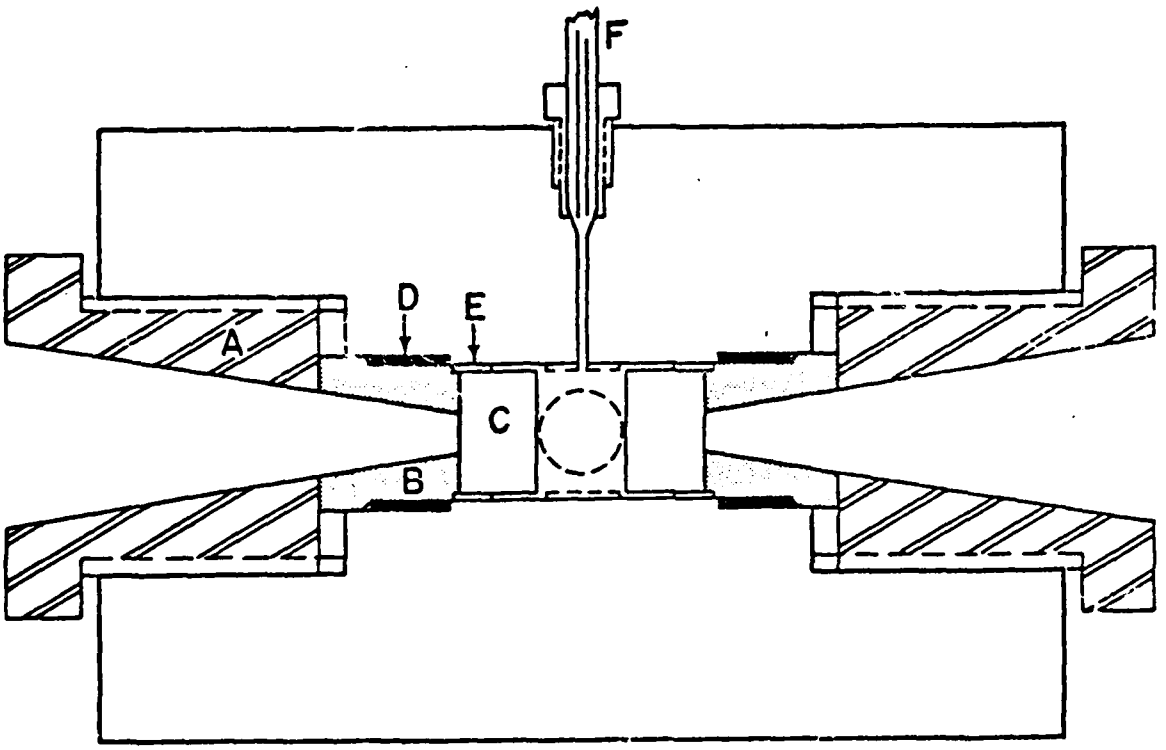

Fig. 1. The high-pressure far infrared cell for transmission spectroscopy in the frequency range 3-400 cm^{-1} and with hydrostatic pressures up to 9 kbar. A, retaining closure; B, window mount; C, window; D, packing; E, window retraining ring; F, gas input line.

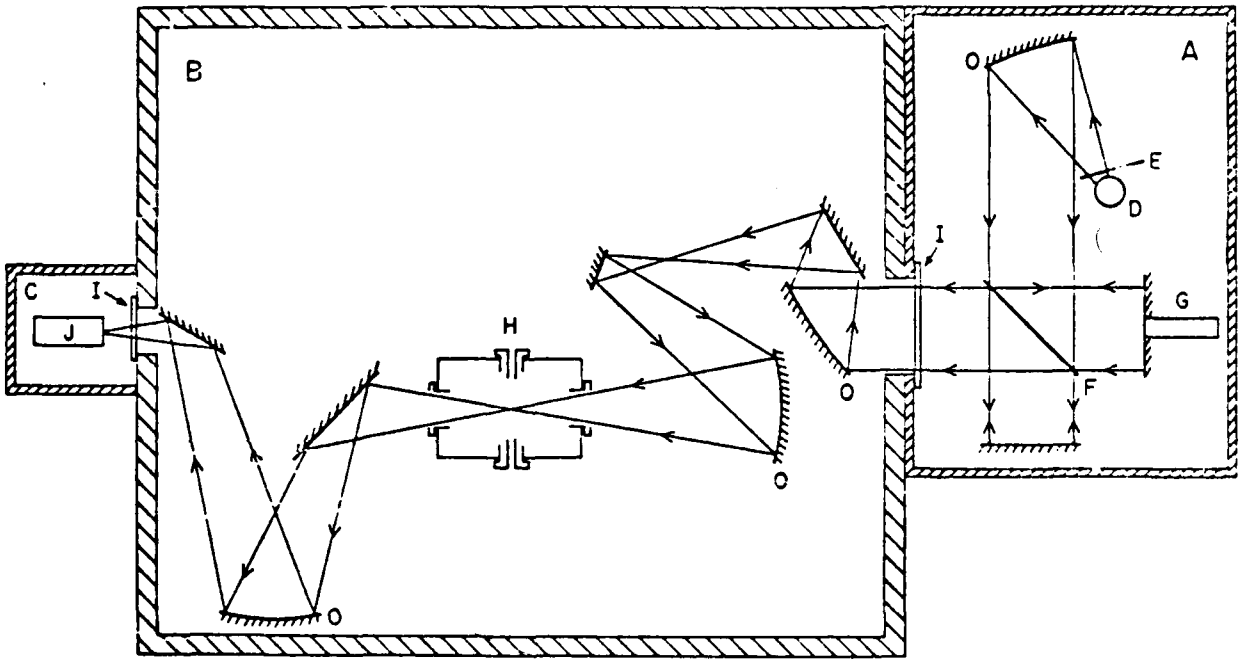

Fig. 2. The experimental layout for high-pressure far infrared spectroscopy. A, Michelson interferometric module; B, high-pressure cell module; C, detector module; D, source; F, beam splitter; G, moving mirror; H, high-pressure cell; I, module vacuum window; J, detector; O, mirrors.

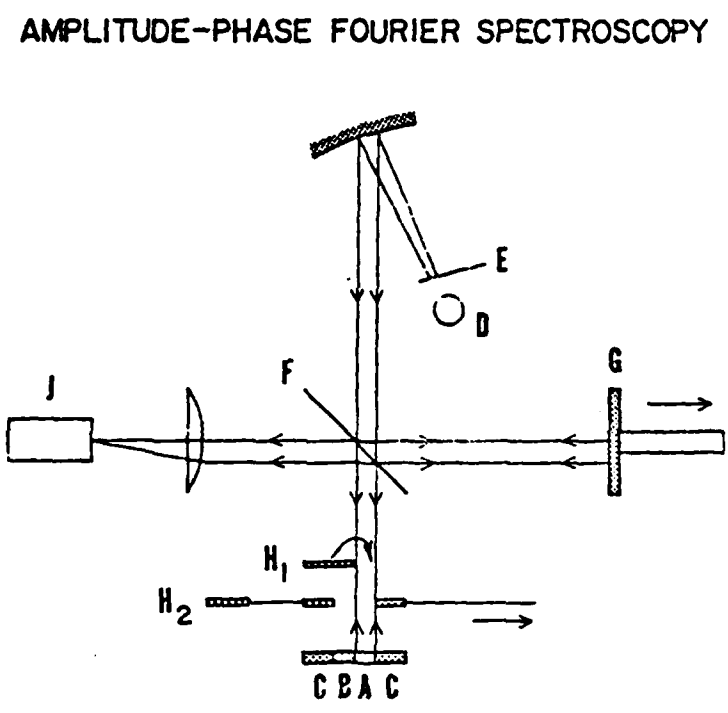

Fig. 3.

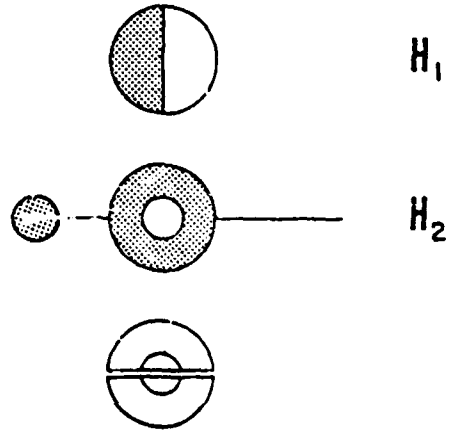

Fig. 4.

Fig. 3. Experimental layout of the dispersive Fourier transform spectrometer.

Fig. 4. Schematic view of the sample and screens used with the dispersive Fourier transform spectrometer.

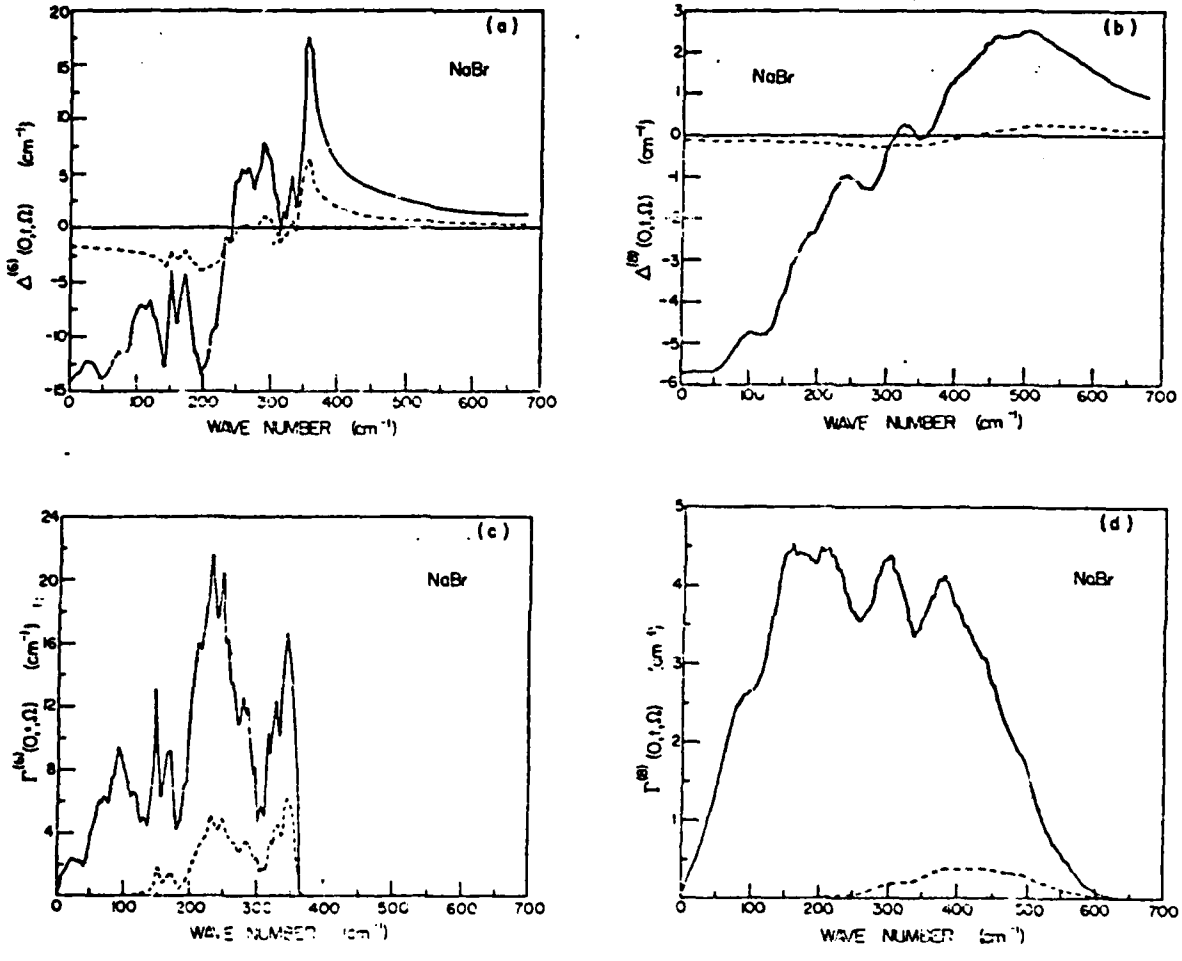

Fig. 5. The calculated frequency dependence of the different contributions to $\tilde{\Delta}^{A}(0,t,\Omega)$ and $\Gamma(0,t,\Omega)$ for NaBr at 5 K (dashed line) and 300 K (solid line).

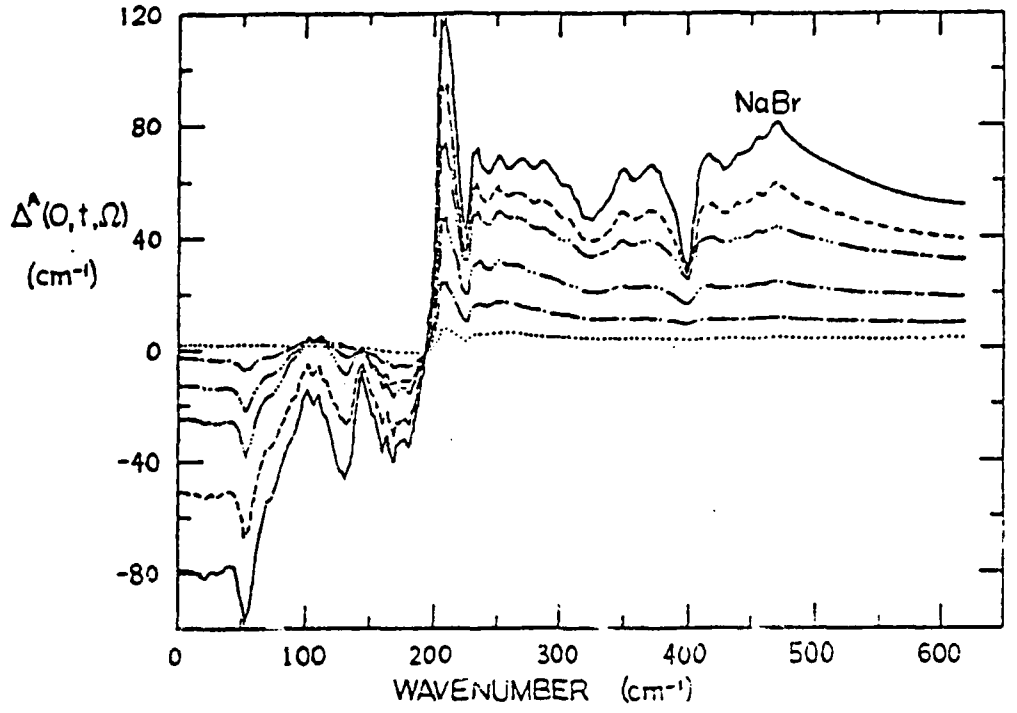

Fig. 6a

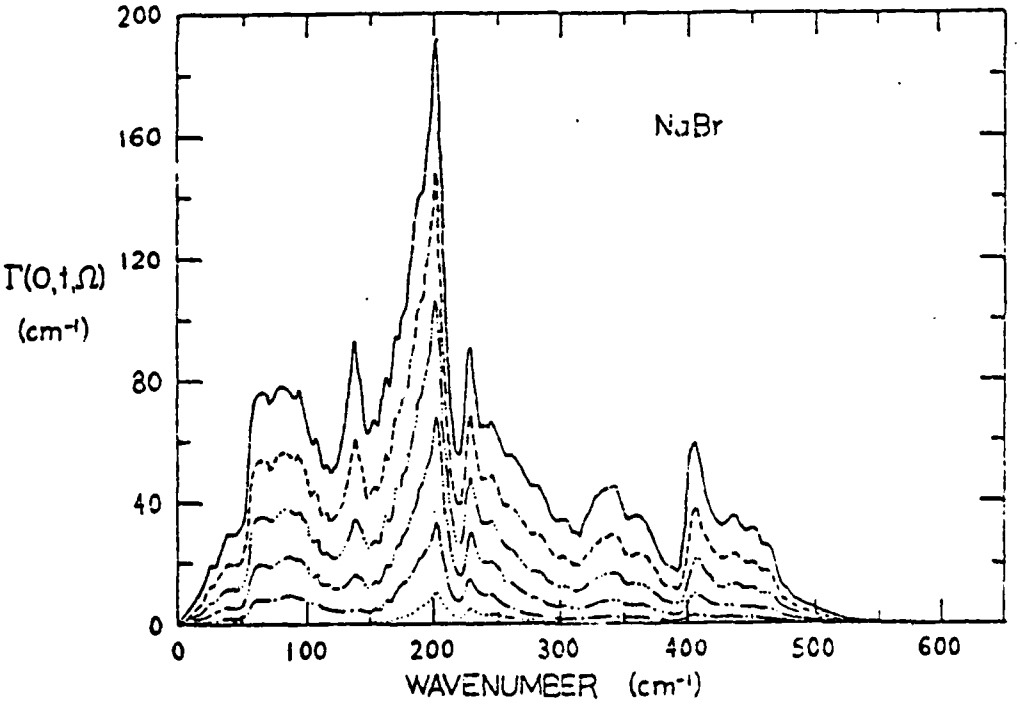

Fig. 6b

Fig. 6. The calculated frequency dependence of (a) $\Delta^A(0,t,\Omega)$ and (b) $\Gamma(0,t,\Omega)$ for NaBr at 5 K (· · ·), 200 K (- · -), 400 K (- ·· -), 600 K (- ···-), 800 K (- - -) and 1000 K (——).

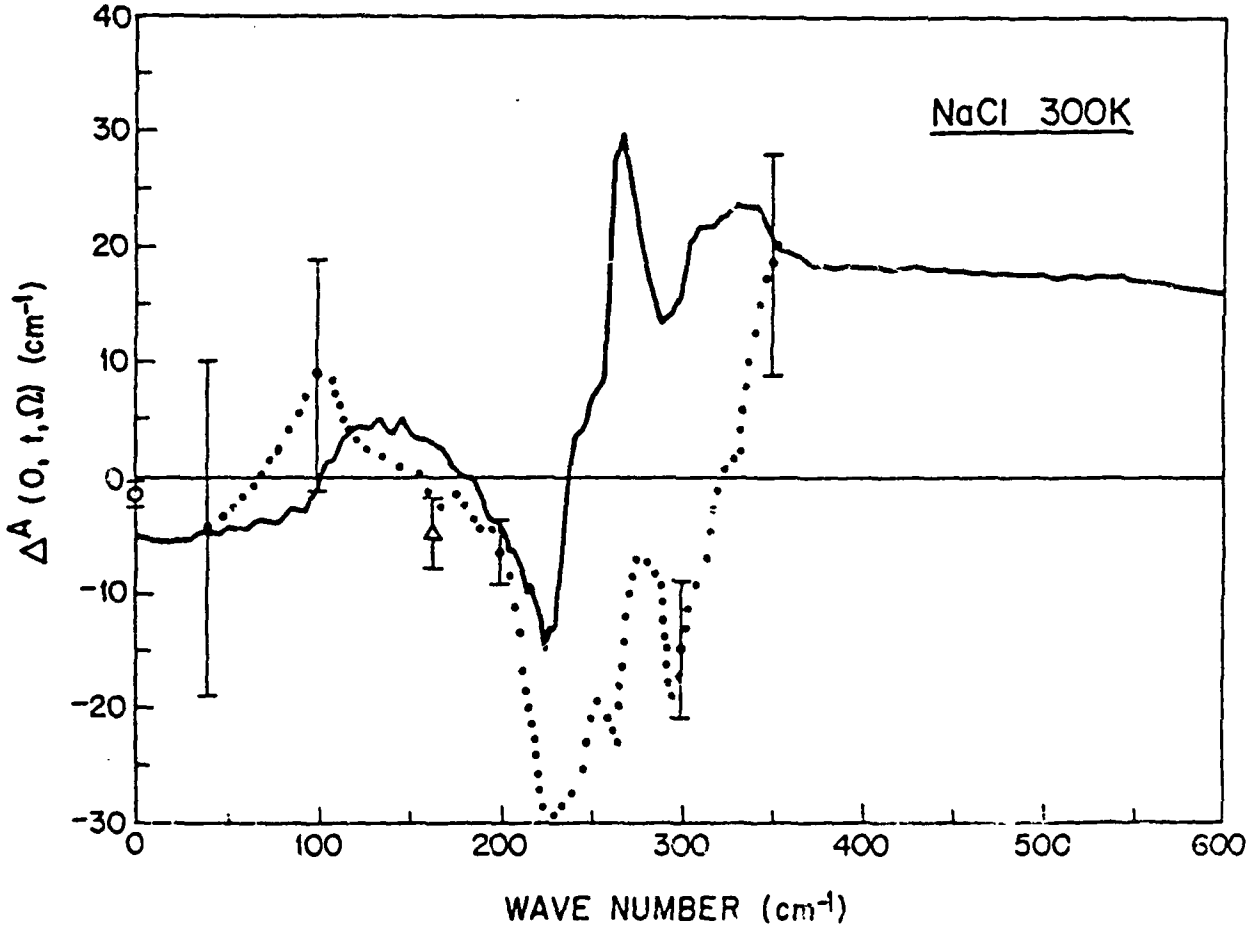

Fig. 7. The experimental (· · ·) and calculated (——) frequency dependence of $\Delta^A(0,t,\Omega)$ for NaCℓ at 300 K. Also shown are values of $\Delta^A(0,t,\Omega)$ determined at $\Omega = 0$ (0) from low-frequency dielectric constant measurements, and at $\Omega = \omega_t$ (Δ) from far infrared transmission measurements.

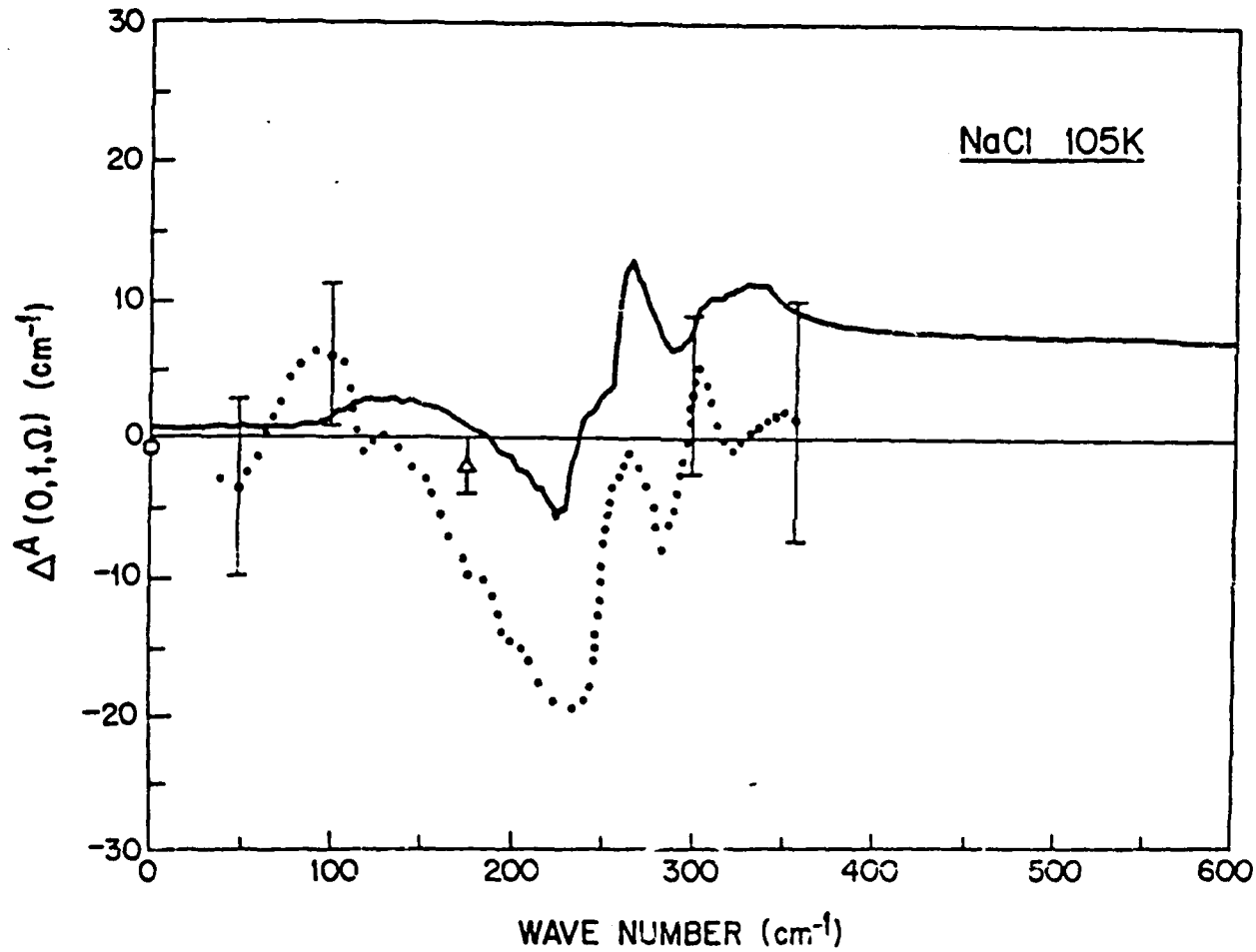

Fig. 8. The experimental (· · ·) and calculated (——) frequency dependence of $\Delta^A(0,t,\Omega)$ for NaCl at 105 K. Also shown are values of $\Delta^A(0,t,\Omega)$ determined at $\Omega = 0$ (0) from low-frequency dielectric constant measurements, and at $\Omega = \omega_t$ (Δ) from far infrared transmission measurements.

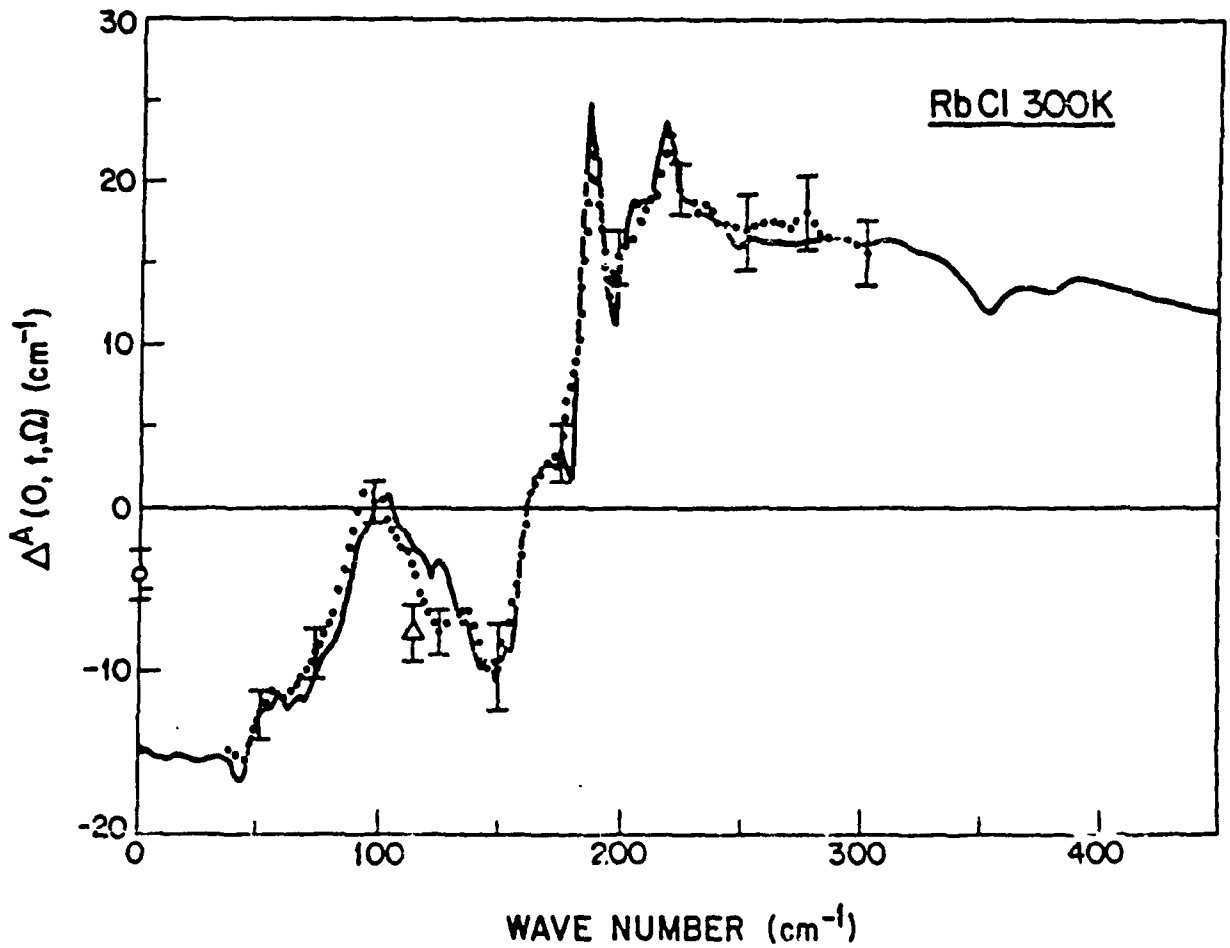

Fig. 9. The experimental (· · ·) and calculated (——) frequency dependence of $\Delta^A(0,t,\Omega)$ for RbCℓ at 300 K. Also shown are values of $\Delta^A(0,t,\Omega)$ determined at $\Omega = 0$ (0) from low-frequency dielectric constant measurements, and at $\Omega = \omega_t$ (Δ) from far infrared transmission measurements.

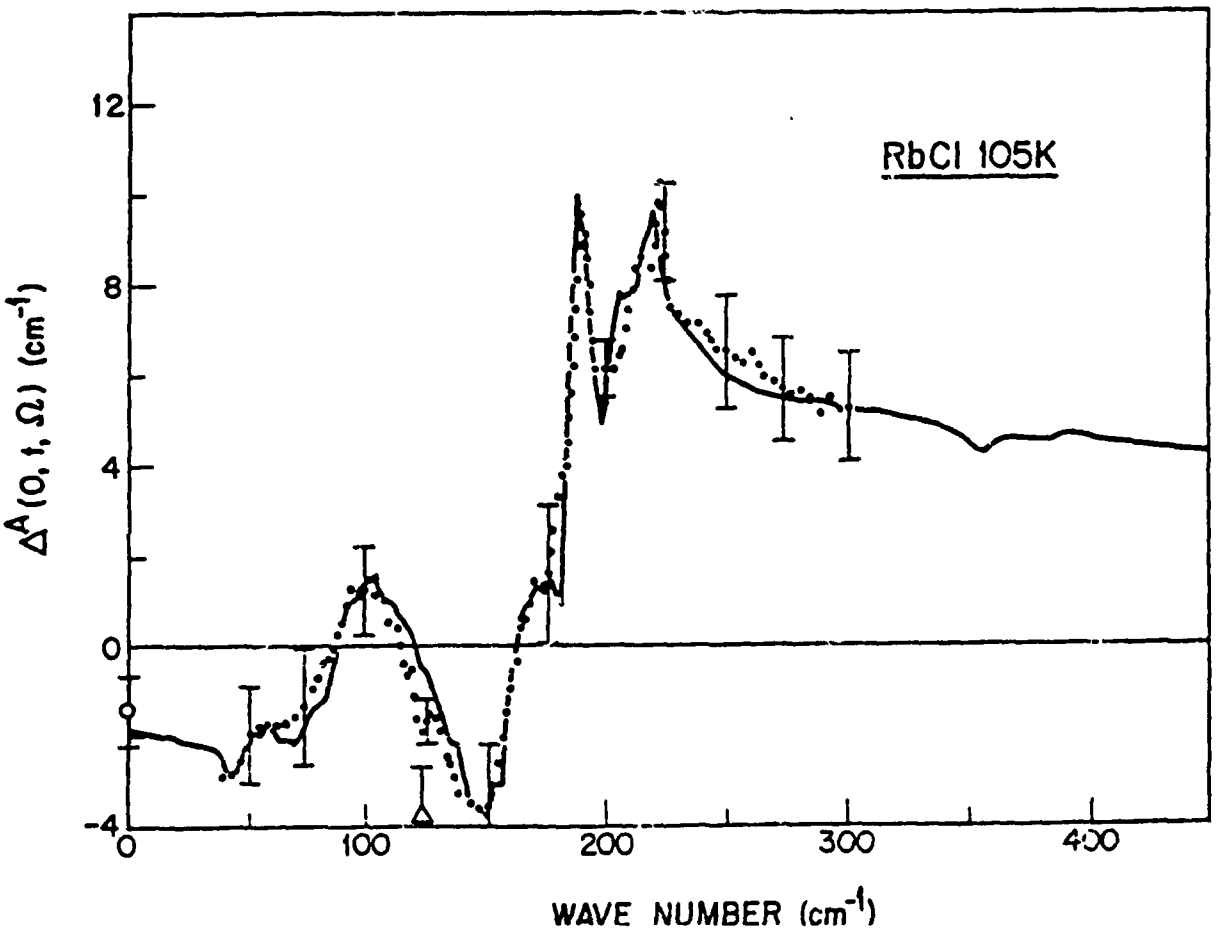

Fig. 10. The experimental (· · ·) and calculated (——) frequency dependence of $\Delta^A(0,t,\Omega)$ for RbCℓ at 105 K. Also shown are values of $\Delta^A(0,t,\Omega)$ determined at $\Omega = 0$ (0) from low-frequency dielectric constant measurements, and at $\Omega = \omega_t$ (Δ) from far infrared transmission measurements.

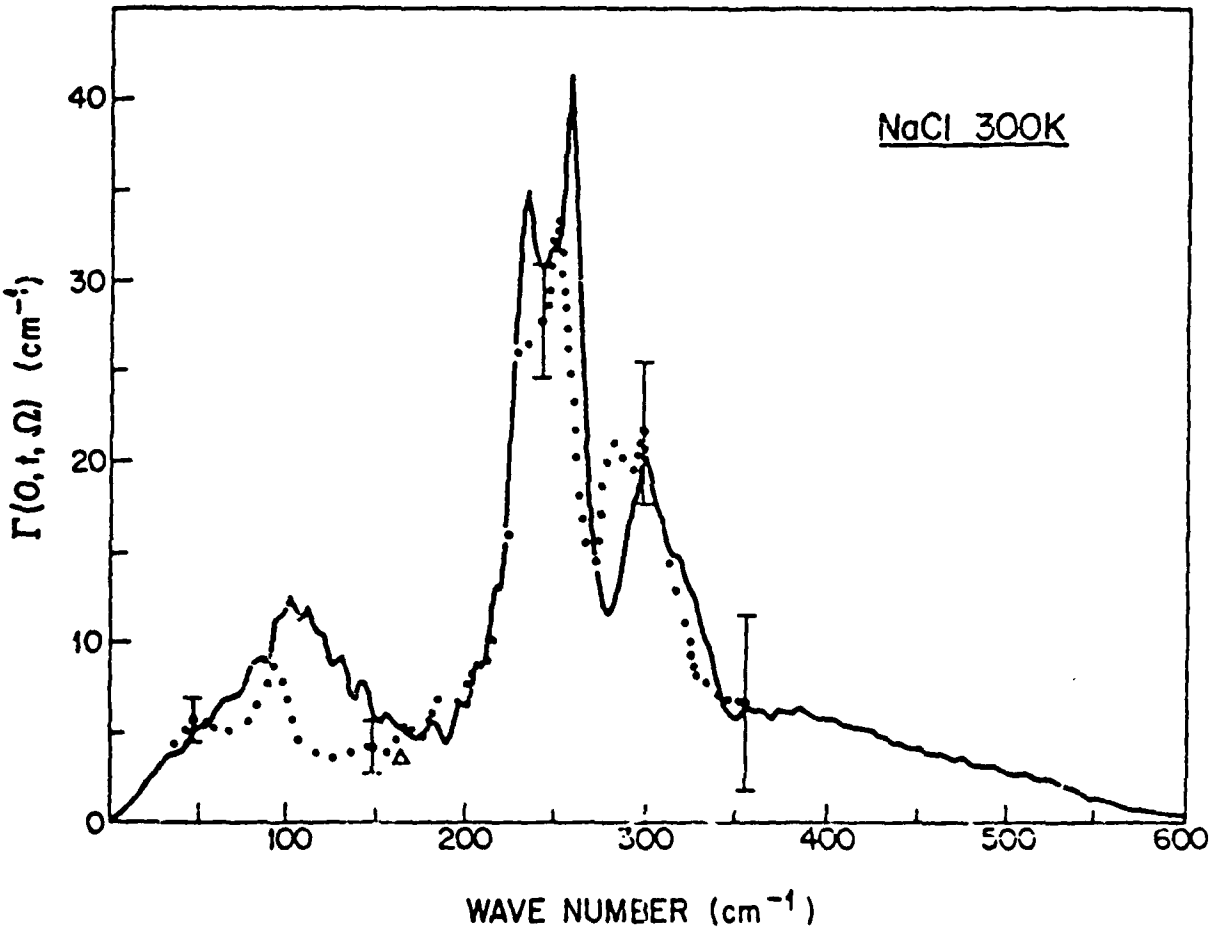

Fig. 11. The experimental (· · ·) and calculated (——) frequency dependence of $\Gamma(0,t,\Omega)$ for NaCℓ at 300 K. Also shown are values of $\Gamma(0,t,\Omega)$ determined at $\Omega = \omega_t$ (Δ) from far infrared transmission experiments.

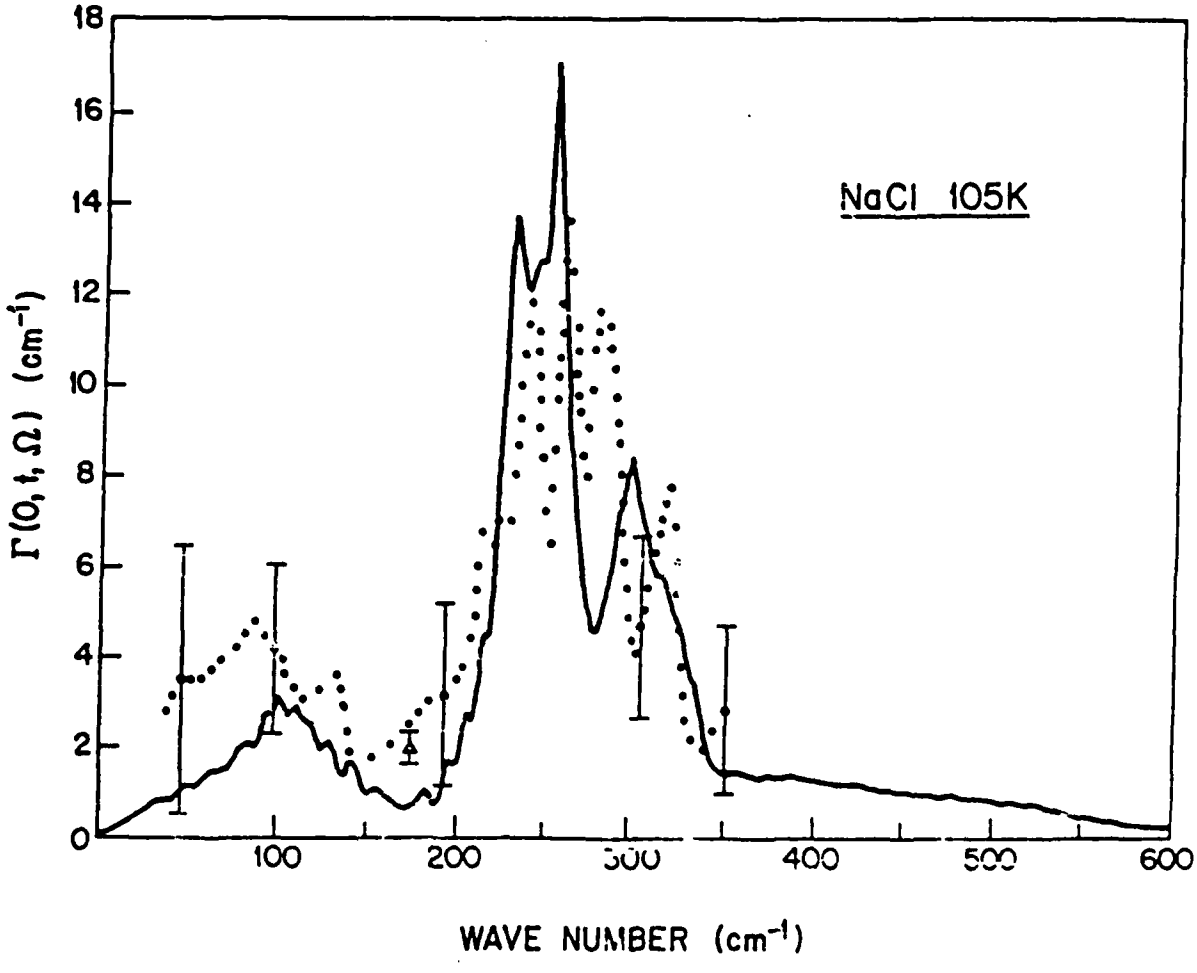

Fig. 12. The experimental (· · ·) and calculated (——) frequency dependence of $\Gamma(0,t,\Omega)$ for NaCℓ at 105 K. Also shown are values of $\Gamma(0,t,\Omega)$ determined at $\Omega = \omega_t$ (Δ) from far infrared transmission experiments.

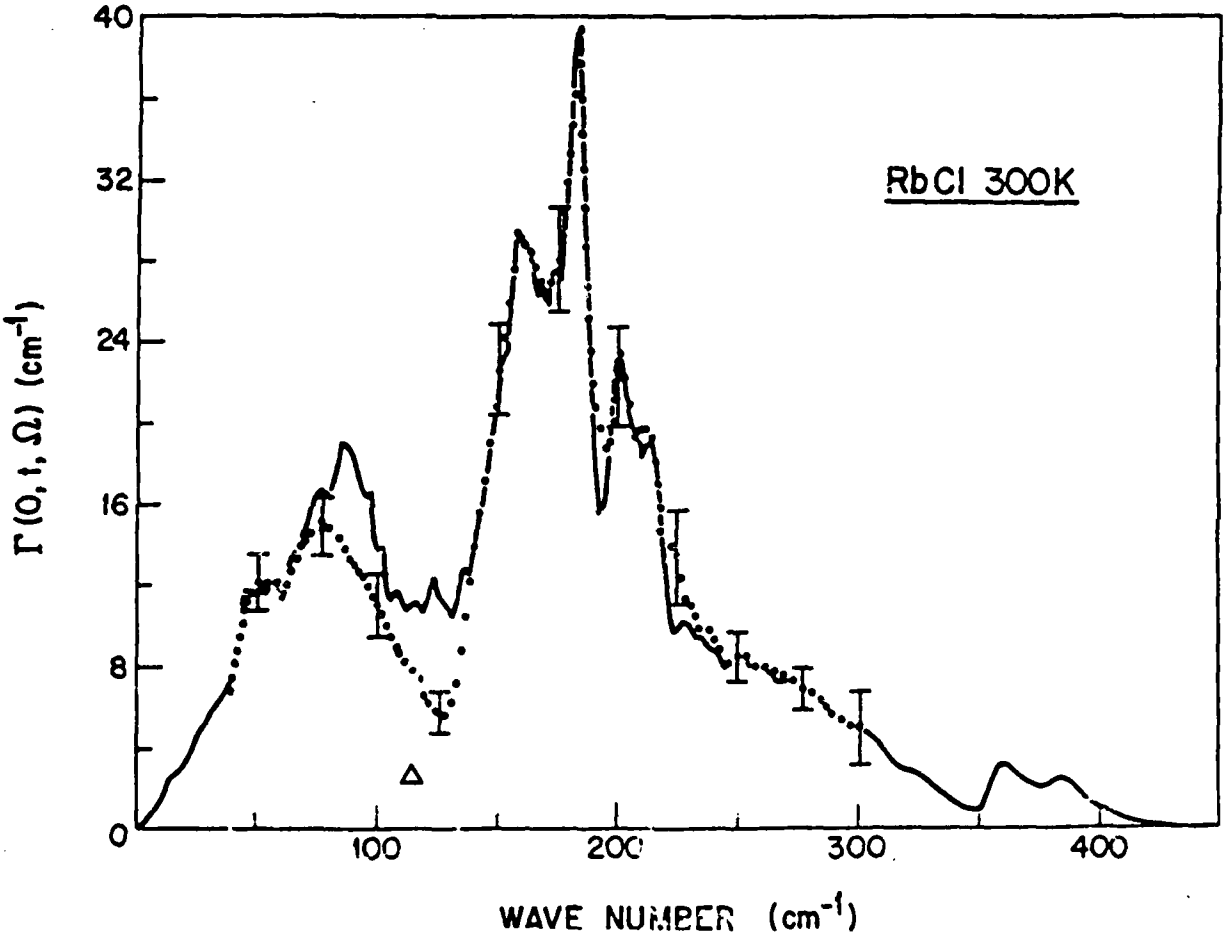

Fig. 13. The experimental (· · ·) and calculated (——) frequency dependence of $\Gamma(0,t,\Omega)$ for RbCl at 300 K. Also shown are values of $\Gamma(0,t,\Omega)$ determined at $\Omega = \omega_t$ (Δ) from far infrared transmission experiments.

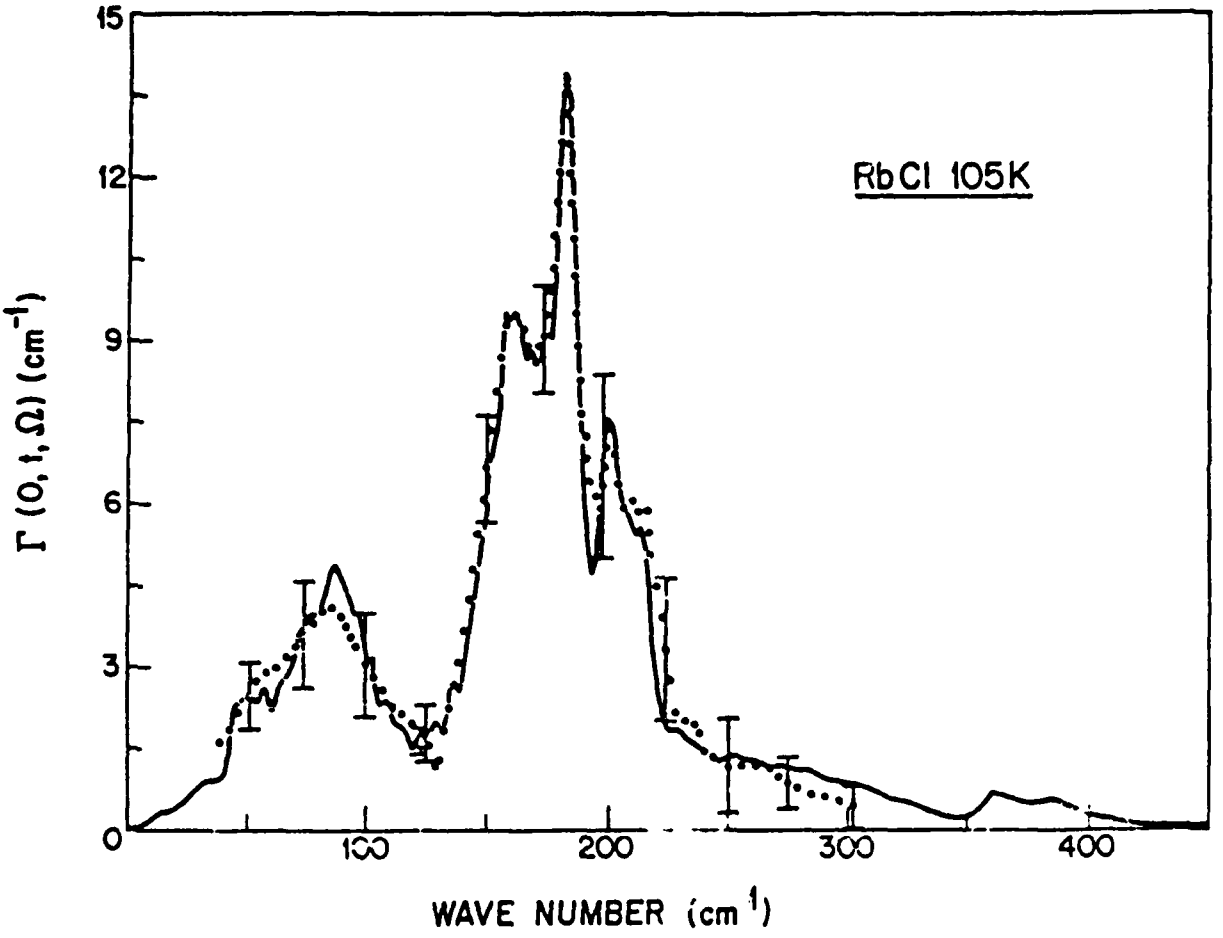

Fig. 14. The experimental (· · ·) and calculated (———) frequency dependence of $\Gamma(0,t,\Omega)$ for RbCl at 105 K. Also shown are values of $\Gamma(0,t,\Omega)$ determined at $\Omega = \omega_t$ (Δ) from far infrared transmission experiments.

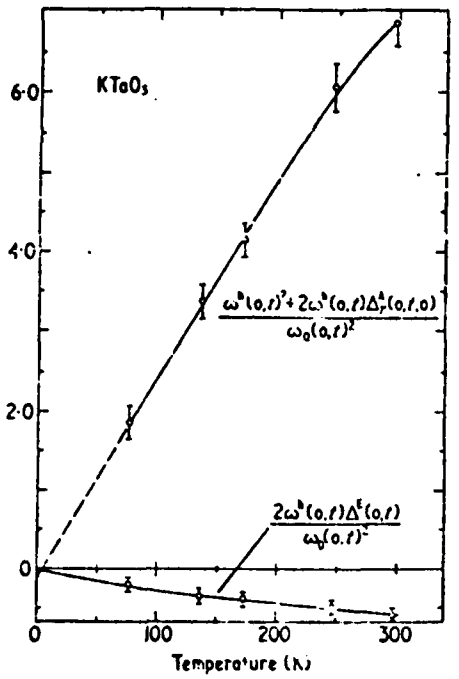

Fig. 15. The temperature dependence of $2\omega^h(0,t)\Delta^E(0,t)$ and $[\omega^h(0,t)^2 + 2\omega^h(0,t)\Delta_T^A(0,t,0)]$ expressed as a fraction of the quasi-normal soft mode frequency (squared) at 0 K for $KTaO_3$. The broken line illustrates the extrapolation used to determine $\omega^h(0,t)^2$.

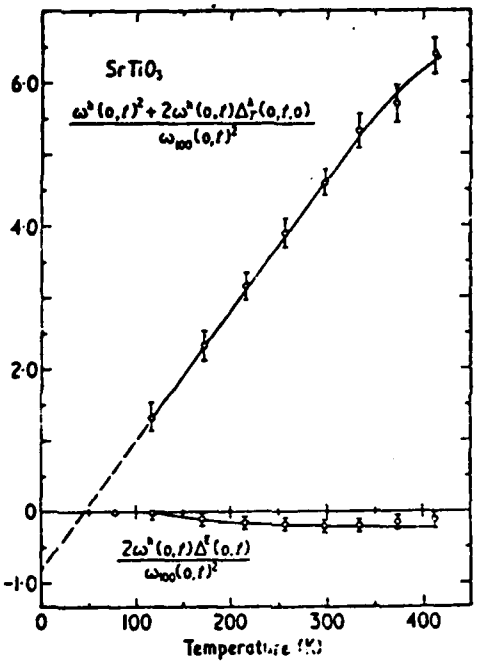

Fig. 16. The temperature dependence of $2\omega^h(0,t)\Delta^E(0,t)$ and $[\omega^h(0,t)^2 + 2\omega^h(0,t)\Delta_T^A(0,t,0)]$ expressed as a fraction of the quasi-normal soft mode frequency (squared) at 0 K for $SrTiO_3$. The broken line illustrates the extrapolation used to determine $\omega^h(0,t)^2$.

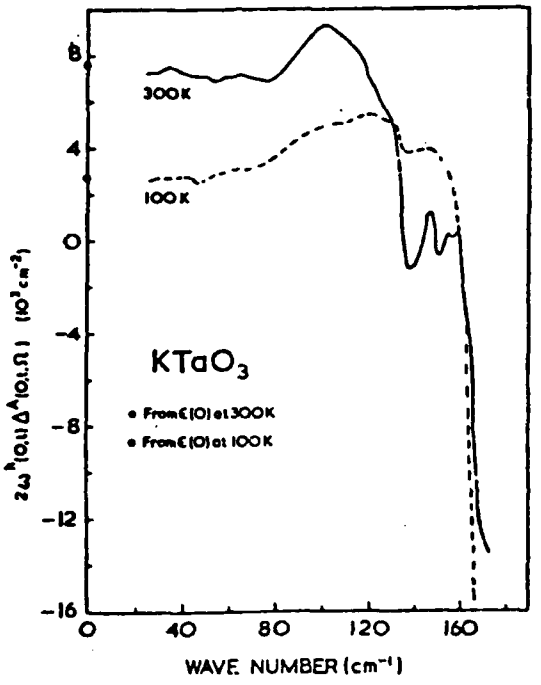

Fig. 17. The frequency dependence of $2\omega^{h}(0,t)\Delta^{A}(0,t,\Omega)$ determined for $KTaO_3$ at 100 and 300 K. The values shown at $\Omega = 0$ are determined from our dielectric constant measurements (see reference 40).

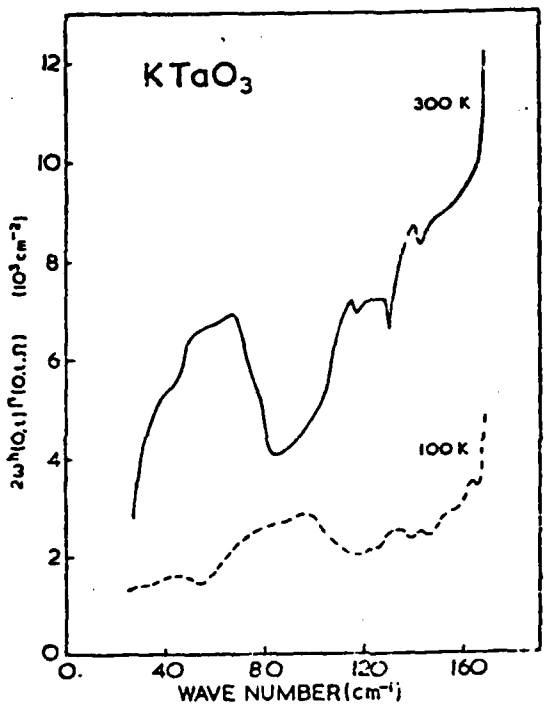

Fig. 18. The frequency dependence of $2\omega^{h}(0,t)\Gamma(0,t,\Omega)$ determined for $KTaO_3$ at 100 and 300 K.

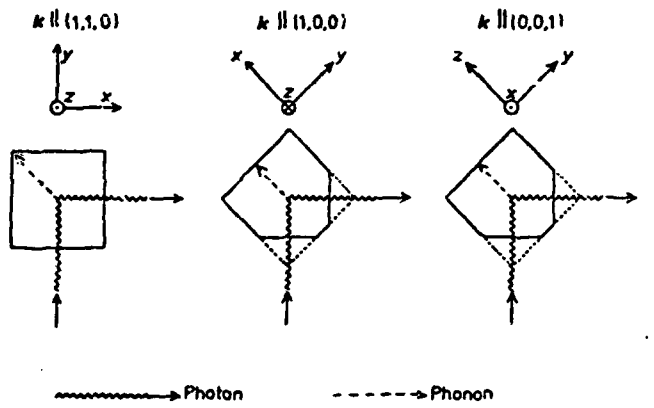

Fig. 19. The three scattering geometries utilized to study the E-mode splittings.

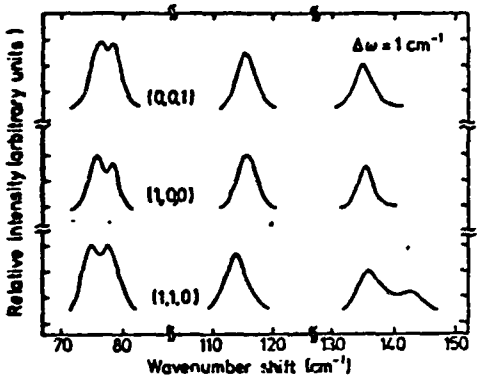

Fig. 20(a)

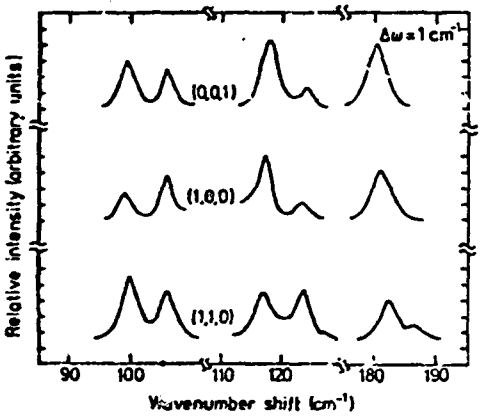

Fig. 20(b)

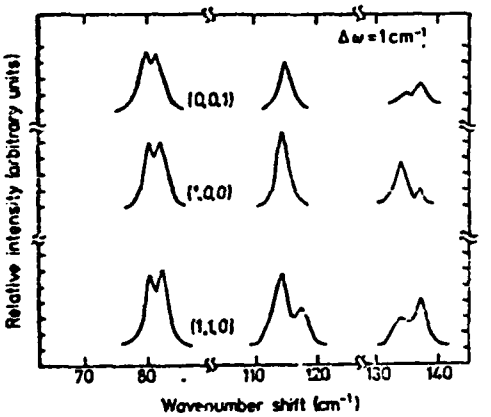

Fig. 20(c)

Fig. 20. The low-frequency B_1, B_2 spectra recorded at 10 K for phonons propagating in the (0,0,1), (1,0,0) and (1,1,0) directions for (a) KDP; (b) KDA; and (c) KD*A.

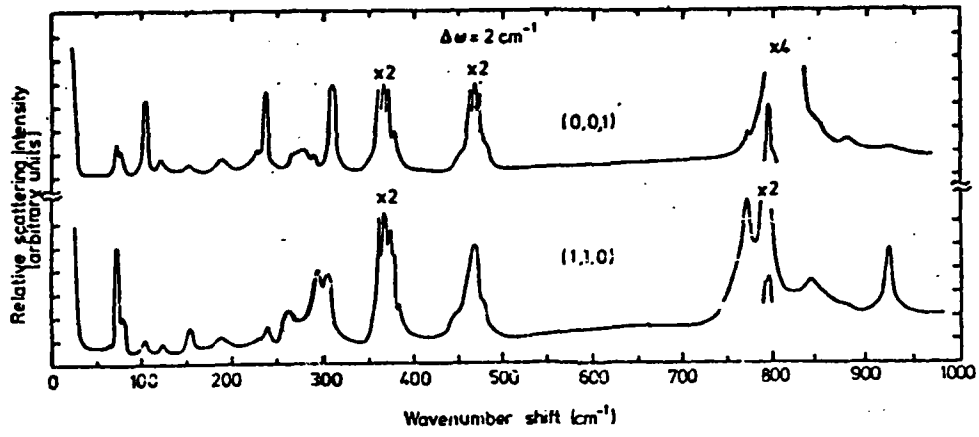

Fig. 21(a)

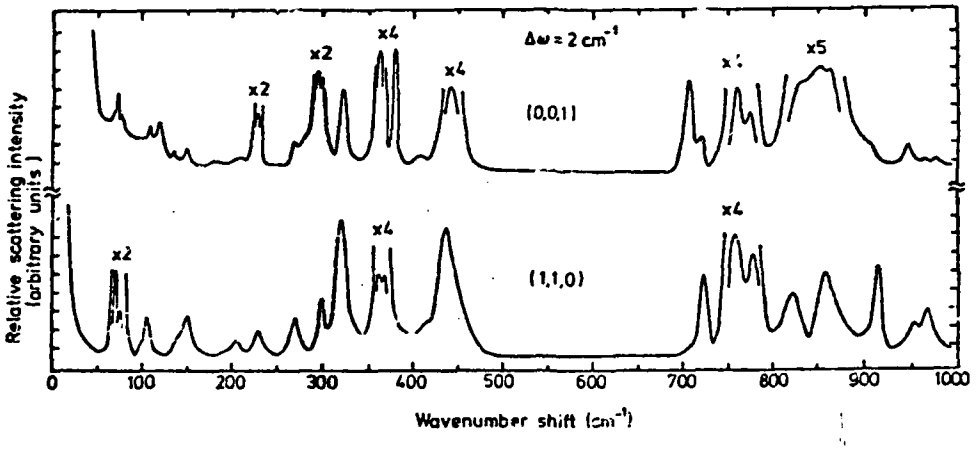

Fig. 21(b)

Fig. 21. The B_1, B_2 spectra recorded at 10 K for phonons propagating in the (0,0,1) and (1,1,0) directions for (a) RbDA; and (b) RbD^*A.

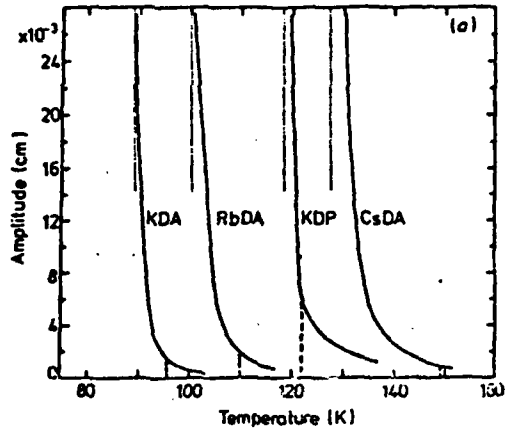

Fig. 22(a)

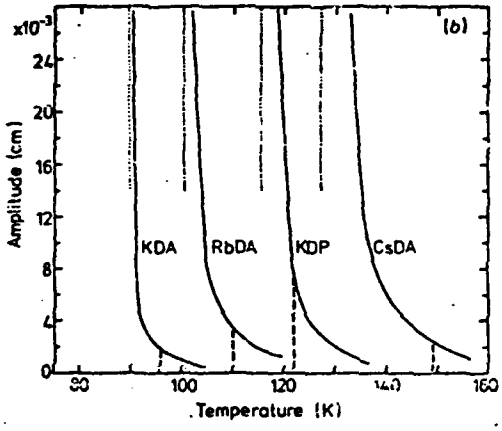

Fig. 22(b)

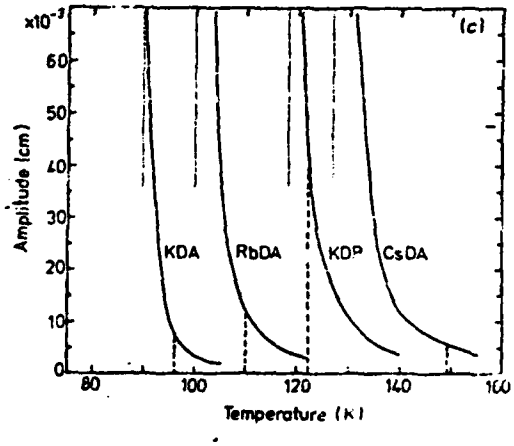

Fig. 22(c)

Fig. 22. The temperature dependence of the amplitude of the central component for KDP, KDA, RbDA and CsDA calculated from equation (53) using (a) $\alpha = \alpha_E$, (b) $\alpha = \langle\alpha\rangle$, and (c) $\alpha = \langle\alpha\rangle_m$. The broken lines indicate the characteristic ferroelectric transition temperature for each compound and the dotted lines the characteristic T_c^x.

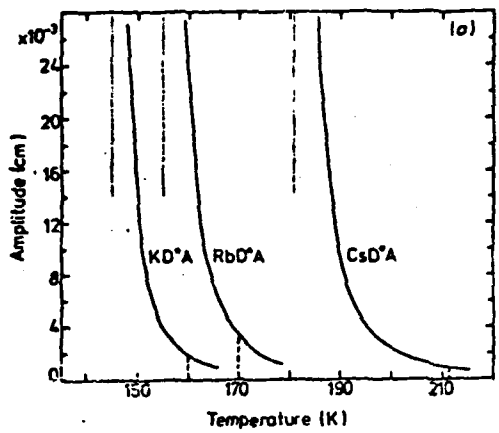

Fig. 23(a)

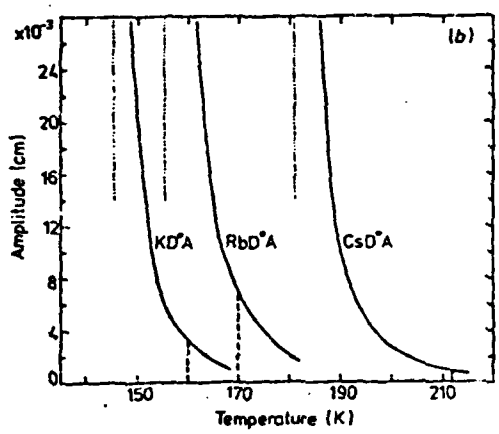

Fig. 23(b)

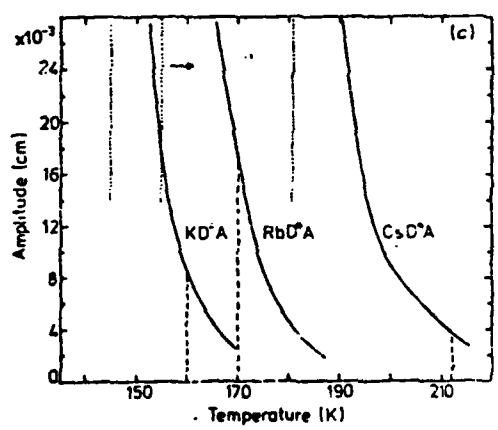

Fig. 23(c)

Fig. 23. The temperature dependence of the amplitude of the central component for KD*A, RbD*A and CsD*A calculated from equation (53) using (a) $\alpha = \alpha_E$, (b) $\alpha = \langle\alpha\rangle$, and (c) $\alpha = \langle\alpha\rangle_m$. The broken lines indicate the characteristic T_c^*.

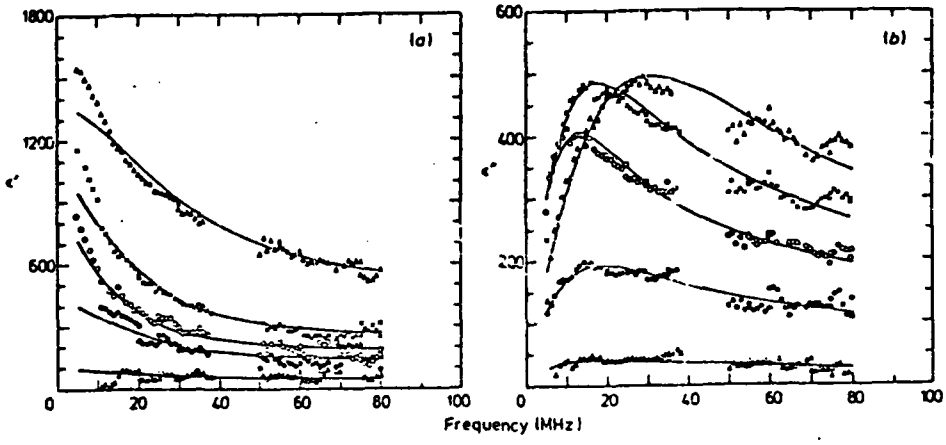

Fig. 24(a)

Fig. 24(b)

Fig. 24. The radiofrequency dependence of (a) ε' and (b) ε'' for KDP at different temperatures in the ferroelectric phase. The full curves represent fits of the experimental data to the Debye form of relaxation given in equation (43). Δ, 91.12 K; ●, 98.47 K; o, 103.36 K; x, 110.46 K; ▲, 122.25 K.

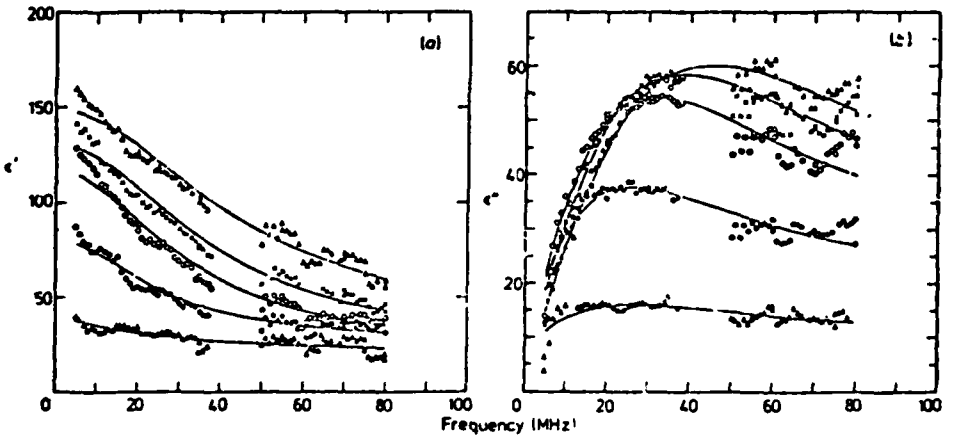

Fig. 25(a)

Fig. 25(b)

Fig. 25. The radiofrequency dependence of (a) ϵ' and (b) ϵ'' for CsDA at different temperatures in the ferroelectric phase. The full curves represent fits of the experimental data to the Debye form of relaxation given in equation (43). Δ, 123.85 K; ●, 128.76 K; ○, 133.78 K; x, 138.75 K; ▲, 144.42 K.

Table 1. Calculated values, in cm^{-1}, of the different contributions to $\Delta^B(0,t)$, $\Delta^A(0,t,0)$, $\Delta^A(0,t,\omega_t)$, and $\Gamma(0,t,\omega_t)$ for the lithium halides.

	LiF				LiCl				LiBr				LiI		
Temperature (K)	5	100	300	500	5	100	200	300	5	100	200	300	5	100	200
$\omega(0,t)$	316.9	316.3	300.8	278.7	220.3	214.8	192.1	153.4	191.5	179.0	146.6	173.0	147.7	127.2	146.0
$\Delta^B(0,t)$	0	−0.6	−10.9	−26.4	0	−4.1	−20.2	−40.8	0	−6.7	−26.7	−50.5	0	−12.8	−43.4
$\Delta^{(4)}(0,t)$	13.0	13.3	19.1	27.7	14.1	16.0	22.4	30.0	12.5	16.1	24.6	34.6	14.5	21.4	35.2
$\Delta^{(8)}(0,t)$	−0.2	−0.2	−0.7	−1.6	−0.4	−0.7	−1.7	−3.6	−0.4	−0.9	−2.9	−6.0	−0.5	−2.2	−7.1
$\Delta^A(0,t)$	12.8	13.1	18.4	26.1	13.7	15.3	20.7	27.0	12.1	15.1	21.8	28.5	13.9	19.2	28.0
$\Delta^{(6)}(0,t,0)$	−9.8	−11.1	−25.2	−41.7	−8.4	−13.3	−25.2	−37.6	−4.6	−10.0	−19.6	−29.4	−5.3	−15.2	−30.0
$\Delta^{(8)}(0,t,0)$	−1.1	−1.2	−5.0	−13.6	−1.6	−3.1	−10.0	−22.0	−1.7	−5.3	−19.1	−42.7	−2.3	−11.8	−45.2
$\tilde{\Delta}^A(0,t,0)$	−10.9	−12.3	−30.2	−55.3	−10.0	−16.4	−35.1	−59.6	−6.4	−15.3	−38.7	−72.1	−7.5	−27.0	−75.3
$\Delta^A(0,t,0)$	2.0	0.8	−11.8	−29.2	3.7	−1.1	−14.4	−32.6	5.8	−0.3	−17.0	−43.6	6.4	−7.9	−47.2
$\Delta^{(6)}(0,t,\omega_t)$	−12.7	−13.1	−19.1	−27.1	−12.7	−14.3	−18.9	−23.1	−5.1	−9.5	−13.8	−25.4	−5.7	−5.6	−11.7
$\Delta^{(8)}(0,t,\omega_t)$	−1.2	−1.4	−5.0	−15.3	−1.9	−3.2	−9.0	−21.0	−2.1	−6.0	−17.6	−43.4	−2.8	−13.6	−47.9
$\tilde{\Delta}^A(0,t,\omega_t)$	−13.9	−14.4	−24.1	−40.4	−14.5	−17.5	−28.0	−44.1	−7.2	−15.5	−31.5	−68.8	−8.4	−19.3	−59.7
$\Delta^A(0,t,\omega_t)$	−1.1	−1.3	−5.7	−14.3	−0.8	−2.2	−7.3	−17.1	4.9	−0.4	−9.7	−40.3	5.5	−0.1	−31.6
$\Gamma^{(6)}(0,t,\omega_t)$	0.3	0.7	6.1	9.3	0.8	2.2	5.4	9.6	4.1	7.8	7.4	18.6	0.02	11.4	6.9
$\Gamma^{(8)}(0,t,\omega_t)$		0.1	2.1	7.2	0	1.0	5.1	9.9	0	2.7	4.9	25.0	0.12	3.7	40.1
$\Gamma(0,t,\omega_t)$		0.8	8.4	16.5	0.8	3.2	10.5	19.6	4.1	10.1	12.2	43.6	0.14	15.1	47.0

Table 2. Calculated values, in cm^{-1}, of the different contributions to $\Delta^B(0,t)$, $\Delta^A(0,t,0)$, $\Delta^A(0,t,\omega_t)$, and $\Gamma(0,t,\omega_t)$ for the sodium halides.

	NaF				NaCl				NaBr				NaI			
Temperature (K)	5	100	200	300	5	100	200	300	5	100	200	300	5	100	200	300
$\omega(0,t)$	255	254	248	239	174	171	164	154	143	140	133	124	123	120	110	92.5
$\Delta^B(0,t)$	0	−0.63	−3.69	−7.79	0	−1.09	−4.56	−8.61	0	−1.39	−4.97	−8.98	0	−1.78	−5.90	−10.38
$\Delta^{(4)}(0,t)$	5.44	7.17	9.55	12.95	3.93	5.81	8.98	12.95	3.27	5.13	8.96	13.02	3.43	6.05	10.60	15.10
$\Delta^{(8)}(0,t)$	−0.08	−0.13	−0.32	−0.65	−0.06	−0.15	−0.47	−1.01	−0.05	−0.19	−0.62	−1.36	−0.06	−0.32	−1.12	−2.46
$\Delta^A(0,t)$	5.36	7.04	9.23	12.30	3.87	5.66	8.51	11.94	3.22	4.94	8.34	11.66	3.37	5.73	9.48	12.64
$\Delta^{(6)}(0,t,0)$	−4.49	−6.42	−11.86	−17.71	−2.82	−5.79	−11.37	−17.04	−1.69	−4.59	−9.10	−13.05	−1.32	−4.57	−9.12	−13.69
$\Delta^{(8)}(0,t,0)$	−0.26	−0.42	−1.27	−2.79	−0.15	−0.47	−1.74	−3.90	−0.13	−0.66	−2.54	−5.71	−0.15	−1.16	−4.56	−10.25
$\tilde{\Delta}^A(0,t,0)$	−4.76	−6.84	−13.13	−20.50	−2.97	−6.26	−13.11	−20.94	−1.82	−5.24	−11.64	−19.36	−1.47	−5.73	−13.68	−23.94
$\Delta^A(0,t,0)$	1.60	0.20	−3.90	−8.20	0.90	−0.61	−4.60	−9.00	1.41	−0.30	−3.30	−7.70	1.91	0	−4.20	−11.30
$\Delta^{(6)}(0,t,\omega_t)$	−6.65	−7.17	−9.20	−12.20	−4.39	−5.32	−7.77	−10.42	−3.40	−4.58	−5.88	−6.86	−1.47	−1.59	−3.03	−7.76
$\Delta^{(8)}(0,t,\omega_t)$	−0.30	−0.45	−1.10	−2.36	−0.18	−0.42	−1.36	−3.17	−0.16	−0.60	−2.09	−4.75	−0.19	−1.11	−4.33	−8.45
$\tilde{\Delta}^A(0,t,\omega_t)$	−6.95	−7.62	−10.30	−14.56	−4.56	−5.75	−9.13	−13.59	−3.55	−5.17	−7.97	−11.61	−1.66	−2.70	−7.36	−16.21
$\Delta^A(0,t,\omega_t)$	−1.59	−0.58	−1.07	−2.26	−0.69	−0.09	−0.62	−1.65	−0.33	−0.23	0.37	0.06	1.71	3.03	2.12	−3.57
$\Gamma^{(6)}(0,t,\omega_t)$	0.20	0.54	1.23	2.36	0.27	0.86	1.41	2.55	0.69	1.74	3.19	5.08	0.72	2.97	7.37	11.38
$\Gamma^{(8)}(0,t,\omega_t)$	0	0.14	0.93	2.29	0	0.27	1.39	3.18	0	0.38	1.60	3.29	0	0.80	2.63	3.50
$\Gamma(0,t,\omega_t)$	0.20	0.67	2.16	4.65	0.27	1.14	2.80	5.74	0.69	2.12	4.79	8.37	0.73	3.77	10.00	14.89

Table 3. Calculated values, in cm^{-1}, of the different contributions to $\Delta^B(0,t)$, $\Delta^A(0,t,0)$, $\Delta^A(0,t,\omega_t)$, and $\Gamma(0,t,\omega_t)$ for the potassium halides.

	KF				KCl				KBr				KI			
Temperature (K)	5	100	200	300	5	100	200	300	5	100	200	300	5	100	200	300
$\omega(0,t)$	201.4	200.1	195.3	186.8	149.8	149.8	146.2	141.9	123.5	122.8	119.8	115.8	110.2	110.2	109.2	107.7
$\Delta^B(0,t)$	0	−1.09	−5.18	−10.19	0	−1.07	−4.04	−7.37	0	−1.15	−3.82	−6.72	0	−0.95	−2.91	−4.99
$\Delta^{(4)}(0,t)$	5.87	7.15	10.91	15.30	3.14	4.57	7.77	11.25	2.28	3.90	6.95	10.18	1.35	2.67	4.90	7.22
$\Delta^{(B)}(0,t)$	−0.09	−0.21	−0.61	−1.28	−0.04	−0.14	−0.48	−1.05	−0.02	−0.14	−0.48	−1.06	−0.01	−0.08	−0.30	−0.67
$\Delta^A(0,t)$	5.78	6.95	10.30	14.02	3.10	4.43	7.29	10.20	2.26	3.77	6.47	9.12	1.34	2.59	4.59	6.55
$\Delta^{(6)}(0,t,0)$	−3.47	−6.46	−12.55	−18.81	−1.80	−4.61	−9.16	−13.75	−1.10	−3.60	−7.17	−10.76	−0.51	−2.09	−4.18	−6.27
$\Delta^{(B)}(0,t,0)$	−0.24	−0.60	−2.15	−4.81	−0.08	−0.38	−1.46	−3.27	−0.05	−0.37	−1.48	−3.32	−0.03	−0.28	−1.10	−2.47
$\tilde{\Delta}^A(0,t,0)$	−3.71	−7.06	−14.70	−23.62	−1.89	−4.99	−10.62	−17.02	−1.15	−3.97	−8.65	−14.08	−0.53	−2.37	−5.28	−8.74
$\Delta^A(0,t,0)$	2.07	−0.12	−4.41	−9.59	1.21	−0.56	−3.33	−6.82	1.11	−0.21	−2.29	−4.97	0.81	0.22	−0.68	−2.19
$\Delta^{(6)}(0,t,\omega_t)$	−5.63	−6.69	−9.43	−12.27	−3.08	−4.27	−6.95	−9.44	−1.69	−2.48	−4.70	−6.98	−0.65	−0.70	−1.09	−1.35
$\Delta^{(B)}(0,t,\omega_t)$	−0.29	−0.59	−1.75	−3.90	−0.10	−0.29	−0.95	−2.20	−0.06	−0.30	−1.06	−2.40	−0.03	−0.24	−0.90	−2.04
$\tilde{\Delta}^A(0,t,\omega_t)$	−5.91	−7.28	−11.18	−16.17	−3.18	−4.56	−7.90	−11.64	−1.76	−2.77	−5.76	−9.38	−0.68	−0.94	−1.99	−3.39
$\Delta^A(0,t,\omega_t)$	−0.13	−0.33	−0.89	−2.14	−0.08	−0.13	−0.61	−1.43	0.50	0.99	0.71	−0.26	0.66	1.65	2.60	3.15
$\Gamma^{(6)}(0,t,\omega_t)$	0.47	0.93	1.90	3.13	0.18	0.51	1.33	1.91	0.60	1.77	3.10	4.10	0.19	0.68	1.44	1.89
$\Gamma^{(B)}(0,t,\omega_t)$	0	0.33	1.73	3.90	0	0.28	1.29	2.93	0	0.26	1.11	2.47	0	0.23	0.97	2.12
$\Gamma(0,t,\omega_t)$	0.47	1.26	3.63	7.04	0.18	0.78	2.62	4.84	0.60	2.03	4.22	6.57	0.19	0.91	2.41	4.01

Table 4. Calculated values, in cm^{-1}, of the different contributions to $\Delta^B(0,t)$, $\Delta^A(0,t,0)$, $\Delta^A(0,t,\omega_t)$, and $\Gamma(0,t,\omega_t)$ for the rubidium halides.

	RbF				RbCl				RbBr				RbI			
Temperature (K)	5	100	200	300	5	100	200	300	5	100	200	300	5	100	200	300
$\omega(0,t)$	164.3	161.9	154.4	145.6	126.1	124.3	120.3	114.7	94.55	93.12	90.0	86.55	61.67	80.54	78.04	75.15
$\Delta^B(0,t)$	0	−2.03	−7.51	−13.76	0	−1.61	−5.25	−9.20	0	−1.33	−3.88	−6.55	0	−1.29	−3.55	−5.88
$\Delta^{(4)}(0,t)$	5.77	7.97	13.03	18.65	3.11	5.16	9.14	13.36	1.60	3.31	6.16	9.11	1.22	2.94	5.57	8.27
$\Delta^{(B)}(0,t)$	−0.11	−0.34	−1.10	−2.35	−0.04	−0.23	−0.80	−1.75	−0.02	−0.13	−0.50	−1.10	−0.01	−0.13	−0.49	−1.10
$\Delta^A(0,t)$	5.66	7.63	11.93	16.30	3.07	4.93	8.34	11.61	1.59	3.18	5.66	8.01	1.21	2.81	5.08	7.17
$\Delta^{(6)}(0,t,0)$	−2.43	−5.83	−11.43	−17.12	−1.43	−4.49	−8.97	−13.46	−0.86	−3.53	−7.06	−10.60	−0.60	−2.98	−5.96	−8.94
$\Delta^{(B)}(0,t,0)$	−0.28	−1.10	−4.18	−9.37	−0.09	−0.58	−2.27	−5.11	−0.03	−0.33	−1.32	−2.97	−0.02	−0.32	−1.28	−2.88
$\tilde{\Delta}^A(0,t,0)$	−2.71	−6.92	−15.61	−26.49	−1.51	−5.07	−11.24	−18.57	−0.88	−3.86	−8.38	−13.57	−0.62	−3.30	−7.24	−11.82
$\Delta^A(0,t,0)$	2.95	0.71	−3.68	−10.19	1.55	−0.14	−2.90	−6.96	0.70	−0.68	−2.72	−5.56	0.60	−0.50	−2.16	−4.65
$\Delta^{(6)}(0,t,\omega_t)$	−3.99	−5.38	−8.47	−10.70	−2.79	−4.42	−6.72	−8.68	−1.48	−2.97	−5.34	−6.97	−1.00	−2.24	−4.06	−5.38
$\Delta^{(B)}(0,t,\omega_t)$	−0.34	−1.29	−4.25	−8.24	−0.11	−0.51	−1.95	−4.49	−0.03	−0.22	−0.87	−2.10	−0.02	−0.22	−0.83	−1.99
$\tilde{\Delta}^A(0,t,\omega_t)$	−4.33	−6.67	−12.72	−18.94	−2.90	−4.93	−8.67	−13.18	−1.52	−3.19	−6.21	−9.07	−1.02	−2.46	−4.90	−7.38
$\Delta^A(0,t,\omega_t)$	1.33	0.96	−0.79	−2.64	0.17	0	−0.33	−1.57	0.06	−0.02	−0.54	−1.06	1.86	0.35	0.18	−0.20
$\Gamma^{(6)}(0,t,\omega_t)$	0.87	2.50	4.83	6.95	0.59	1.26	1.96	2.86	0.24	0.98	1.05	1.77	0.27	1.17	1.47	2.27
$\Gamma^{(B)}(0,t,\omega_t)$	0	0.72	2.24	4.62	0	0.46	1.88	3.65	0	0.28	1.17	2.58	0	0.26	1.07	2.32
$\Gamma(0,t,\omega_t)$	0.87	3.22	7.06	11.57	0.59	1.72	3.84	6.51	0.24	1.26	2.22	4.35	0.27	1.43	2.54	4.60

Table 5. Comparison of the calculated and experimental values, in cm^{-1}, of $\Delta^B(0,t)$, $\Delta_T^A(0,t,\Omega)$, determined at $\Omega=0$ and $\Omega=\omega_t$, and of $\Gamma(0,t,\omega_t)$ for the lithium halides.

		$\Delta^B(0,t)$			$\Delta_T^A(0,t,0)$		$\Delta_T^A(0,t,\omega_t)$			$\Gamma(0,t,\omega_t)$		
			Expt.				Calc.		Expt.	Calc.		Expt.
Ω	T (K)	Calc.	$\Omega=0$	$\Omega=(\omega_t)_{expt}$	Calc.	Expt.	$(\omega_t)_{calc}$	$(\omega_t)_{expt}$	$(\omega_t)_{expt}$	$(\omega_t)_{calc}$	$(\omega_t)_{expt}$	$(\omega_t)_{expt}$
LiF	5	0	0	0	2.0	0.8	− 1.1	− 1.1	0.2	0.3	0.4	3.7
	100	− 0.6	−0.5	− 0.4	0.8	−1.5	− 1.3	− 1.2	−1.5	0.8	0.8	5.4
	200	− 4.6	−2.7	− 3.7	− 5.1	−3.0	− 2.8	− 2.8	−3.0	3.7	3.8	7.0
	300	−10.9 ± 1.6	−8.2 ± 0.9	−11.4 ± 1.6	−11.8 ± 2.2	−4.5 ± 3.0	− 5.7 ± 3.7	− 5.5 ± 3.7	−4.4 ± 3.6	8.4 ± 0.5	8.8 ± 0.5	8.7 ± 1.5
LiCl	5	0	0		3.7	3.0	− 0.8	− 0.8		0.8	0.8	7.2
	100	− 4.1	−2.3		− 1.1	0.2	− 2.2	− 2.2		3.2	3.2	8.8
	200	−20.2	−7.8		−14.4	0.1	− 7.3	− 8.4		10.5	12.4	11.6
	300	−40.8 ± 6.1	−9.3 ± 1.4		−32.5 ± 4.2	0 ± 1.5	−17.1 ± 7.0	−19.9 ± 7.1		19.6 ± 1.2	23.2 ± 1.4	17.9 ± 3.0
LiBr	5	0			5.8		4.9	3.7		4.1	3.9	7.7
	100	− 6.7			− 0.3		− 0.4	0.5		10.1	10.7	10.6
	200	−26.7			−17.0		− 9.7	−14.6		12.2	28.3	13.4
	300	−50.5 ± 7.5			−43.6 ± 5.2		−40.7 ± 10.6	−40.3 ± 10.0		7.3 ± 0.4	43.6 ± 2.6	17.8 ± 3.7
LiI	5	0			6.4		− 8.4	5.1		0.1	0.2	12.5
	100	−12.8			− 7.9		−19.3	− 1.6		15.1	12.4	14.3
	200	−43.4 ± 6.4			−47.2 ± 5.5			−31.6 ± 9.3			47.0 ± 2.6	17.5 ± 3.8

Table 6. Comparison of the calculated and experimental values, in cm^{-1}, of $\Delta^E(0,t)$, $\Delta_T^A(0,t,\Omega)$, determined at $\Omega = 0$ and $\Omega = \omega_t$, and of $\Gamma(0,t,\omega_t)$ for the sodium halides.

		$\Delta^E(0,t)$			$\Delta_T^A(0,t,0)$		$\Delta_T^A(0,t,\omega_t)$			$\Gamma(0,t,\omega_t)$		
			Expt.				Calc.		Expt.	Calc.		Expt.
	T (K)	Calc.	$\Omega = 0$	$\Omega = (\omega_t)_{expt}$	Calc.	Expt.	$(\omega_t)_{calc}$	$(\omega_t)_{expt}$	$(\omega_t)_{expt}$	$(\omega_t)_{calc}$	$(\omega_t)_{expt}$	$(\omega_t)_{expt}$
NaF	5	0	0	0	1.6	2.2	−1.6	−1.9	−1.2	0.2	0.2	3.3
	100	− 0.6	−1.0	−0.7	0.2	0.2	−0.6	−0.8	−2.8	0.7	0.7	5.2
	200	− 3.7	−3.9	−4.4	− 3.0	−1.6	−1.1	−1.5	−5.2	2.2	2.3	6.4
	300	− 7.8 ± 1.2	−8.8 ± 1.3	−8.7 ± 1.0	− 8.2 ± 1.5	−2.5 ± 1.8	−2.3 ± 2.4	−2.3 ± 2.4	−7.7 ± 2.8	4.6 ± 0.3	4.7 ± 0.3	8.4 ± 1.0
NaCl	5	0	0	0	0.9	2.3	−0.7	−0.8	−1.4	0.3	0.3	1.3
	100	− 1.1	−1.3	−1.3	− 0.6	−0.2	−0.1	−0.5	−1.9	1.1	1.1	1.8
	200	− 4.6	−4.0	−3.3	− 4.6	−1.0	−0.6	−1.0	−3.3	2.8	3.2	2.7
	300	− 8.6 ± 1.3	−6.8 ± 1.0	−9.0 ± 0.5	− 9.0 ± 1.5	−1.5 ± 1.1	−1.6 ± 2.2	−1.8 ± 2.2	−5.0 ± 2.9	5.7 ± 0.4	5.7 ± 0.4	3.5 ± 0.3
NaBr	5	0	0	0	1.4	1.0	−0.3	−0.1	−3.2	0.7	1.3	1.7
	100	− 1.4	−1.5	−1.6	− 0.3	−0.6	−0.2	−0.8	−3.6	2.1	2.7	2.2
	200	− 5.0	−1.9	−4.7	− 3.3	−1.2	0.4	−1.4	−4.5	4.8	5.4	3.5
	300	− 9.0 ± 1.3	−3.9 ± 0.8	−7.9 ± 0.5	− 7.7 ± 1.5	−1.8 ± 1.4	0.1 ± 2.2	−1.3 ± 2.3	−6.5 ± 1.6	8.4 ± 0.5	8.5 ± 0.5	4.2 ± 0.4
NaI	5	0	0		1.9	1.1	1.7	1.7		0.7	0.7	2.2
	100	− 1.8	−1.7		0	−0.3	3.0	3.0		3.8	3.7	3.1
	200	− 5.9	−4.6		− 4.2	−0.7	2.1	1.4		10.0	9.6	4.8
	300	−10.4 ± 1.5	−6.8 ± 1.0		−11.3 ± 1.9	−1.0 ± 0.5	−3.6 ± 2.9	1.2 ± 2.8		14.9 ± 0.9	16.9 ± 1.0	6.9 ± 1.5

Table 7. Comparison of the calculated and experimental values, in cm^{-1}, of $\Delta^R(0,t)$, $\Delta_T^A(0,t,\Omega)$, determined at $\Omega=0$ and $\Omega=\omega_\ell$, and of $\Gamma(0,t,\omega_\ell)$ for the potassium halides.

		$\Delta^R(0,t)$			$\Delta_T^A(0,t,0)$		$\Delta_T^A(0,t,\omega_\ell)$			$\Gamma(0,t,\omega_\ell)$		
			Expt.				Calc.		Expt.	Calc.		Expt.
	T (K)	Calc.	$\Omega=0$	$\Omega=(\omega_\ell)_{expt}$	Calc.	Expt.	$(\omega_\ell)_{calc}$	$(\omega_\ell)_{expt}$	$(\omega_\ell)_{expt}$	$(\omega_\ell)_{calc}$	$(\omega_\ell)_{expt}$	$(\omega_\ell)_{expt}$
KF	5	0			2.1		−0.1	−0.1		0.5	0.5	5.9
	100	−1.1			−0.1		−0.3	−0.3		1.3	1.3	7.0
	200	−5.2			−4.4		−0.9	−0.9		3.6	3.6	8.3
	300	−10.2 ± 1.5			−9.6 ± 1.7		−2.1 ± 2.7	−2.1 ± 2.8		7.0 ± 0.4	6.9 ± 0.4	9.5 ± 1.2
KCl	5	0	0	0	1.21	0.2	−0.1	−0.1	−1.1	0.2	0.2	0.7
	100	−1.1	−1.9	−1.2	−0.56	−2.2	−0.1	−0.1	−1.1	0.8	0.8	1.0
	200	−4.0	−3.5	−4.3	−3.33	−4.5	−0.6	−0.6	−1.6	2.6	2.6	1.7
	300	−7.4 ± 1.1	−6.3 ± 0.9	−7.6 ± 1.2	−6.82 ± 2.0	−6.9 ± 2.7	−1.4 ± 2.0	−1.4 ± 2.0	−2.4 ± 2.4	4.8 ± 0.3	4.8 ± 0.3	2.3 ± 0.2
KBr	5	0	0	0	1.1	0.7	0.5	0.5	−2.0	0.6	0.6	0.5
	100	−1.1	−1.0	−0.9	−0.2	−1.6	1.0	0.8	−2.3	2.0	2.0	0.9
	200	−3.8	−3.2	−3.3	−2.2	−3.3	0.7	0.7	−3.6	4.2	4.1	1.4
	300	−6.7 ± 1.0	−5.4 ± 0.6	−5.8 ± 0.6	−5.0 ± 1.1	−4.8 ± 2.0	−0.3 ± 1.7	0 ± 1.7	−5.5 ± 1.6	6.6 ± 0.4	5.7 ± 0.3	2.4 ± 0.1
KI	5	0	0	0	0.8	1.2	0.7	0.7	−1.4	0.2	0.2	1.0
	100	−0.9	−0.9	−1.3	0.2	−1.4	1.6	1.7	−1.5	0.9	0.9	1.5
	200	−2.9	−2.9	−3.7	−0.7	−3.0	2.6	3.0	−1.7	2.4	2.4	2.6
	300	−5.0 ± 0.7	−5.0 ± 0.5	−6.2 ± 0.6	−2.2 ± 0.7	−4.5 ± 1.2	3.1 ± 0.9	3.9 ± 0.9	−2.5 ± 1.6	4.0 ± 0.3	4.8 ± 0.3	3.1 ± 0.3

Table 8. Comparison of the calculated and experimental values, in cm^{-1}, of $\Delta^E(0,t)$, $\Delta_T^A(0,t,\Omega)$, determined at $\Omega = 0$ and $\Omega = \omega_t$, and of $\Gamma(0,t,\omega_t)$ for the rubidium halides.

		$\Delta^E(0,t)$			$\Delta_T^A(0,t,0)$		$\Delta_T^A(0,t,\omega_t)$			$\Gamma(0,t,\omega_t)$		
			Expt.				Calc		Expt.	Calc.		Expt.
	T (K)	Calc.	$\Omega = 0$	$\Omega = (\omega_t)_{expt}$	Calc.	Expt.	$(\omega_t)_{calc}$	$(\omega_t)_{expt}$	$(\omega_t)_{expt}$	$(\omega_t)_{calc}$	$(\omega_t)_{expt}$	$(\omega_t)_{expt}$
RbF	5	0			2.9		1.3	1.4		0.9	0.9	3.2
	100	−2.6			0.7		1.0	1.0		3.2	3.2	3.8
	200	−7.5			−3.7		−0.8	−1.5		7.1	7.9	4.8
	300	−13.8 ± 2.1			−10.2 ± 2.1		−2.6 ± 3.4	−6.1 ± 3.8		11.6 ± 0.7	13.1 ± 0.7	5.5 ± 0.7
RbCl	5	0	0	0	1.5	0.6	0.2	0.2	−3.5	0.6	0.6	1.3
	100	−1.6	−0.9	−1.1	−0.1	−1.4	0	−0.1	−3.7	1.7	1.9	1.6
	200	−5.2	−2.8	−3.4	−2.9	−2.7	−0.3	−0.5	−5.1	3.8	3.9	2.0
	300	−9.2 ± 1.8	−4.5 ± 0.5	−5.9 ± 0.6	−7.0 ± 1.6	−4.2 ± 1.5	−1.6 ± 2.6	−1.6 ± 2.6	−7.6 ± 1.6	6.5 ± 0.4	6.7 ± 0.4	2.6 ± 0.2
RbBr	5	0	0	0	0.7	−0.1	0.1	0.1	−1.4	0.2	0.2	0.7
	100	−1.3	−1.1	−1.1	−0.7	−1.2	0	0	−1.7	1.3	1.3	0.9
	200	−3.9	−3.0	−3.2	−2.7	−1.8	−0.5	−0.7	−2.2	2.2	2.3	1.2
	300	−6.5 ± 1.0	−4.8 ± 0.5	−5.4 ± 0.5	−5.6 ± 1.0	−2.6 ± 1.1	−1.1 ± 1.5	−1.1 ± 1.5	−3.2 ± 1.5	4.4 ± 0.3	4.4 ± 0.3	1.5 ± 0.2
RbI	5	0	0	0	0.6	−0.7	1.9	1.9	−0.5	0.3	0.3	0.6
	100	−1.3	−0.9	−1.0	−0.5	−1.9	0.4	0.2	−0.9	1.4	1.4	0.8
	200	−3.5	−2.4	−2.8	−2.2	−2.8	0.2	0.5	−1.7	2.5	2.6	1.1
	300	−5.9 ± 0.9	−3.7 ± 0.4	−4.5 ± 0.4	−4.6 ± 0.9	−4.1 ± 1.5	−0.2 ± 1.4	−0.2 ± 1.4	−2.5 ± 1.4	4.6 ± 0.3	4.7 ± 0.3	1.5 ± 0.1

Table 9. Experimental values, in cm^{-1}, of $\Delta^E(0,t)$ and $\Delta^A_T(0,t,\Omega)$, determined at $\Omega = 0$ and $\Omega = \omega_t$, for the cesium halides.

		$\Delta^E(0,t)$			
	T (K)	$\Omega = 0$	$\Omega = \omega_t$	$\Delta^A_T(0,t,0)$	$\Delta^A_T(0,t,\omega_t)$
CsCl	5	0	0	−1.1	−0.7
	100	−1.6	−2.0	1.2	−0.1
	200	−2.9	−5.8	3.5	1.5
	300	−3.8 ± 0.4	−9.8 ± 1.0	5.1 ± 2.4	2.3 ± 2.0
CsBr	5	0	0	0.4	−1.2
	100	−1.2	−1.6	0.8	−0.2
	200	−3.2	−4.2	1.7	0.6
	300	−5.2 ± 0.6	−6.8 ± 0.7	2.6 ± 1.5	0.9 ± 1.5
CsI	5	0	0	0.2	0.5
	100	−1.0	−1.4	0.5	1.3
	200	−2.3	−3.4	1.0	1.8
	300	−3.7 ± 0.4	−5.5 ± 0.5	1.4 ± 1.3	2.2 ± 1.1

Table 10. Experimental values, in cm^{-1}, of $\Delta^E(0,t)$ and $\Delta^A_1(0,t,\omega)$, determined at $\Omega = 0$ and $\Omega = \omega_t$, for the silver and thallium halides.

		$\Delta^E(0,t)$			
	T (K)	$\Omega = 0$	$\Omega = \omega_t$	$\Delta^A_1(0,t,0)$	$\Delta^A_1(0,t,\omega_t)$
AgCl	5	0	0	3.5	− 4.5
	100	− 0.8	−1.7	0.3	− 5.3
	200	− 3.7	−5.2	−2.1	− 7.2
	300	− 8.8 ± 0.8	−9.5 ± 1.0	−3.0 ± 2.0	−10.5 ± 5.0
AgBr	5	0	0	3.0	− 1.4
	100	− 0.6	−1.3	−0.3	− 2.0
	200	− 5.2	−4.6	−0.7	− 3.2
	300	−11.2 ± 0.8	−8.6 ± 0.8	−1.2 ± 2.0	− 4.8 ± 2.3
TlCl	5	0	0	1.0	3.0
	100	− 0.6	−0.9	3.9	4.5
	200	− 3.4	−4.4	7.1	8.4
	300	− 4.6 ± 0.7	−8.3 ± 1.0	10.8 ± 2.0	12.6 ± 2.1
TlBr	5	0	0	1.0	3.0
	100	− 0.6	−0.6	3.1	4.4
	200	− 2.0	−3.5	6.0	8.6
	300	− 4.3 ± 0.6	−7.6 ± 0.9	8.9 ± 2.0	12.8 ± 1.8

Table 11. Measured values of the temperature and pressure dependence of $2\Gamma(0,t,\omega_t)$ for the alkali and heavy metal halides.

	$2\Gamma(0,t,\omega_t)$ (cm^{-1})				$\frac{d2\Gamma(0,t\ \omega_t)}{dP}$ ($cm^{-1}kbar^{-1}$)
T (K)	2	90	200	290	290
LiF	7.3±3.2	10.4±2.9	13.9±2.3	17.1±1.9	
LiCl	14.4±1.4	17.4±1.4	23.1±1.4	34.5±1.4	
LiBr	15.3±3.8	20.5±4.7	26.8±4.6	34.6±5.4	
LiI	25.0±4.7	27.9±4.7	35.0±7.5	39.7±8.8	
NaF	6.5±1.3	10.4±2.1	12.7±2.1	16.8±2.0	0.10±0.07
NaCl	2.5±0.7	3.[illegible]±0.7	5.3±0.5	7.0±0.5	−0.50±0.13
NaBr	3.4±0.9	4.3±0.7	7.0±0.7	8.4±0.7	−0.32±0.14
NaI	4.3±1.3	6.1±1.9	9.5±3.0	13.7±2.9	
KF	11.9±2.1	14.0±2.1	16.6±2.1	19.0±2.4	
KCl	1.4±0.6	1.9±0.4	3.4±0.5	4.5±0.4	−0.08±0.07
KBr	0.9±0.5	1.6±0.4	2.8±0.2	4.7±0.2	−0.03±0.03
KI	2.0±0.6	2.7±0.5	5.0±0.5	6.2±0.5	0.03±0.02
RbF	6.4±0.9	7.4±1.2	9.6±1.3	10.9±1.3	
RbCl	2.5±0.4	3.1±0.4	4.0±0.4	4.8±0.4	−0.04±0.03
RbBr	1.3±0.3	1.7±0.3	2.4±0.3	3.0±0.3	0.14±0.11
RbI	1.1±0.2	1.4±0.2	2.1±0.2	2.8±0.2	0.12±0.04
CsF	9.2±1.4	9.9±2.0	16.2±2.0	19.7±2.0	
CsCl	3.4±0.5	3.7±0.5	5.1±0.5	6.1±0.5	−0.02±0.02
CsBr	1.5±0.2	2.3±0.2	3.1±0.2	4.0±0.2	−0.04±0.02
CsI	1.0±0.2	1.4±0.3	2.1±0.3	2.6±0.3	−0.04±0.02
AgCl	3.5±0.5	6.0±0.5	9.5±0.5	13.2±1.0	0.02±0.01
AgBr	2.5±0.5	4.5±0.5	8.5±0.5	13.2±1.0	0.04±0.02
TlCl	4.0±0.5	5.0±0.5	6.3±0.5	7.7±0.5	−0.05±0.04
TlBr	2.7±0.3	3.0±0.3	3.5±0.4	4.0±0.4	−0.03±0.02

AD-A095 151 NORTHEASTERN UNIV BOSTON MASS F/G 20/12
PHONON SELF-ENERGIES IN WEAKLY AND STRONGLY ANHARMONIC SYSTEMS.(U)
DEC 80 R P LOWNDES DA-ARO-D-31-124-72-G125
UNCLASSIFIED ARO-10392.14-P NL

2 OF 2
AD A095151

END
DATE FILMED
3-81
DTIC

Table 12. The different values of α determined as defined in the text. Note that the errors quoted for α_s and α_p reflect only the inaccuracies involved in the linear extrapolation of the ferroelectric mode spectral characteristics and do not contain any estimate of the inaccuracy of the fitting procedure.

	$\alpha_s \times 10^2$	$\alpha_p \times 10^2$	$\alpha_E \times 10^2$	$\alpha_\perp^2 \times 10^2$	$\langle\alpha\rangle \times 10^2$	$\langle\alpha\rangle_m \times 10^2$
KDP	6·7	6·7	0·20 ± 0·02	0·25 ± 0·03	0·51	2·06
KDA	5·4 ± 0·4	30·6 ± 3·1	0·10 ± 0·02	0·10 ± 0·02	0·30	0·61
RbDA	3·6 ± 0·2	11·1 ± 0·9	0·25 ± 0·05	0·26 ± 0·05	0·84	1·88
CsDA	0·24 ± 0·01	1·1 ± 0·1	0·47 ± 0·03	0·52 ± 0·03	1·11	2·51
KD*A	−5·6 ± 0·4	−6·8 ± 0·3	0·39 ± 0·03	0·43 ± 0·03	0·70	1·95
RbD*A	−7·0 ± 0·2	−5·0 ± 0·2	0·58 ± 0·02	0·75 ± 0·03	1·50	4·18
CsD*A	−7·3 ± 0·1	−5·4 ± 0·1	0·65 ± 0·02	0·73 ± 0·03	0·75	3·01

Table 13. Values of the parameters characterizing the Debye relaxation process in the ferroelectric phase of KDP and CsDA determined from fits of the experimental data to the form of equation (43). The transition occurs at 122.4 K and 149.5 K in KDP and CsDA, respectively

	T (K)	$\epsilon'(\infty)$	$\epsilon''(\infty)$	A	$1/\tau$ (MHz)
	122·35	446·3	38·6	914·6	30·78
	120·53	339·9	51·0	917·4	27·89
	118·89	283·9	59·6	895·3	26·71
	117·13	255·6	60·1	892·4	23·23
	115·55	279·1	101·5	796·7	21·31
KDP	114·06	251·2	92·7	808·1	20·73
	110·46	230·8	101·2	763·1	18·07
	106·93	197·2	88·2	751·7	15·63
	103·36	172·8	95·2	617·8	13·39
	98·47	117·7	45·2	340·0	19·13
	91·12	46·1	16·5	48·9	18·84
	149·47	89·8	1·7	91·0	75·39
	146·73	39·7	2·9	112·0	52·60
	144·42	31·3	1·2	122·7	45·04
	141·74	25·7	1·7	121·1	41·52
CsDA	138·75	23·3	4·8	111·5	38·08
	133·78	21·9	7·1	98·5	31·92
	128·76	26·2	10·9	56·0	26·21
	126·41	24·3	9·7	37·8	24·78
	123·85	21·9	8·2	16·6	25·93

Unclassified

SECURITY CLASSIFICATION OF THIS PAGE (When Data Entered)

REPORT DOCUMENTATION PAGE		READ INSTRUCTIONS BEFORE COMPLETING FORM
1. REPORT NUMBER	2. GOVT ACCESSION NO. AD-A095151	3. RECIPIENT'S CATALOG NUMBER
4. TITLE (and Subtitle) PHONON SELF-ENERGIES IN WEAKLY AND STRONGLY ANHARMONIC SYSTEMS		5. TYPE OF REPORT & PERIOD COVERED Final June 1975-December 1980
		6. PERFORMING ORG. REPORT NUMBER
7. AUTHOR(s) Robert P. Lowndes		8. CONTRACT OR GRANT NUMBER(s) DA-ARO-D-31-124-72-G125 DAHC04-75-G-0166
9. PERFORMING ORGANIZATION NAME AND ADDRESS Northeastern University Boston, Massachusetts 02115		10. PROGRAM ELEMENT, PROJECT, TASK AREA & WORK UNIT NUMBERS
11. CONTROLLING OFFICE NAME AND ADDRESS U. S. Army Research Office Post Office Box 12211 Research Triangle Park, NC 27709		12. REPORT DATE December 11, 1980
		13. NUMBER OF PAGES 91
14. MONITORING AGENCY NAME & ADDRESS (if different from Controlling Office)		15. SECURITY CLASS. (of this report) Unclassified
		15a. DECLASSIFICATION/DOWNGRADING SCHEDULE NA

16. DISTRIBUTION STATEMENT (of this Report)

Approved for public release; distribution unlimited.

17. DISTRIBUTION STATEMENT (of the abstract entered in Block 20, if different from Report)

NA

18. SUPPLEMENTARY NOTES

The findings in this report are not to be construed as an official Department of the Army position, unless so designated by other authorized documents.

19. KEY WORDS (Continue on reverse side if necessary and identify by block number)

Anharmonic Self-Energy; Central Component; Soft Mode; Ionic Solid; Alkali Halide; Heavy Metal Halide; Displacive Ferroelectric; Hydrogen-Bonded Ferroelectric; High Pressure Far Infrared; Dispersive Fourier Transform Spectroscopy; Radiofrequency Dielectric.

20. ABSTRACT (Continue on reverse side if necessary and identify by block number)

This report describes investigations of phonon anharmonic self-energies in weakly anharmonic systems, in strongly anharmonic systems like displacive ferroelectrics, and in hydrogen bonded ferroelectrics. Section II of the report describes the experimental determination of the thermal strain component and the frequency dependence of the anharmonic self-energy and damping function of the $q \approx 0$ transverse optic mode in a number of simple ionic systems and compares them with numerical evaluations using current anharmonic theories. The results strongly support the current theories of weak anharmonicity. Section III

DD FORM 1 JAN 73 1473 EDITION OF 1 NOV 65 IS OBSOLETE

Unclassified

SECURITY CLASSIFICATION OF THIS PAGE (When Data Entered)

describes analogous experimental determinations of the various self-energy components associated with the soft mode in the displacive ferroelectrics $KTaO_3$ and $SrTiO_3$. Section IV describes the results of an experimental search for the central component in hydrogen bonded ferroelectrics, and of our subsequent observation and theoretical analysis of a central component in the power spectrum of homogeneous polarization fluctuations in the ferroelectric phase of these materials.

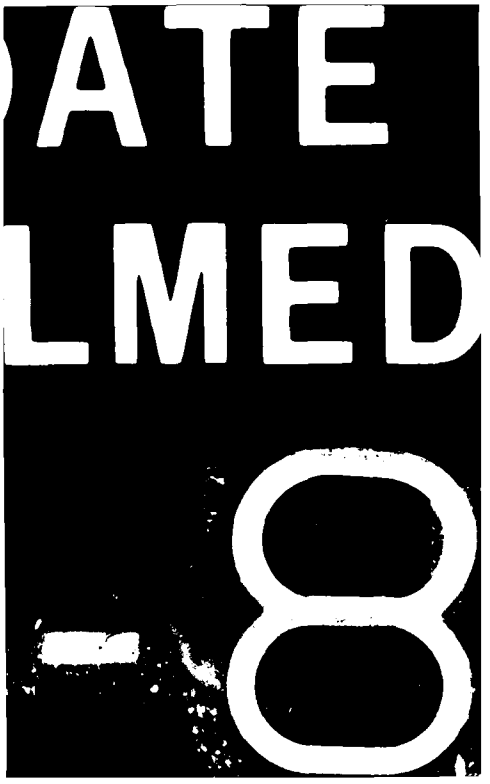
ATE
LMED
8